Detection and Visualization of Anatomical Structures for Radiation-Therapy Planning

by

Neculai Archip

DISSERTATION

Submitted to the Faculty of Science in fulfillment of the requirements for the degree of

"Docteur ès Sciences"

University of Neuchâtel
Department of Computer Science
Emile Argand 11
CH-2007 Neuchâtel
Switzerland

IMPRIMATUR POUR LA THESE

Detection and visualization of anatomical structures for radiation therapy planning

de M. Neculai Archip

UNIVERSITE DE NEUCHATEL

FACULTE DES SCIENCES

La Faculté des sciences de l'Université de Neuchâtel sur le rapport des membres du jury,

MM. P.-J. Erard (directeur de thèse),
H. Hügli, J.-M. Haefliger (La Chaux-de-Fonds),
et M. Egmont-Petersen (Utrecht NL)

autorise l'impression de la présente thèse.

Neuchâtel, le 11 juin 2002

Le doyen:

F. Zwahlen

To my parents.

Table of Contents

Abstract

Accurate planning of radiation therapy entails the definition of treatment volumes and a clear delimitation of normal tissue to which unnecessary exposure should be prevented. Is also needed 3D visualization of these structures. Being performed manually this procedure is a very consuming time process. In this thesis a computer based method for automatically detection of structures of interest on CT images is presented. The approach relies on a knowledge-base which consists of a so-called *Anatomical Structures Map* and a task-oriented architecture called the *Plan Solver*. 3D segmentation algorithms for medical images inspired from human operator procedure are introduced. Two important problems related to radiation therapy planning are solved using this approach: spinal cord segmentation and lung tumors detection. The algorithms were tested on real patient data obtained from *La Chaux-de-Fonds* Hospital, Switzerland. For spinal cord segmentation, 23 patient CT scans have been used, and 20 patients for the lung metastases detection. Evaluation was performed using a visual inspection of the contours projected on the CT image slices. A radiologist has decided for each of the contours obtained with our system whether it is acceptable or not. The solution proposed has a high clinical quality and it is very fast.

A method for reconstruction of 3D surface and volume models of anatomical structures is also introduced. The technique was tested on real clinical data as well. Models for different organs have been obtained. The quality surfaces has been judged satisfactory for display purposes in medical applications (*Computer Aided Diagnostic* and *Computer Assisted Surgery*).

Acknowlegments

The thesis was possible due to the support and encouragement I had from my supervisor Prof. Pierre-Jean Erard.
I acknowledge also the members of the jury Dr. Michael Egmont-Petersen, Prof. Jean-Marie Haefliger and Prof. Heinz Hugli, for their comments and improvements on the original manuscript.
The kindly collaboration of the members of the Oncology Department of the La Chaux de Fonds Hospital, especially PD Dr. Jean-Francois Germond was essential for the success of this thesis.
Some part of this thesis was facilitated by the work done together with Medivision AG and Muller Institute Bern. Special thanks to Dr. Vincent Dessenne and Prof. Lutz-Peter Nolte.
Finally ...[1]

[1] ...I thank to all the persons who were beside me all these years : $(A|B|...|Z)^*$

Chapter 1

Introduction

Medicine offers now many application areas for computer science. Neurosurgery, surgical planning, anatomic modeling for prosthesis production and radiation therapy are major application areas. Other areas include robotic assistance, virtual endoscopy, and anatomic atlases. In the last years, a big volume of intersiciplinary research work has been performed in areas as radiology, physics, biology, electrical engineering and computer science. The work presented in this thesis, deals with development of *Computer Aided Diagnosis* techniques applied in cancer treatment.

1.1 Problem statement

The three primary modalities of cancer treatment are: surgery, chemotherapy and radiation therapy. The goal of radiation therapy is to destroy tumor cells by maximizing the radiation dose to the tumor while minimizing the dose to surrounding healthy tissue. Radiation treatments may be just one part of an integrated cancer treatment strategy involving other modalities of treatment including surgery and chemotherapy. Radiation therapy is delivered in a number of different ways including x-ray or electron beams and brachytherapy, or implant therapy, which is the temporary or permanent internal placement of radioactive sources. Each patient is treated with the type of radiation most appropriate to their situation.

Successful radiotherapy relies also on an precise planning and a thorough implementation of the radiation procedure. Radiation therapy planning has to find a balance between ineffective underdosing of the tumor (the target volume) and dangerous overdosing of surrounding tissue (organs at risk).

The problem of radiotherapy planning which is addressed here, requires that the tissues of interest, including the tumor and the surrounding (vital) organs, be located with a high accuracy. The current planning procedure entails manual delineation of the organs at risk and of tumors in each separate slice followed by an automatic reconstruction performed by the image analysis workstation that is connected with the CT-scanning device. Despite the existence of several semi-automatic approaches for planning repetitive radiotherapy [19, 43], automatic identification and delimitation of some organs and pathologies remains an unresolved problem. Being now performed manually, it is a very consuming time process. Our goal is to introduce a computer-based method more efficient and faster than the one which is used now in the hospitals. In this aim, the research presented was focused on the development of a general methodology which can be applied for detection of different normal and pathological anatomical structures on CT images. Special emphasis was also given on the creation of a method for $3D$ visualization of the structures detected.

1.2 Research focus

The performed research work was oriented to solve clinical problems. The work was focused on the following directions:

- *develop an anatomical knowledge base* - the anatomical information present in our image material is very complex and hard to formalize in way that makes computer-based image interpretation feasible. Our image material is characterized by a large amount of inter-patient variation. This variation makes it difficult to develop standardized low-level image processing algorithms that make feasible an automatic detection of the organs in CT images. Instead, a novel knowledge-based top-down approach for image interpretation was developed.

- *medical image interpretation* - several existent basic image processing algorithms can be successfully applied to segment certain organs on the CT images. The problem consists in connecting the knowledge base with these algorithms, in what we have called *knowledge guided image processing.*

- *image segmentation* - several image processing algorithms used in other fields should be adapted to the specific of CT images.

- *solve clinical problems* related to radiotherapy planning using the knowledge based approach.

- *3D reconstruction* - once the objects contours are detected in a stack of CT slices, the 3D object should be displayed using a surface and volume model.

1.3 Contribution highlights

Four major novelties are introduced in this thesis:

1. *top-down knowledge-based approach for a flexible interpretation of CT images.* The method developed can cope with a large amount of inter-patient variation.

2. *3D segmentation algorithms for medical images inspired from the human operator procedure.* Our approach is based on 2D processing in each slice of a CT scanner. It uses local information found in the current slice, and/or information from adjacent slices. The 3D structures are reconstructed from series of contours thus obtained in slices. This way is similar to the method used now by radiotherapists and radiologists to perform the radiation therapy planning. They detect the first slice where the anatomical structure of interest can be precisely detected. Than, they are navigating through the slices to delimitate the organ of interest, using the contours and information from adjacent slices. The use of transversal slices, was the choice of a computer engineer which solves medical problems, using the experience and expertise of the medical doctors. At the beginning of this project, the process of knowledge acquisition was performed, by multiple interviews and observations of the specialists in clinical problems.

3. *the general developed methodology for image interpretation was tested on two real medical problems.* Problems related to detection of organs at risk (e.g. spinal cord) and pathologies (lung metastases) are solved using a general knowledge-based approach. The algorithms tested on more than 20 patients data have shown to be fast and achieve a good clinical quality.

A subordinate task, which has been addressed in depth, is the development of a visualization method for surface and volume models generation. The quality of initial data, in form of contours on parallel slices, is improved using smoothing techniques and B-spline interpolation. Then, the convex hull is obtained applying a $3D$ Delaunay triangulation. A sculpting process of tetrahedra is performed using original image information. The surface quality was judged to be satisfactory for displaying purposes in medical applications. The execution time, another important issue, is also reasonable.

1.4 Medical validation of methods

Interdisciplinary collaboration with a hospital is a very important aspect in this field of research. In our case, we have a profound and efficient cooperation with *La Chaux-de-Fonds* Hospital, Switzerland. Interactivity with the medical team from the Oncology Department, the meetings and their suggestions have been very important for the results we obtained. For a computer scientist, three kind of resources are needed for a joint-project related to medical imaging:

- access to medical expertise;
- access to medical data, in form of CT images;
- validation of the obtained results.

More details on this topic can be found in Chapter 3.

1.5 Overview of the thesis

Chapter 2 reviews the state of the art of methods and techniques for medical image processing used in this thesis. The next chapter presents briefly the process of radiotherapy planning and situates the work presented here. Chapter 4 presents the knowledge based image interpretation method developed, as well the knowledge base that we have called *Anatomical Structures Map*. The task (e.g. *Find spinal cord*) oriented architecture and the plan solver are also introduced here. The problems solved, related to radiotherapy planning are also introduced in this chapter. Chapter 5 provides the solution to the problem of spinal cord segmentation, using the general approach of Chapter 4. In the next chapter, the solution offered to the problem of lung metastases detection is presented. Chapter 6 shows the method we have developed for object reconstruction from parallel contours, and the way we obtain both surface and volume models of organs. The thesis ends with some conclusions about the present work.

Chapter 2

State of the Art

This chapter reviews the methods and techniques for medical image processing used in this thesis. First, different image modalities are briefly presented, followed by information about the DICOM standard for images obtained from the medical scanner. Then, the techniques for image segmentation currently used are introduced. The main methods for object recognition are also illustrated. The applications of computer vision in medical imaging are than presented. Then, some advance approaches for medical interpretation are discussed. The chapter ends with a description of $3D$ reconstruction techniques.

2.1 Diagnostic imaging modalities

In this paragraph the main diagnostic imaging techniques are presented. The focus is mainly on *Computed Tomography*, which is used in our research work. In the Figure 2.1 samples image acquired with different scanner are presented.

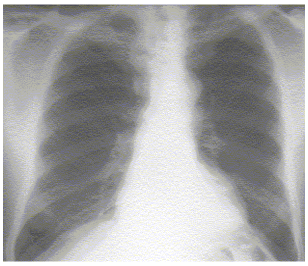

a.

b.

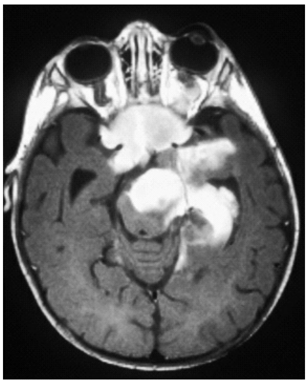

c.

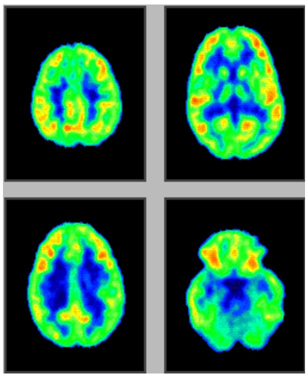

d.

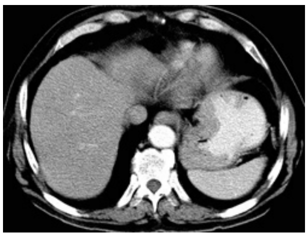

e.

Figure 2.1: Illustrations of images obtained from five diagnostic imaging modalities:
a. Standard X-Ray;
b. Ultrasound;
c. MRI;
d. PET;
e. CT.

2.1.1 X-ray

X-ray can penetrate visually opaque objects with essentially unrestricted orientation to generate two-dimensional semitransparent projection views. Such procedures are relatively inexpensive and widely available. Standard X-ray procedures are excellent for routine examinations of pulmonary and skeletal disorders, but cannot provide direct images of soft tissue.

2.1.2 Ultrasound

Ultrasound uses acoustic windows to measure the time delay between an ultrasonic pulse and its echo, the reflection of the pulse, from a surface where there is discontinuity in characteristic impedance. Ultrasound makes pictures in the same way that sonar equipment in submarines *sees* objects underwater. It is useful in the diagnosis of common vascular disease by showing blood flow abnormalities. Blood velocity and the direction of flow are shown in color to help detect blockage to blood flow. Also prenatal imaging and ultrasound imaging during surgical procedures are medically effective, relatively safe and inexpensive. The disadvantage is its inability to penetrate beyond bone structures. Only soft tissue that is unrestricted by intervening bone is properly imaged.

2.1.3 Magnetic resonance

MR uses magnetism to induce the emission of radio frequency energy from tissue to form a picture of internal patient anatomy; it can discriminate many types of tissue. MR is quite versatile, providing information from anatomic views that show the proton density of all tissue such as water, fat, gray and white brain matter to views that highlight the presence of specific molecules. MR's ability to reveal important chemical properties of tissue is one of its most powerful features. MR scanners are also being used to illustrate blood vessel disorders.

2.1.4 Nuclear medicine as aided diagnosis

Nuclear medicine procedures rely on the physiological uptake and detection of radioactive isotopes. Nuclear medicine images show the functional distribution of the isotope within a target organ against an adjacent surrounding anatomic structure. Because high metabolic activity is common to many forms of cancerous tissue, nuclear medicine helps physicians locate pathology and monitor therapy for such disorders. Nuclear medicine procedures use several types of equipment: PET (positron emission tomography) and SPECT (single photon emission computed tomography).

2.1.5 Computed Tomography

This imaging technique was conceived by G.N. Hounsfield, in 1972 a senior research scientist in Middlesex, England. In the last 30 years, his discovery has completely revolutionized the practice of medicine, so has MRI. Although the first CT scanners could only image the head, they now have primary roles in diagnosing disorders of the chest, abdomen, and pelvis. Conventional radiographs project a three dimensional objects onto a two dimensional image. Their main limitation is that overlying tissues are superimposed on the image. Computed tomography overcomes this problem by scanning thin slices of the body with a narrow x ray beam which rotates around the body, producing an image of each slice as a cross section of the body. Another limitation of the conventional radiograph is its inability to distinguish between two tissues with similar density, such as soft tissue and fluid. Computed tomography can differentiate between tissues of similar density because of the narrow x ray beam and the use of "windowing". In an ideal world, the image would be displayed with a different shade of gray for every different computed tomography number. The radiographer selects the range of computed tomography numbers to be displayed and all the numbers within this range are spread over the available gray scale. By convention, high computed tomography numbers are displayed as white and low as black. To image an area of the body in which many of the tissues have a similar density - for example, the mediastinum or abdomen - a narrow range of computed tomography numbers is selected. These can be spread out over the available gray scale so that two tissues with only a little difference in density will be ascribed separate shades and which makes differentiation possible.

2.2 DICOM standard

The images acquired with a medical scanner should be transfered to a computer-based planning station, using a common protocol for all the scanner manufactures. In this aim, *The American College of Radiology* (ACR) and the *National Electrical Manufactures Association* (NEMA) formed a joint committee in 1983 to develop a standard to :

- Promote communication of digital image information, regardless of device manufacturer;
- Facilitate the development and expansion of picture archiving and communication systems (PACS) that can also interface with other systems of hospital information;
- Allow the creation of diagnostic information data bases that can be queried by

a wide variety of devices distributed geographically.

The result was in 1985 the DICOM (Digital Imaging and Communication in Medicine) standard, a document which defines a new method of communication and storage for the different types of digital medical imaging equipment. This standard is now used by most of the companies active in the field of medical imaging. This norm allows communication between the equipment locally, at the distance or across a media, and assures the compatibility of equipment, eliminating the particular formats. A Radiology Service produces thousands of images every day, so it is not possible to store those images in an current format as JPEG or GIF, because at the risk of loosing demographic dates of the images (patient name, exam type, hospital, date of the exam, acquisition type). The DICOM standard allows storing of every image together with its associated information.

2.3 Computer vision in medical imaging

There is a large number of applications of computer vision techniques in medical imaging. Radiation therapy, surgery planning, studying degenerative disease, construction of rendered 3D models of anatomical structures are some domains with a huge development in the last years. One of the main roles of computer vision systems is to enhance the qualitative information obtained from the produced images.

Radiotherapy is an important ingredient in the often complex treatment procedures that are initiated in other to suppress different kinds of malignant tumors. The purpose of radiation therapy is to eradicate the tumor while minimizing the damage attributed to the surrounding healthy tissues. For certain vital organs, a certain amount of exposure to radiation can induce a number of undesired neurological complications (e.g. for the spinal cord paralysis) [13, 51, 72]. The risk of such serious complications implies much smaller dosage tolerances for the organs at risk than for the tumors. That is why also normal tissue volume (e.g. spinal cord, glottic larynx, heart) are also contoured on CT images [32]. The dosage constraints to critical normal tissues is as in table 2.1. Meanwhile, the tumors (e.g. nodules) should get at least 70 **Gy**. The normal tissues are contoured and considered as solid organs. The treatment plan used for each patient is based on an analysis of the volumetric dosage, including Dose Volume Histogram analyses of the Planning Target Volume (PTV) and critical normal structures. The treatment aim is to deliver the radiation to the PTVs and the exclusion of nonivolved tissue as feasible.

Within this goal, successful radiotherapy relies on a precise planning and a thorough implementation of the radiation procedure. One of the problems of radiotherapy planning addressed in this thesis, is the requirement that the different tissues of interest, including the tumor and the surrounding organs, are located with a high accuracy. Nowadays, radiation therapy is being planned by a radiologist and a radiotherapist, based on a careful analysis of a CT scan that covers the tumor and the surrounding tissues. The current planning procedure entails manual delineation of the spinal cord in each separate slice followed by an automatic reconstruction performed by the image analysis workstation that is connected with the CT-scanning device. Despite the existence of several semi-automatic approaches for planning of repetitive radiotherapy [19, 43], automatic detection of the spinal cord remains an unresolved problem.

Tumors are heterogeneous lesions, which exhibit growth patterns that are unique to each patient. As a consequence, the CT images cannot in our application domain be

Critical normal structure	Radiation dosage suported
Glottic Larynx	2/3 bellow 50 **Gy**
Brainstem	54 **Gy**
Spinal cord	42 **Gy**
Heart	Not more than 35 **Gy** to > 50% cardiac volume
Rectum	55 **Gy**

Table 2.1: Maximum radiation dosage values for some critical normal structures

acquired according to a standardized protocol but are subject to much inter-patient variation, e.g., compared with mammograms [113] or standard thorax radiographs [118] that are acquired in large numbers in Europe and North America. This rather high amount of variation in our image material impedes the application of a standard low-level image processing technique.

In the analysis of the objects in images it is essential that we can distinguish between the objects of interest and *the rest*. The techniques that are used to find the objects of interest are usually referred to as segmentation techniques. A survey of state-of-the-art techniques for image segmentation is presented in the next section. It is important to understand that there is no universally applicable segmentation technique that will work for all images, and no segmentation technique is perfect for all possible applications. A lot of research work is dedicated to the so-called low level image processing. Different operators for gradient approaximation, different filters, different edge operators have been developed in ths last years. The main drawback is a lack of use of knowledge regarding the expected image content. The objects thus detected do not always have a semantic meaning because of just the matematical properties of the image which have been use.
A typical edge detector (e.g. Canny operator) will only give information about where possible contours may be located, but no information about where a specific boundary

structure is. The low-level image processing algorithms can be used just in combination with a-priori anatomical information. The problem is to formalize this knowledge, e.g. by encorporating in a computer reprezentation the inter-patient variation. Even two CT scans of the same patient at different moment in time are not the same. This is the case with all the scanner images due to the biological variation (e.g. age, sex, race). But, certain general facts are valid for all the normal people (everyone has a spine, a brain, lungs, liver). This kind of information could be used as *static knowledge*. The pathologies would in this case be the *dynamic knowledge*. To be successful in our application, an image processing algorithm should be *flexible* as well *transparent* to the radiologist and radiotherapist. A flexible approach can better cope with a high amount of inter-patient variation. Transparency of the image processing system ensures that the experts can take over the image analysis, in case the automatic approach fails to give the desired result.

In the next two sections, the low level image segmentation algorithms and high level methods for image interpretation are presented.

2.4 Image segmentation

Image segmentation is the process that partitions a digital image into disjoint (non-overlapping) regions, where each region is a connected set of pixels - i.e. all pixels are adjacent. Object extraction refers to the particular case of image segmentation where only specific regions of an image are of interest: this segmentation process therefore seeks only to determine the pixels that belong to objects of interest, and all other pixels are assumed to belong to a generic *non-object* category.

Thresholding

Thresholding techniques may be adequate for the segmentation task if the intensity distribution in the image is bimodal (where the object(s) of interest are of different brightness than the background). Locally adaptive thresholding chooses different threshold levels for different regions of an image. It is sometimes more successful than simple (global) thresholding, particularly in cases where the background varies slowly over the entire image, which depends of modality and anatomy.

Edge Detection

The first step in image segmentation is often the application of an edge extraction operation, which determines how different pixels are discriminated from their neighbors: abrupt changes in brightness are interpreted as the edges of objects. The aim is to provide evidence for the automatic delineation of objects in a scene, which are assumed to be characterized by their edges. Convolution kernels for edge detection are often of the gradient type. Edge detection is very often preceded by smoothing, which reduces the effect of noise. The following smoothing filters are most frequently used: used:

- *Uniform Blur* - averages a pixel and its neighbors;
- *Median* - replaces a pixel with the median, rather than the mean, of the pixel and its neighbors;
- *Gaussian* - a filter that produces a smooth response (unlike uniform blur and median filtering) by weighting more towards the center.

The problem of filtering is the trade-off between how much noise the filter removes and how much important information is lost.

Gradient Magnitude Edge Detection

For a continuous image, we use an intensity function $I(x,y)$ and its derivatives $I_x(x,y) = \frac{\delta}{\delta x}I(x,y)$ and $I_y(x,y) = \frac{\delta}{\delta y}I(x,y)$. The gradient function of $I(x,y)$ is then the vector $\nabla I(x,y) = (I_x(x,y), I_y(x,y))$. For a digitized image, we use instead of $I(x,y)$, a pixel discretized function $I(i,j)$, where i and j are integer values for x and y. To express the derivatives, we use:

$$I_x(i,j) = \sum_{k=1}^{m}\sum_{l=1}^{n} g_i(k,l)I(i+k-\frac{m}{2}-1, j+l-\frac{n}{2}-1)$$
$$I_y(i,j) = \sum_{k=1}^{m}\sum_{l=1}^{n} g_j(k,l)I(i+k-\frac{m}{2}-1, j+l-\frac{n}{2}-1)$$

where $g_i(m,n)$ and $g_j(m,n)$ are the weight coefficients of the derivative operator.

The resulting vector contains information about how strong the edge is at that pixel (i,j), and in which direction the slope is maximum.

Gradient Operators

In this way, some operators were introduced in the literature which attempt to approximate the value of the gradient for the discrete case, such as Frei and Chen [38] and Marr edge detection [79]. One of the most common used is the Sobel operator [109], given by:

$$G_x = \begin{pmatrix} -1 & 0 & 1 \\ -2 & 0 & 2 \\ -1 & 0 & 1 \end{pmatrix} \tag{2.1}$$

and

$$G_y = \begin{pmatrix} 1 & 2 & 1 \\ 0 & 0 & 0 \\ -1 & -2 & -1 \end{pmatrix} \tag{2.2}$$

Most recently, Ando [8] introduced a new operator which has a good quality improvement of this approximation; he calculates matrices to be used as convolution operators with the original image:

3 x 3:

$$\mathcal{G}_{3X3} = \begin{pmatrix} -0.112737 & 0.000000 & 0.112737 \\ -0.274526 & 0.000000 & 0.274526 \\ -0.112737 & 0.000000 & 0.112737 \end{pmatrix} \tag{2.3}$$

4 x 4:

$$\mathcal{G}_{4X4} = \begin{pmatrix} -0.022116 & -0.025526 & 0.025526 & 0.022116 \\ -0.099381 & -0.112984 & 0.112984 & 0.098381 \\ -0.099381 & -0.112984 & 0.112984 & 0.098381 \\ -0.022116 & -0.025526 & 0.025526 & 0.022116 \end{pmatrix} \tag{2.4}$$

Boundary Tracking

Boundary tracking is a more algorithmically complex gradient method for edge extraction. A point is located on the boundary of an object, and an algorithm is used to iteratively search for neighboring pixels that are assumed to be also on the boundary. The Canny [23] algorithm, for example, begins by smoothing the image, and then applies a standard edge operator. It then thins the extracted edges to single pixel width by tracking gradient magnitude ridges and setting all pixels in their neighborhoods that are not of maximal gradient to zero (the process is referred to as non-maximal suppression). The tracking process only starts at points with an edge strength greater than a preset threshold, but tracks ridges as long as their edge strength does not fall below a lower preset threshold. This hysteresis process helps to ensure that noisy edges are not broken up into multiple edge fragments.

Deformable Templates and Active Contours

Active Contours are used to extract objects from an image, given an approximate location. The algorithm seeks to (locally) minimize an "energy function" which is the sum of the "energy" at each snaxel. A survey can be found in [80, 81]. Different improvements of the original model introduced in [60] can be found in [21, 57, 69].

Region Growing

Region growing techniques represent another major category of segmentation approaches. They operate by firstly dividing the image into many tiny regions (even single pixels). The properties that reflect object membership for each region are computed - for example, average gray level, texture, color. The boundaries between adjacent regions are then examined. If properties between regions on either side of a boundary do not differ strongly, the two regions are merged. Object membership properties are then recomputed and again weak boundaries are dissolved. This continues until no weak boundaries exist.

There are many techniques for improving the performance of this type of segmentation: see [93, 106] for details.

Region growing techniques are useful in the segmentation of certain types of images, for example natural scenes, where no strong or previous knowledge is available.

They are generally only useful where regions of interest are defined through information other than morphological (shape): this makes them complementary to edge detection-based techniques such as template matching

The Watershed Algorithm

Image data may be interpreted as a topographic surface where the gradient image gray-levels represent altitudes. Region edges correspond to high watersheds and low-gradient region interiors correspond to catchment basins. Attachment basins of the topographic surface are homogeneous in the sense that all pixels belonging to the same catchment basin are connected with the basin's region of minimum altitude (gray-level) by a simple path of pixels that have monotonically decreasing altitude (gray-level) along the path. Such catchment basins then represent the regions of the segmented image. A good survey of watershed algorithms can be found in [102]. Due to its complexity, some work has been performed on its parallelization as in [87].

2.5 Object recognition

Object recognition is the task of finding and labeling parts of a two or three dimensional image. Since the major task in object recognition is to outline areas in an image identifiable as model instances, it is tempting to use one of the edge detection or region segmentation described previously by itself. The results may result in homogenous regions, which do not always belong to the region of interest. These results cannot be used as they are. But these simple techniques may be useful when we need a starting point for a more sophisticated object recognition.

We can classify the strategies for object recognition according their suitability for complex models and for complex data in four major classes :

- *Feature vector classification.* Features vector methods rely on a trivial model of an object's image characteristics and are typically applied only to simple data.

- *Fitting Models to Photometry.* When simple models are sufficient but the photometric data are noisy and ambiguous, a number of methods that fits simple models instances may be effective. Such methods search for features with predetermined global shapes and photometric properties.

- *Fitting Models to Symbolic Structures.* When complex models are required but reliable symbolic structures can be accurately inferred from simple data, procedures that tie these structures into complex model hierarchies may be appropriate. Such approaches typically look for instances of objects by matching data structures that represent relations among object parts and may use a hierarchy of intermediate models to prune the search tree.

- *Combined Strategies.* When both the data and the desired model instances are complex, successful object recognition requires a combination of strategies.

Feature Vector Classification

In this approach, objects are modeled as vectors of characteristic features, each of which corresponds to a point in the multidimensional feature space. Examples of features include gray value, color, infrared or ultraviolet intensity, area, perimeter, compactness, textural properties. To use the feature vector approach, we must select which features are relevant, determine a way to measure them, and define a criterion for distinguishing the desired objects. Two types of approaches are :

- *Pixel Classification.* It is the simplest and most straightforward application of the feature-space strategy. Each pixel is potentially a member of a different model class, and the classification of pixels is based solely on their intensities or frequency spectrum.

- *Classification from a feature vector.* We may use features that characterize regions of a partitioned image; such regions are typically obtained by some photometry-based method that groups adjacent pixels into coherent areas with homogeneous local characteristics. This requires images with simple photometric statistics. The features-space approach works well when the problem involves simple models that do not include constraints relating different parts of a model and when we can restrict ourselves to either pixel classification or classification of labels with good photometry. A major limitation of the feature-space approach is its inappropriateness for the representation and handling of models that include constraints on the relationships between the chosen features. The technique does not easily make use of more global information, such as spatial relationships and model context.

Fitting Models to Photometry

The most straightforward object recognition techniques are those that fit their models directly to the photometric data. These methods improve upon feature-based recognition by incorporating more model knowledge into their procedures and replacing local pixel classification by more global considerations. The basic strategies are divided into two categories :

- *Rigid Model Fitting.* The shape or photometry of the target object is known a priori; the model shape can be either rigid or parametric, depending on a limited set of free parameters. The method is based on template matching. We include strategies as quantifying photometric statistics and hough transform methods.

- *Flexible Model Fitting.* This class of computational strategies uses more flexible models, specified by a set of generic constraints on object characteristics such as smoothness, rectilinearity, curvature, compactness, symmetry and homogeneity. The fit of the model to the image data is usually measured by an objective function, and matching is performed by minimizing this measure. We include techniques as gradient descent, closed-form solution, relaxation, and heuristic pruning. The main disadvantages are related to the initialization and optimization process.

Fitting Models to Symbolic Structures

Fitting models to symbolic structures assumes that a set of features has been reliably extracted from the image data by some preprocessing operation. These features are usually found by a local statistics-based operator, without using shape information or contextual scene knowledge. This process is often referred to as segmentation. Important categories are:

- *Graph Matching.* Objects are modeled as a relational structure or graph of primitives. The nodes are components of the object or scene, whereas the arcs denote relationships. Labels are assigned by searching for the optimal match between the model graphs and the graph derived from the image data. Heuristics can be used to prune the search tree and reduce the computation time at the possible risk of finding a nonoptimal solution.

- *Composite (Hierarchical) Model Fitting.* A reduction of the search space is obtained by working hierarchically, that is, by finding partial matches using a hierarchy of intermediate models and then refining them. The techniques used in this strategy are : structural grouping, refining matches using multiple information sources and knowledge-based systems.

2.6 Medical image interpretation

The literature on computer-based image interpretation describes a large number of architectures, systems and approaches. Some focus on architectural aspects of the scene (the spatial configuration composed by the objects that are present); in other approaches an extensive knowledge base and an advanced reasoning strategy form the major components [83, 110, 119, 126]. Also probabilistic systems were developed for knowledge-guided image interpretation [58, 66, 116]. Several blackboard and other knowledge-based systems were developed specifically for interpretation of medical images. The ERNEST system has been developed for interpretation of scintigraphic images and MR images [67]. The system VIA-RAD [103] applies four diagnostic strategies, obtained from the radiological domain, to perform image interpretation. Brown *et al.* [22] present a knowledge-based system for lung detection in CT images. A system for object recognition in CT images of the brain is presented in [74]. An architecture has been developed for interpretation of abdominal CT images [35]. A task-based architecture to interpretation of MR images of the brain, is introduced by Gong et al. [45]. Another systems for magnetic resonance images analysis are presented in [59, 96].

In computer-based systems for interpretation of medical images, one or more of the following archetypes of knowledge are generally modeled [30]: *structural knowledge*, *dynamic knowledge* and *procedural knowledge*.

In some applications, a satisfactory image interpretation can be obtained from solely one type of knowledge. For example, in perfusion analysis of bone tumors dynamic knowledge is sufficient for making a distinction between viable tumor and necrosis [31]. In other applications, all three types of knowledge may be a prerequisite for a successful image synthesis. Spinal cord detection and subsequent planning of radiotherapy rely primarily on structural knowledge components: where is the tumor located, the spine and on the procedural knowledge that is needed to describe how the CT images should be analyzed [2, 98]. A semi-automatic method for ultrasound images segmentation is shown in [37]. In case-based reasoning there are a few examples of systems that are concerned with medical images. In the ROENTGEN system [17], therapy planning based on tomographic images is the object of reasoning. Radiologic image retrieval based on image captions and content related queries is the focus in the MacRad system [78]. A case based system that interprets medical images is the SCINA system [50], which is based on the commercially available ESTEEM CBR tool. Grimnes in [48] described a two layer case-based reasoning architecture for medical image understanding. It combines low-level structure analysis with high-level interpretation of image content, within a task-oriented model. A case based reasoner working on a segment case-base contains the individual image segments. These cases with labels are considered indexes for another case based reasoner working on an organ interpretation case base.

Yanai, in [124] described a multi-agent architecture to integrate and cooperate object recognition modules for individual target objects. In their system, object candidates generated by different agents are integrated not only on the evaluations by each modules themselves but also on spatial relations among objects. By checking spatial relation, the agents also estimate actual objects from parts seen in the image. For scene exploration, the knowledge base contains information about camera movements and objects.

In [63] it was shown that regarding remote sensing data and maps from different kinds of sensors allow a similar approach for both in the domain of landscape interpretation. The prior knowledge about the landscape objects is represented explicitly by semantic nets. Based on the semantics of the network language a problem independent set of rules controls the scene interpretation. Important is that the scene analysis employs a partial interpretation derived from a Digital Land-scape Model (ATKIS DLM 25/1). This partial interpretation is used to generate an initial scene description. Consecutively the scene description is verified in aerial images and maps. Interpretation proceeds iteratively mixing top-down and bottom-up strategies.

In [64] a black-board infrastructure for object-based image interpretation applications was presented. The infrastructure is based on an abstract definition of important concepts in image interpretation: data objects, relationships, algorithms, strategies and models.

Some research has been performed to automate the task of tumor detection in CT images. In [25], a technique to detect the nodules in the lungs is presented which first removes the vessels on the images, using a 3D region growing. Using different geometric features to distinguish nodules from vessels, a method was tested on eight CT scans in [86]. A technique based on object deformation is presented in [77]. In [12], Armato presented a method which combines threshold techniques with geometrical and intensity properties for classifying the nodules in the CT images. A genetic algorithm is used in [71] for detection of lung nodules. An spatial filter to detect the nodules is used in [91]. Ko in [62] developed a gray-level-threshold-based automated nodules detection method. Some similar methods are presented in [100, 110] for lung analysis from CT high resolution images.

2.7 3D Reconstruction

The problem of 3D reconstruction arises in medical imaging where human organs are scanned using an image modality already discussed in Section 2.1 (CT or MRI). Cross-sections are obtained and then a reconstruction of a surface connecting these cross-sections is sought. The input to the surface reconstruction problem is a series of parallel slices, each representing a cross-section of the solid to be modeled. An appropriate edge detection technique is assumed to have detected the boundary of the contours from their raw images. Each slice contains possibly several contours, whose boundaries consist of non-intersecting closed polygon curves. In the case of a contour with hole(s), these polygonal curves are nested. Given the slices of contours, the goal is to reconstruct a triangulated surface that bounds an object, called solid connection, whose geometry is more likely to resemble the original (sampled) object. This uncertainty in reconstruction is bound to crop up in the absence of any apriori knowledge about the sampled object. Branching and correspondence problem arise from this uncertainty [15, 85]. Almost all known approaches reconstruct the solid connection between two consecutive slices and then concatenate them in series to model the object. Much of the earlier work assumes a single contour without any holes in image, thus concentrating primaly on the tiling problem of generating a non self-intersecting surface with certain optimization. Representative works appear in

[24, 39, 40, 61]. A survey for this one-to-one case appears in [108]. Various optimization criteria such as minimum surface area, maximum volume, minimum edge length were considered while constructing the surface, but none could guarantee a non self-intersecting surface. Finally, Gitlin in [44] explained this shortcoming by exhibiting two contours that cannot be triangulated without self-intersection unless new vertices are inserted on the contours. Subsequent approaches allow extra points on the contours and concentrated more on the problem of correspondence and branching with multiple contours on slices. Several approaches that cope with multiple contours on two slices have been proposed [15, 16, 20, 33, 42, 85, 107]. The methods proposed in [33, 85, 107] only work for restricted cases as pointed out in [15]. The algorithm in [16] is reported to work well in practice based on the substantial experimental evidence presented. However, it requires to dicretize the contour boundary sufficiently fine and given an arbitrary data set, it is not clear how to determine a good discretization quantitatively. The method in [15] combines the approach of [16] and [42] to handle the branching problem. However, it implies a strong assumption on the input sampling distance. A competing approach appears in [20] which is based on Delaunay triangulation. This is refined further in [42]. Different types of surface reconstruction algorithms from a set of points can be identified [54].

Algorithms exploiting structure information

Many surface reconstruction algorithms exploit structure in the data. For instance, algorithms solving the surfaces from contours problem make heavy use of the fact that the data points are organized into contours, and the contours lie in parallel planes. Also, algorithms to reconstruct surfaces from multiple range images typically make use of the adjacency relationship of the data within each range image. In [84], two methods for merging range images are given: a *virtual milling* technique that intersects polyhedral constructed from the different range images, and a pruning technique that first constructs the 3D Delaunay Triangulation of the points and then prunes the tetrahedra exposed in the various range images. A *mesh zippering* method is presented in [117], which stitches overlapping surfaces together. The main drawbacks of these approaches is that they dependent on the initial structure of points (methods solving the surfaces from contours problem cannot be used when presented with several sets of intersecting contours).

Algorithms exploiting orientation information

Knowledge of the orientation of the surface at each data point is extremely valuable in surface reconstruction. Many of previous reconstruction methods assume that such orientation information is supplied with the data. When the data points X are obtained from volumetric data, the gradient of this data can provide orientation information that helps guiding the reconstruction. In [88], Moore and Warren fit a piecewise polynomial implicit surface to a set of points, and make use of auxiliary volumetric samples (off the surface) to assign correct orientations to the surface pieces and to prevent spurious surface sheets. Other reconstruction procedures assume that each point is also provided with a normal vector. For example, algorithms for reconstructing surfaces from range data typically exploit the fact that each surface point is known to be visible from the sensor, and make use of these direction vectors in orienting the surface. Szeliski and Tonnesen [112] reconstruct a surface using an optimization problem involving oriented particles. By local interaction, these particles align themselves on a 2-dimensional manifold. The initial orientations of the particles are crucial to the success of their method, and must be specified as input.

Algorithms for triangulating noise-free data

Some recent computational geometry methods come close to addressing the general surface reconstruction problem. They find meshes of arbitrary topological type that interpolate sets of unorganized points. Since they interpolate the data, their main limitation is that they require the data to be noise free.

Favardin in [36] presents a modified gift-wrapping algorithm for triangulating a set of points. Gift-wrapping is a standard algorithm from computational geometry for computing the convex hull of a set of points. It creates a triangulation by successively pivoting planes about boundary edges of the triangulation until these planes encounter other points. Favardin modifies the standard procedure to allow the creation of non-convex surfaces by only considering points in a local neighborhood of the pivoting edge. Favardin also describes a heuristic for detecting and dealing with surface boundaries.

Chapter 3

Radiation Therapy Planning

The aim of radiation therapy is to decrease the number of tumor cells to a level that achieves permanent local tumor control.

Three-dimensional treatment planning ($3DTP$) was developed more than two decades ago. Its aim is to increase tumor control probability by improving the spatial distribution of dosage relative to that achievable with traditional techniques. The objectives of this chapter are to:

- briefly describe the clinical rationale for $3DTP$;
- describe the major components of a $3DTP$ system;
- specify where exactly work presented in this thesis is situated in the context of radiotherapy planning;
- describe a model of collaboration with a hospital.

3.1 Introduction

There are three primary modalities of cancer treatment: surgery, chemotherapy and radiation therapy. The goal of radiation therapy is to destroy tumor cells by maximizing the radiation dosage to the tumor while minimizing the dosage to surrounding healthy tissue. About 50% of all cancer patients will require radiation therapy during some phase of their cancer care. Radiation treatments may be just one part of an integrated cancer treatment strategy involving other modalities of treatment including surgery and chemotherapy. Radiation therapy is delivered in a number of different ways including x-ray or electron beams and brachytherapy, or implant therapy, which is the temporary or permanent internal placement of radioactive sources. Each patient is treated with the type of radiation most appropriate to their situation. Very important is the ethical aspect of radiotherapy treatment. There are cases where by employing it, different secondary effects may appear. Some of these effects can be very damaging for the patient health (like paralysis if the spinal cord receives a high dosage of radiation). In these cases, usually, some trade-offs are made, and the radio oncologists together with the patient have to make a decision about the preferred treatment strategy.

Radiotherapy is particulary useful when the tumor is restricted to its primary site (no metastases) and when the site is inaccessible for surgery (brain tumors). Radiation therapy planning has to find a balance between ineffective underdosing of the tumor (the target volume) and dangerous overdosing of surrounding tissue (organs at risk). Treatment plans are commonly based on desired dosage levels, which are specified for the tumor and each organ at risk. These desired dosage levels are chosen so that a high tumor control probability is realized, but also that probability of complications in any organ at risk is low. Desired dosage levels are specified in terms of the equivalent uniform dosage (EUD), which is defined as that uniform dosage in any given organ. It has the same effect as the actual inhomogeneous dosage that is delivered by radiation therapy equipment. The EUD can be determined based on organ structure using simulation methods and historical data.

3.2 The Three-Dimensional Treatment Planning Process

Three-dimensional treatment planning systems may vary in their design, but all are based on the same principles. The steps required are further presented. It should be noted that not all steps are carried out for all radiation plans. The components of a *Three-Dimensional Treatment Planning* are:

- Localization of the disease and normal organs in 3D:
  - *Initial simulation.*

    The simulation process is a combination of conventional simulation and computed tomography (CT) imaging. Conventional simulators are used to determine the best position of the patient, to define a provisional isocenter, and to place reference localization marks (tattoos) on the patient's skin. The patient is transferred immediately to the CT suite and scanned in the treatment position, that is, on a flat tabletop in the immobilization device. The patient is arranged using the reference localization marks and the CT alignment lasers. Radio-opaque catheters are placed on the localization marks to identify the provisional isocenter location on the CT scans. Anterior and lateral radiographic scout views are acquired to confirm the isocenter position and also the alignment of the patient's skeletted anatomy.

- *3D imaging (CT, MRI).*

  The number of CT slices (or images) required depends on the size, shape and anatomical location of the structures of interest and also the treatment technique to be used. To produce high-resolution 3D reconstructions, the interslice spacing is generally 3-5 mm, with smaller spacing employed in regions where structures of interest are small or vary rapidly in size or shape. The slice thickness is chosen so as to avoid gaps in the CT data set. However, as the number of CT images increases, so does the amount of effort needed to extract the relevant information from them. The actual number of images acquired for a given anatomical site is thus a compromise between accuracy and practicality.

- *Delineation of the target and normal organs.*

  This thesis focuses on this aspect. In the next section, more details are presented about this topic.

• 3D Treatment Planning:

- *Use of Beams-eye-view (BEV).*

  Treatment planning attempts to arrange the treatment fields so as to conform the high dosage region to the target, minimize dosage attributed to normal structures and constrain the dosage to critical structures to below a tolerance. In $3D$ treatment planning, oblique non-coplanar beams can be used, which gives rise to many more possible beam arrangements, thus making the selection of the optimum treatment technique a complex process.

- *3D dosage calculations.*

  Having defined the beam apertures the next step in the 3D treatment planning process is to perform the dosage calculations to estimate the effect of the treatment plan. It is essential that dosage calculations are accurate as there is a close relationship between dosage and clinical outcome, and also so that meaningful comparisons of treatment plans can be made. The most accurate means of dosage calculation is by Monte Carlo simulation of radiation transport [53].

- *Qualitative plan evaluation.*

  Once the dosage distribution has been calculated for a treatment plan it is necessary to have some method by which to determine the merit of that plan. The first step in the plan evaluation process is qualitative and usually consists of a visual inspection of the dosage distribution depicted graphically in relation to the anatomy. There is a variety of ways of displaying dosage distributions. The most common is to superimpose color-coded isodose curves on 2D transverse, sagittal, coronal CT images as well as any reconstructed oblique plane.

- *Quantitative plan evaluation.*

  Objective criteria are used to summarize the large amounts of three-dimensional dosage distribution data into single plots or scores that can be used for plan comparison. However, it should be noted that as we condense information we tend to loose spatial information regarding the dosage distribution. Quantitative measures of a plan merit can be as simple as the minimum, maximum or mean target dosage. An useful commonly evaluation tool is the dose-volume histogram, which indicates how much dosage is received by how much volume for the organ/organs of interest.

- 3D Treatment Plan Delivery:

  - *Resimulation.*

    Once the treatment plan is completed and approved, the CT image set is used to produce digitally reconstructed radiographs (*DRRs*) for each treatment field. In addition to each of the treatment fields, anterior and the lateral orthogonal "setup field" DRRs are also produced. The *DRRs* provide a link between planning and treatment and are used at time of verification simulation, or resimulation, to determine whether the patient is in the prescribed treatment position as determined from the $3D$ CT data set.

  - *Transfer of beam apertures to simulation film.*

    It is the simulator radiographs that represent the reference images for the patient. They are used in comparison with portal films for treatment verification and also as templates for Cerrobend block fabrication. Thus, it is necessary to transfer the beam apertures with the simulator radiographs. This is performed by first registering the DRRs, either manually or automatically, to the simulator radiographs and then transferring the apertures.

- *Transfer of treatment parameters to treatment machine.*

  The traditional method of transferring the planned treatment parameters (number of fields, machine settings, monitor units etc.) for a patient to the treatment machine is via the delivery of the patients folder containing the plan information. The radiation therapist enters the parameters, for each patient, into the treatment machine at time of treatment. Since $3DCRTplans$ are generally more complex than conventional $2D$ plans, they tend to contain a greater amount of information. However, all, or part, of this increased amount of information can be transferred directly to the treatment machine via computer.

- *Semi-automated or automated treatment delivery.*

  Since a greater number of fields will in general improve the therapeutic ratio, that is, the ratio of the tumor dosage to normal tissue dosage, $3DCRT$ treatment plans commonly involve a greater number of treatment fields than conventional plans. Although $3DCRT$ plans can be delivered on conventional treatment machines with Cerrobend blocks, the full benefit of $3DCRT$ can only be realized on treatment machines capable of rapidly delivering a large number of arbitrarily shaped fields under computer control.

• Treatment Delivery Verification:

- *Record and verify systems.*

  The $3DCRT$ plans are more sensitive to delivery errors and therefore it becomes more important to verify that $3DCRT$ treatments are delivered correctly. Record and verify $(R\&V)$ systems can be used to check that machine parameters have been entered correctly. The *R&V* computer and treatment machine control computer communicate over a local area network. For each treatment field, for each patient, the *R&V* system accesses the relevant data from the patient data base and compares it to the machine parameters entered for that field.

- *Portal imaging.*

  Once the machine settings have been verified the next step is to check that the patient has been positioned correctly. Portal films, or more recently electronic portal images, are acquired on the beam exit side of the patient. This record of the treatment position is then compared to the prescribed treatment position as represented by the *DRRs*. The comparison is usually a two step process - comparing DRRs to simulator films at time of resimulation and then simulator films to portal images at time of treatment. Comparisons are usually made visually, however with the advent of electronic portal imaging devices (*EPIDs*) more quantitative methods of patient setup evaluation are being developed and will be discussed later.

• Plan Documentation

A detailed summary of the 3*DCRT* treatment plan should be included with the patients records. In addition to the conventional information the plan summary should contain isodose distributions and quantitative dosage and volume information. Isodose distributions on three planes, coronal, sagittal and central axis CT slice, showing the prescription isodose and other significant levels (e.g. hot spot), are included to document target coverage. Target coverage and dosage to critical normal organs are also reported by the inclusion of target and normal structure $DVHs$.

3.3 Delineation of the target and normal organs

Once the $3D$ information has been acquired the next step is to delineate the target volume and normal structures. Different volumes may be defined, often with varying concentrations of demonstrated or suspected malignant cells. Furthermore, considerations have to be given to probable changes in the spatial relationships between the volume(s) and therapy beam(s) during treatment, movements of the tissues/patient and possible inaccuracies in the treatment setup. Two volumes are defined prior to treatment planning:

- **Gross Tumor Volume - GTV.**

  The **GTV** is the gross palpable or visible/demonstrable extent and location of malignant growth. It consists of primary tumor, metastatic lymphadenopathy, or other metastases. It is the region where the tumor cell density is largest. Different medical image sources can be used to determine the shape, size and location of **GTV** (CT,US,MRI).

- **Clinical Target Volume - CTV.**

  The **CTV** is a tissue volume that contains a demonstrable **GTV** and/or sub-clinical microscopic malignant disease, which has to be eliminated. This volume thus has to be treated adequately in order to achieve the aim of therapy.

During the treatment planning process, other volumes are defined:

- **Planning Target Volume (PTV).**

  The **PTV** is a geometrical concept, and it is defined to select appropriate beam

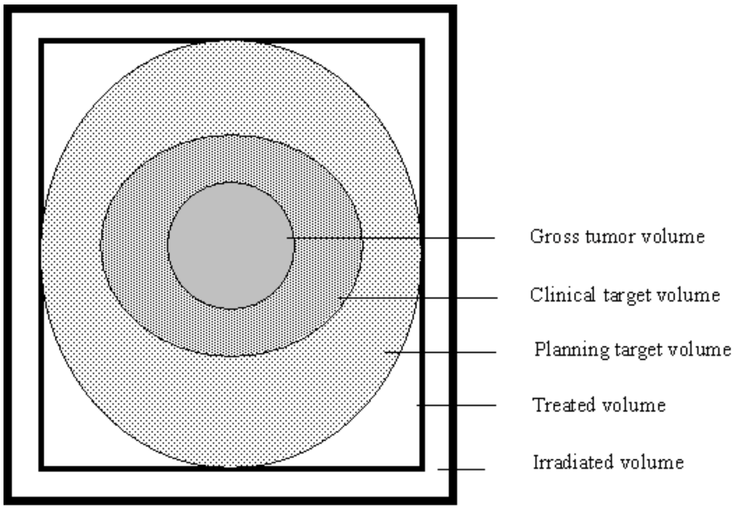

Figure 3.1: Different volumes for radiotherapy

sizes and beam arrangements, taking into consideration the net effect of all the possible geometrical variations, in order to ensure that the prescribed dosage is actually absorbed by the **CTV**.

- **Organ at Risk.**

  Organs at risk are normal tissues whose radiation sensitivity may significantly influence treatment planning and/or prescribed dosage.

Two volumes result from treatment planning: **Treated Volume** and **Irradiate Volume**. The scheme representing these volumes is shown in Figure 3.1.

The problems of radiotherapy planning are illustrated in the Figure 3.2. A hypothetical cancer is present. It should receive at least 70 **Gy** radiation. Meanwhile the spinal cord should be protected. It can not receive more than 42 **Gy**. That is why it should be precisely delimited. In a typical radiotherapy planning station, contouring tools that are currently available include image contrast adjustment, image processing

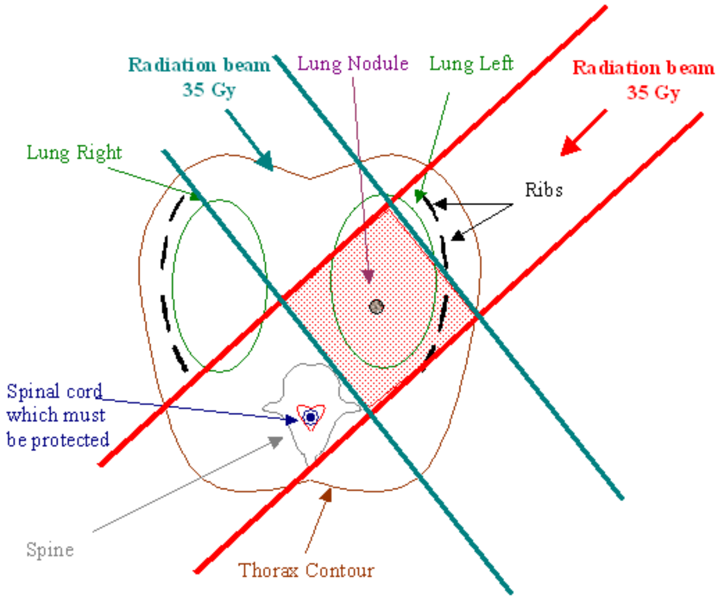

Figure 3.2: An hypothetical lung nodule. A simplified scheme for radiation therapy planning is presented. The tumor should receive at least 70 **Gy**. Meanwhile the spinal cord should be protected. It can not receive more than 42 **Gy**.

(e.g. adaptive histogram equalization), manual contouring (contours can be entered using point or vector drawing modes), interpolation and editing (reshaping of any contour that has been drawn, copied or interpolated).

The manual delineation is particularly important for the definition of the tumor volume. In general, the physician outlines the clinical target volume, **CTV**.

The identification of normal critical structures is necessary as the planning process must take their exposure into account. The structures of interest are contoured on a stack of typically 30 to 40 CT slices. This is a labor intensive, time consuming operation.

This motivated us in creating a computer-based automatic method, which can delimit different structures with a high accuracy and in a reasonable time.

3.4 A model of collaboration with a hospital

A project related to medical image analysis entails a strong collaboration with a hospital. In this section within the framework of radiotherapy planning process, we present also the most important aspects of our cooperation with the Oncology Department of *La Chaux-de-Fonds* hospital. This is a model for a joint-project between computer scientists and medical specialists.

3.4.1 Access to medical expertise

At the beginning of the project, fruitful discussions took place with the specialists from the Oncology Department of *La Chaux-de-Fonds* hospital. Together, we identified clinical problems that can be solved by computer scientists. We also acompanied them during a routine radiotherapy planning procedure. The methods that they used were carefully studied. Few automated tools are available for the oncologists in the process of delineation of the contours of interest. Some tasks are performed with a higher frequency than others (e.g. spinal cord segmentation). Our original idea was to use a knowledge-based approach enclosing medical information about anatomical structures involved in a daily clinical examination. Within this development, medical literature (e.g. medical atlases) provided kindly by specialists from this clinic, has been studied. During the progress of the project we hold several meetings with oncologists and physicians with the goal of clarifying different medical questions that an usual computer scientist could not answer.

3.4.2 Access to medical data

For radiotherapy imaging, a CT scanner is mostly used. At the *La Chaux-de-Fonds*, a Picker CT scanner is available at the Oncology Department. The access to the medical images data is mandatory for the success of a medical imaging project. The algorithms developed must be able to cope with the patient variation. To achieve this goal, the developed methodologies for medical image analysis should be tested on real clinical data. The algorithms created should be robust enough to cope with the appearance differences of organs images depending on the person physiology. Moreover, two consecutive CT scans of the same person will not be the same. Still general anatomical facts are valid for all the patients (spine is in the middle of the thorax, liver is in the right side, spinal cord is located in the middle of spinal canal). This kind of information can be used by a computer-based approach to medical image interpretation. A problem is to assure the privacy data. In this aim, it is common to establish formal agreements between partners. In the hospitals having installed a *Picture Achievement and Communication System (PACS)*, the task of recovering images is easier. Electronical databases are available and queries may be performed considering different parameters (e.g. disease, patient age or gender).

By our partners, the images are stocked on a usual network system in *DICOM* format. We used *DICOM* server software to transfer the images from the hospital to one station at the university. During these operation valuable assistance was provided from the *DICOM* specialist from the Oncology Department.

3.4.3 Results validation

The automatic procedures for image analysis have been developed in the university laboratories. The algorithms have been applied to real CT medical images. The results, in the form of contours have then been inspected by an oncologist who validated them by visual inspection. His observations have been taken into account for further development and improvement of the techniques. Meanwhile, we have been invited to several national radiologists meetings where our results have been presented in front of the medical community. This was a good opportunity to obtain feedback from the potential users of our system.

Chapter 4

Knowledge Guided Image Processing

In this chapter the knowledge-based approach used for automatic identification of anatomical structures is presented. The *Anatomical Structure Map* the name we used for our knowledge-base is introduced here. Than, the plan solver which for a specific task (e.g. *find spinal canal*) detects the sub-task to be performed, is presented. The $3D$ general image processing algorithm is presented as well. Some considerations about implementation of the knowledge base are than illustrated. The chapter ends with the description of contouring problems we have solved and medical data used (in form of CT images).

4.1 Knowledge guided image processing

The anatomical information present in our image material is very complex and hard to formalize in way that makes computer-based image interpretation feasible. Our image material is characterized by a large amount of inter-patient variation. This variation makes it difficult to develop standardized low-level image processing algorithms that make feasible an automatic identification of the organs in CT images.

Instead, we present a novel, knowledge-based top-down approach for image interpretation. Our approach was originally inspired by the manner in which a radiologist and radiotherapist interpret the CT images before plan the radiotherapy can be planned.

4.1.1 Image acquisition and interpretation

In clinical routine, the radiotherapist performs a request containing the questions which should be resolved by the radiological examination (e.g. where is the tumor located? how far is it from the spine? are there other healthy tissues that will be exposed to radiation?). The image acquisition is performed according to a standard protocol, which contains general guidelines for how CT images should be obtained for planning of radiotherapy. The details of an acquisition are chosen such that the tumor of the particular patient is visualized in the best possible way. In general, a number of aspects should be taken into account in order to acquire CT images in such a way that the relevant findings can be established. Wegener [120] points out that there is a strong relationship between what region, organ or lesion is examined and how the image should be acquired, including imaging parameters (slice thickness, slice interval, scanning time), and contrast administration (presence/type of contrast agent, injection speed, concentration). After CT images have been acquired, the interpretation is performed by a radiologist and a radiotherapist in concert. The image assessment relies on both morphological and densitometric findings. Grimnes mentions a number of general aspects that influence the interpretation of CT images [48]:

- the typical size and shape of the objects (organs);
- the variation in size and shape of the objects;

- the expected HU value range associated with each tissue;
- the variation in the HU value range associated with each tissue;
- typical response of an organ to the contrast tracer that is used;
- organs and blood may change their expected HU range in light of disease;
- biological variation;
- and social context.

The radiological analysis results in a *synthesis* of the clinical by relevant findings that were present the CT images, while taking the abovementioned aspects into account. The ultimate goal of any computer system for image interpretation should be to produce such an image synthesis, either automatically or in an interactive manner, e.g., through a dialogue with the radiologist. In computer-based systems for interpretation of medical images, one or more of the following types of knowledge are generally modeled:

- *structural knowledge*, which can contain information about the physical world e.g., normal structures (lungs, spinal canal, lamina, spinal cord, thorax) or pathologies (lung nodules which have a circular shape);
- *dynamic knowledge*, which can contain information about possible abnormal processes;
- *procedural knowledge*, which divides a request (e.g. image synthesis) into a sequence of subtasks that can be performed by specific image processing algorithms.

In some applications, a satisfactory image synthesis can be obtained from solely one type of knowledge. For example, in perfusion analysis of bone tumors dynamic knowledge is sufficient for making a distinction between viable tumor and necrosis [31]. In other applications, all three types of knowledge may be a prerequisite for a successful image synthesis. For example, spinal cord segmentation as subsequent planning of radiotherapy relies primarily on structural knowledge components: where is the tumor located, the spine and on procedural knowledge that is needed to describe how the CT imagesshould be analyzed [2][98]. Meanwhile, lung tumors detection relies on all three types of knowledge.

4.1.2 Knowledge representation in medical image analysis

We will present an approach for semi-automatic image interpretation that uses a knowledge base to link different low-level image processing algorithms. The knowledge base contains medical knowledge about organs and possible pathologic structures, i.e., components of the tumor. The knowledge-base is used to guide the image interpretation but also to specify the parameters of these algorithms. The model presented here is inspired by *frame* [56] systems. *Frames* are structures containing a collection of mutually associated data. They are usually relatively large blocks of knowledge about a particular object, event, situation, or location, describing it in the required detail. They are equivalent to the records in conventional databases having, in general, a slot-facet-value organization of the knowledge to be represented. This model introduced in *AI* is suitable to represent the anatomical information we need, for each structure of interest. Each anatomical structure is represented as a prototype, and its properties as *slots*.

Relation	Description
isInside	Object1 *isInside* Object2 ⇔ allmost all the pixels of Object1 are included in Object2
isSorounded	Object1 *isSurrounded* Object2 ⇔ almost all the pixels of Object1 are included in Object2 and Object1 is the only object which respect Object1 *isInside* Object2
isAtMedialAxis	Object1 *isAtMedialAxis* Object2 ⇔ the center of Object1 is approximately the same as the center of Object2
isNeighbor	Object1 *isNeighbor* Object2 ⇔ the Object1 has a common border with Object2
isAtLeft	Object1 *isAtLeft* Object2 ⇔ allmost all the pixels of Object1 are at the left border of Object2
isAtRight	Object1 *isAtRight* Object2 ⇔ almost all the pixels of Object1 are at the right border of Object2

Table 4.1: Relationships between structures

Structural knowledge

The core of our system is the so-called anatomical structures map (Fig.4.1). (ASM), which was presented earlier in [10]. A set of properties (related to shape, position, densitometric ranges) is used to characterize each of the normal structures (the organs, bones and the vascular system). These normal organs are the **static knowledge**, which is represented in the **ASM**. In the same way any tumors are represented, being also structural knowledge. The tumors are usually connected to an anatomical organ. Identification of the organ, helps further detection of possible tumors. Two types of tumors are represented: nodules which are located inside the lungs, and metastases which can appear at the border of the lungs. The spatial relationships between objects (normal and pathological) are represented as a semantic network. A very simple grammar was also introduced that makes it feasible to express the semantic relations that pertain to our application, see Table 4.1.

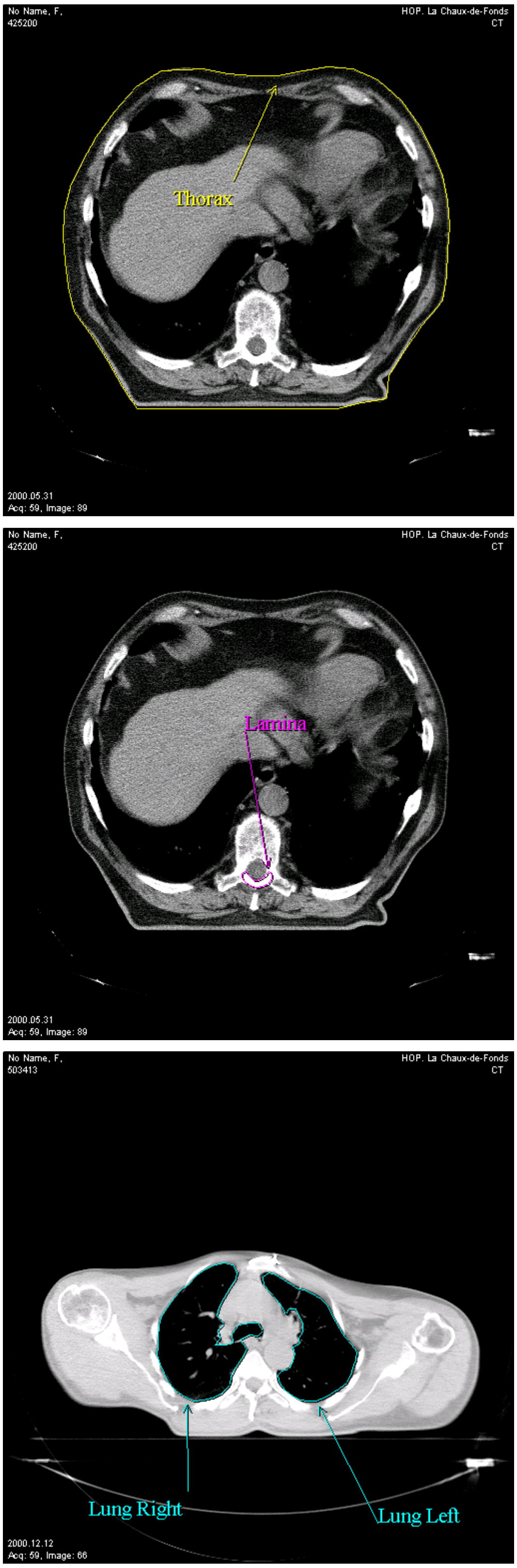

Figure 4.1: Some samples of reference objects.

Procedural knowledge

The structural knowledge base is merged with a *task oriented* architecture, the *plan solver*, which contains the procedural knowledge that is needed to perform the image interpretation. The involved clinicians make use of so-called reference objects (e.g., body or lamina) to direct their focus of attention. Although the architecture of the plan solver was originally inspired by the approach followed by the involved clinicians, the task-based structure also makes it possible to recognize complex objects while benefiting from more simple (basic) object segmentation. Algorithms developed for the recognition of complex objects use so-called reference objects to set their initial configuration or constrain the final solution. The task oriented architecture is responsible for running the plan solver, which dispatches a task, e.g., segment spinal canal, into sub-tasks [45]. Which sub-task should be dispatched, depends on so-called *reference objects*. $Object_x$ is reference object for $Object_y$ if:

- there is a direct, spatial relation between $Object_x$ and $Object_y$ (e.g., *isNeighbor*, *isInside*)
- $Object_x$ has an segmentation algorithm that does not depend on $Object_y$. Hence, $Object_x$ can be identified without any knowledge of $Object_y$.

When the plan-solver is called with the request *Find* $Object_x$, it identifies the sub-tasks that should be performed in order to fulfill the request, i.e., which objects are reference objects to $Object_x$. The list with reference objects found is the list with the sub-tasks to be performed. The task-planner module relies on a global positioning system (along the axes x, y, z), (Fig.6.2) that maps each of the segmented organs to world coordinates.

4.2 Anatomical structures map

The anatomical structures map establishes a number of spatial relations between the objects that are typically distinguished in the CT images used for planning of radiotherapy in our clinic (see Fig. 4.3). The architecture of the anatomical structures map lends its inspiration from frame systems, a well-known concept in the artificial intelligence literature. We choose to represent the anatomical information in 2D slices. More specifically, the ASM represents spatial relations between the typical objects (e.g., spine, lamina and tumor) as well as the general category of each object: bone, air and tissues (see Fig. 4.2). We discern these particular categories for the following reasons. Objects belonging to the first two categories have either a very low or a very high HU level (e.g., the air compartment in a lung versus, e.g., bones). For these two types of objects, a threshold-based technique is in most cases sufficient for a reliable segmentation result. Tissues (e.g., organs), on the other hand, cannot be identified by thresholding within a specific HU range. For objects belonging to this third category, a reliable segmentation needs to be based on the already segmented reference objects.

The main object represented is the *body contour*, which comprises all the other organs. It has a so-called *independent* segmentation scheme as it is possible to identify the body by a basic image processing algorithm, in this case by thresholding (see section 5.1.1). The structures that are more difficult to segment include the spine, the lamina, the lungs, the ribs and the spinal canal. The spine contains mainly bone so it has a very high HU and thresholding is used to segment it. All the sub-parts of the spine consist of mainly bone cortex so a threshold method is also used to segment these objects. The spinal canal consists mainly of tissue but is completely surrounded

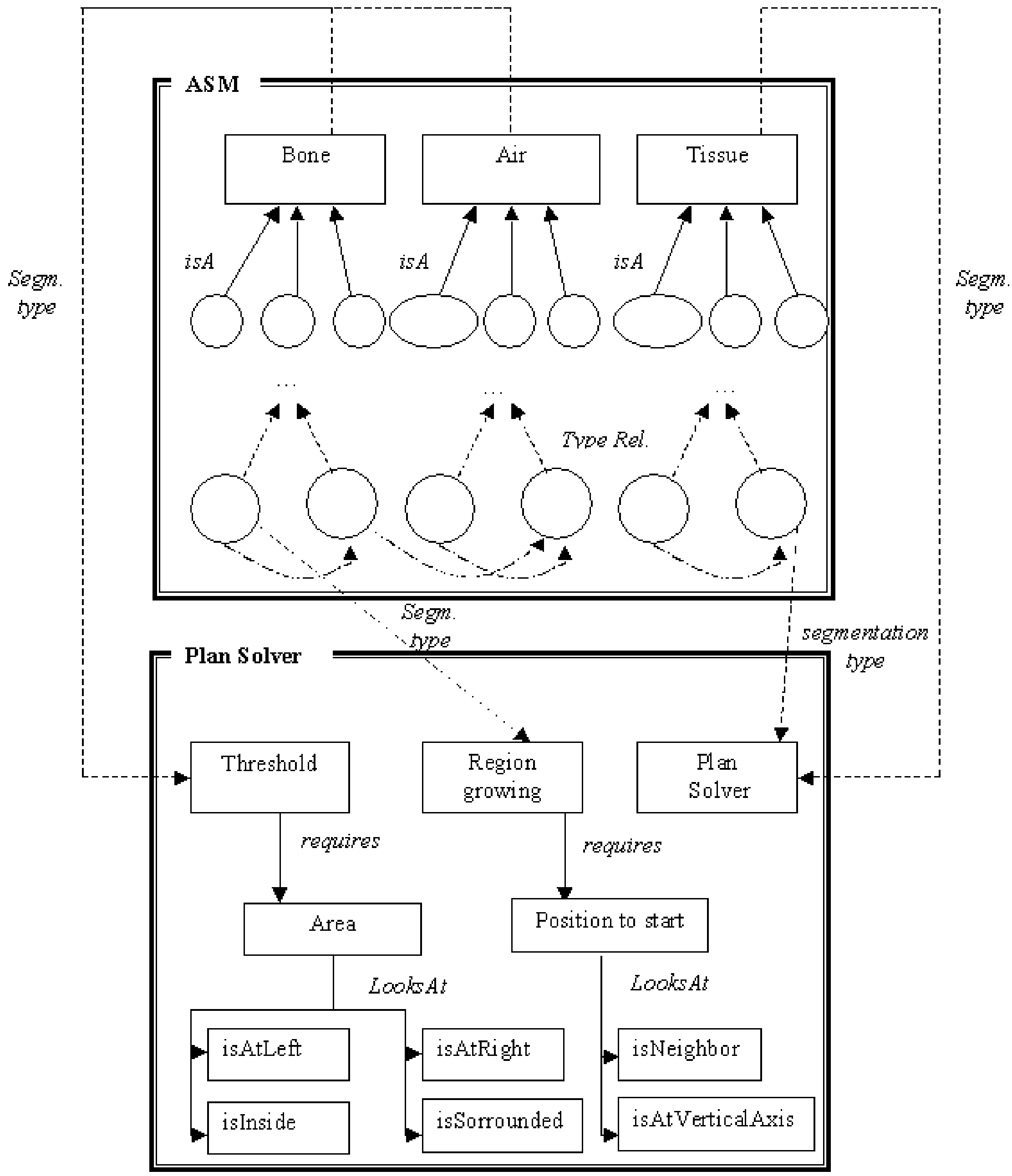

Figure 4.2: Relationships in the *Anatomical Structures Map - Plan Solver*. On the *ASM* relationships between structures are presented, and on the *Plan Solver* side segmentation methods as well as parameters for each of it. Also the connections between structures and corresponding segmentation methods are presented

by the spine, i.e., *Spinal Canal* **IsInside** *Spine.* We use a region growing scheme to segment it, mainly because the border of the spinal canal has a high contrast compared with the surrounding bone (difference *HU* bone - tissue) - see section 5.1.3.

The ribs are bones and again a threshold technique will segment them properly. Their position is given by relationships *Ribs Left* **isAtRight** *Lung Left* and *Ribs Right* **isAtLeft** *Lung Right.* The threshold area is thus delimited.

4.3 Plan solver

The anatomical structures map help to partition a request (e.g., locate spine) into subtasks and further into atomic image processing tasks that are performed by dedicated routines. This hierarchical partitioning takes place in the *plan solver* module, which links the spatial relations in the anatomical structures map (see the figure 4.3) with the atomic image processing algorithms. The plan solver uses an *inheritance scheme* to determine the appropriate segmentation approach for a particular object or tissue (see Fig. 4.2). An object connected with another (basic) object by an **isA** relationship inherits the segmentation method of that basic object.

We make a distinction between different types of atomic segmentation methods that are used for object recognition in our application: the threshold-based methods (for the bones in this case, but also for the lungs in the context of lung tumors detection) and region based methods (for the spinal canal in this case). For the threshold-based methods it is important to restrict the area to which they are applied. This is accomplished by using so-called reference objects. Reference objects are specified by the following relations in the anatomical structures map: **isAtLeft**, **isAtRight**, **isInside** and **isSurrounded** by a recursive top-down search (see the line

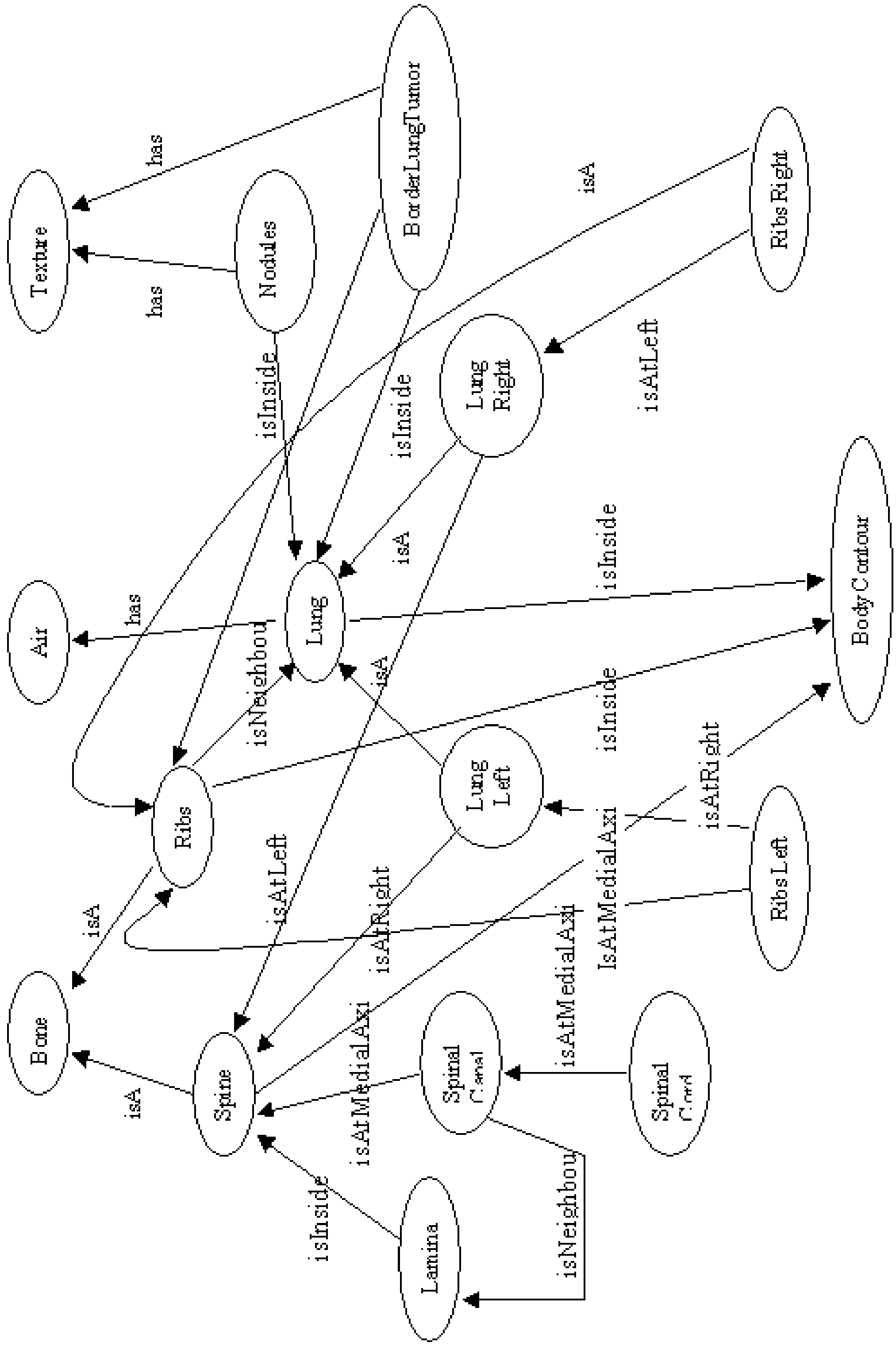

Figure 4.3: Relationships between structures

7, in Algorithm 1). For region based approaches, the reference objects are found between the objects with the relationship **isNeighbor** or **isVerticalAxis** (see line 5, in Algorithm 1). When a certain sub request *Find* $Object_x$ is dispatched, the plan solver tries to fulfill the request choosing the appropriate segmentation methods. These are either specified directly (for certain organs like the spinal canal, which is segmented by region growing), or indirectly by inheritance from the reference objects by the relationship **isA**. Depending on the chosen segmentation method, the reference objects are found. The functionality of the plan solver is illustrated by two example requests: *Find Lamina* and *Find Spinal Canal.* The first object *Lamina* does not have its own dedicated segmentation methods so Lamina is found by the inheritance structure based on the link **isA**. *Lamina* **isA***Spine* which also does not have its own dedicated segmentation method. Finally, *Lamina* **isA** *Bone* which has a thresholding segmentation method attached. As *Lamina* is connected by the link **isA** to *bone* via *Spine*, *Lamina* is segmented by thresholding. The inference mechanism proceeds by looking for the objects linked to *Lamina* by the relation *isInside.* The only object where *Lamina* is inside, is the body (body contour), which this way becomes reference object for *Lamina.* So the task *Find Lamina* has as sub-tasks: *Find Body Contour* and *thresholding*, the latter takes place only inside the *Spine.*

In the second example, *Find Spinal Canal*, a dedicated segmentation method is specified: region based segmentation. So we are looking for the objects which could give us a starting point for the region growing algorithm. Thus we are looking for the objects connected with relationships **isNeigbor**, **isAtVerticalAxis**, which are *Body Contour* and *Lamina. Body contour* has its own segmentation scheme, which is why it is reference object for the *Spinal Canal.* The *Lamina*, as it is presented earlier, has as reference object *Body Contour*, which does not involve the *Spinal Canal*. So the *Lamina* is the second sub-task for the task *Find Spinal Canal*.

The algorithm 1 connects the image processing part with the knowledge-base, using the task oriented architecture (presented in the figure 5.3).

Algorithm 1 IdentifyStructureUsingASM

Require: the structure X to be found
Ensure: the contour of the structure X

Search X in the list with the anatomical structures represented in ASM
if X **not** $found$ **then**
  $exit$ **with** $failure$
else
  if SegmentationType(X)= *RegionBased* **then**
    RefObjList $\leftarrow$ *Structures Connected* **by isNeighbor, isVerticalAxis**
  else
    /* *Threshold method for segmentation* */**RefObjList** $\leftarrow$ *Structures Connected* **by isAtLeft, isAtRight, isInside, isSurrounded**
  end if
  for $\forall X_i \in RefObjList$ **do**
    IdentifyStructureUsingASM(X_i)
  end for
  Segment X *using* $X_i \in RefObjList$
  return X
end if

The general schema is presented in 5.3.

4.4 The use of snakes

In the cases where the general schema fails, because the spinal canal is not completely surrounded by bone, the system uses a snake based method. Snakes were introduced in the literature by Kass [60], and formulated as an energy-minimizing spline. Given the spline $v(s) = (x(s), y(s))$, he defined the energy function:

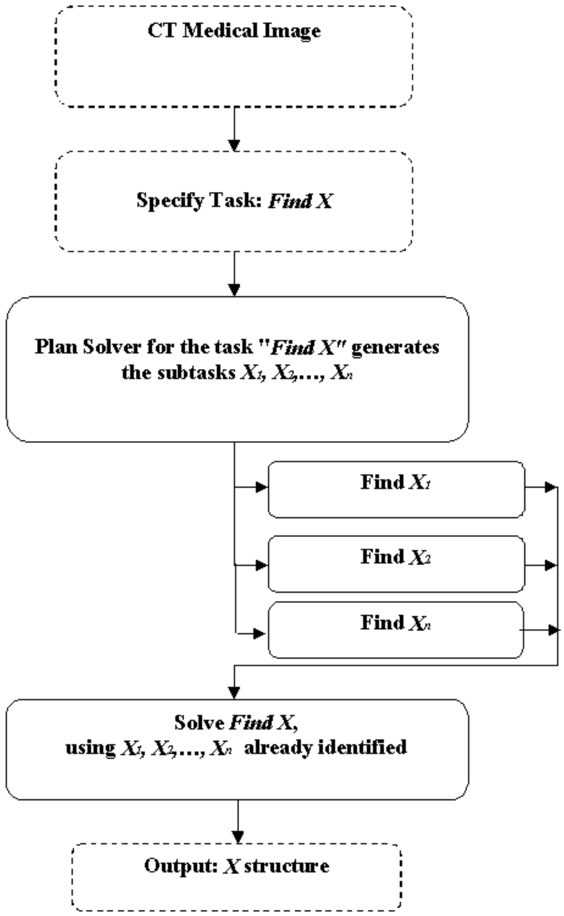

Figure 4.4: Plan for a task: General Architecture. Different sub-tasks are executed to solve the original task.

$$E_{total} = \int_0^1 E_{int}(v(s)) + E_{image}(v(s)) + E_{con}(v(s))\, ds \tag{4.1}$$

where E_{int} represents the internal energy of the spline, composed of a first-order term controlled by $\alpha(s)$, which makes the snake act like a membrane, and the second-order term controlled by $\beta(s)$, making the snake to act like a thin plate.

$$E_{int} = (\alpha(s)|v_s(s)|^2 + \beta(s)|v_{ss}(s)|^2)/2 \tag{4.2}$$

E_{image} is given by:

$$E_{image} = -|\nabla I(x, y)|^2 \tag{4.3}$$

so that the snake is attracted by the contours with large gradients. Finally E_{con} gives rise to the external constraint forces given by the user.

The problem of initialization of the snake is solved by using the result obtained in the previous slice. The specific of the spinal cord shape implies the use of control points and intervals on which we use different coefficients. The curvature estimation plays an essential role.

To approximate the curvature, the finite difference are used. If $v_i(x_i, y_i)$ is a point on the contour, the following approximations are used:

$\left|\frac{dv_i}{ds}\right|^2 \approx |v_i - v_{i-1}|^2 = (x_i - x_{i-1})^2 + (y_i - y_{i-1})^2$

and

$\left|\frac{d^2 v_i}{ds^2}\right| \approx |v_{i-1} - 2v_i + v_{i+1}|^2 = (x_{i-1} - 2x_i + x_{i+1})^2 + (y_{i-1} - 2y_i + y_{i+1})^2$

In respect to these considerations we choose a Greedy strategy as in [122]. The main algorithm is the algorithm 2. The input consists in the set of points which represent the contour to be modified. It improves the quality of the contour using

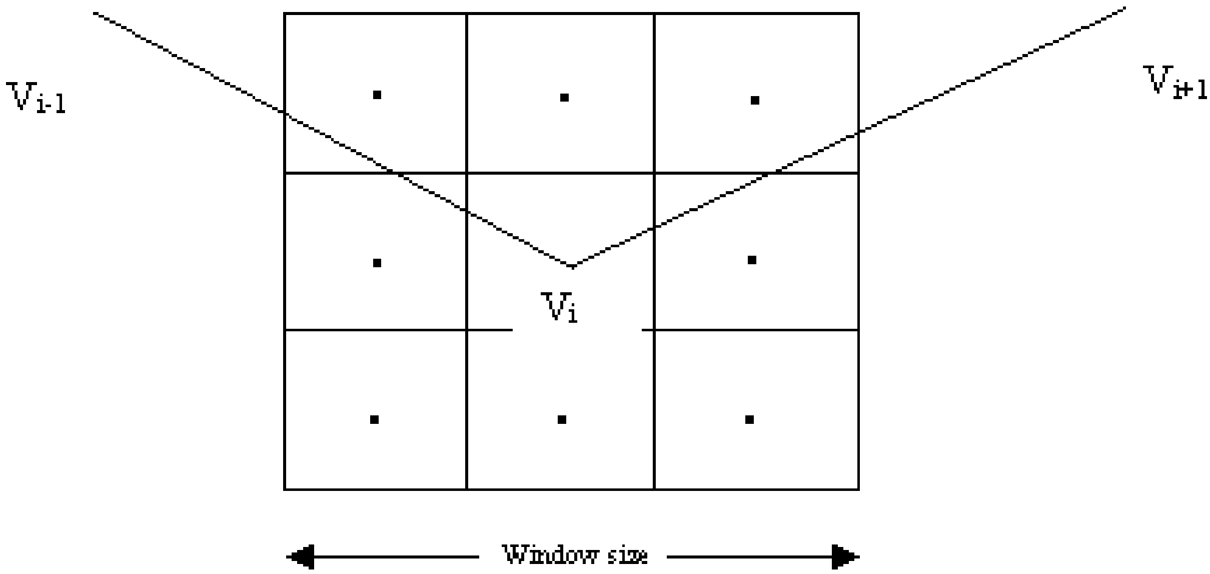

Figure 4.5: Modifying a point on the snake. The new position is obtained by a search in a neighbor window where the energy function is optimal, according to the Greedy strategy.

Algorithm 2 Snake general

Require: Image I, snakes parameters α, γ, window size w, contour v, $nrPoints$
Ensure: the contour v modified

$G \leftarrow$ **ComputeGradient(I)**
$\forall i = 1, nrPoints\ \beta(i) \leftarrow 1$
$finish \leftarrow false$
while NOT $finish$ **do**
    for $i = 1$ **to** $nrPoints$ **do**
        ModifyPoint(i, newX, newY,α, γ,β, w **)**
        $v(i) \leftarrow (newX, newY)$
        Evaluateβ**()**
    end for
    if ConditionsFinishOk() then
        $finish \leftarrow true$
    end if
end while
return v

intensity properties of the image. For every point the optimum position referring to the energy function, in a neighborhood is searched. The algorithm stops when either a number of iterations is done, either when the number of points positions changed is small. After every iteration, the β coefficients (which control the curvature term in the energy function) are computed to detect the corners.
To find the optimum position for a point in its neighborhood, algorithm 3 is used. In each surrounding point the energy function is approximated. The point where the energy is minimal, is chosen (see Figure 4.5), as the new position for the i^{th} point.

Of course, a number of initial parameters for the snakes need to be specified, which will control the behavior of the snake. Depending on the shape of the object to be detected the parameters settings have to be optimezed. A bias variance trade-off has to be made. This is done by tuning the parameters α, β, γ in the energy function for each structure which use snakes as a segmentation method. For the case of the spinal canal, the shape is not complicated and that is why the external energy given by the image gradient properties decides more about the final snake contour. Contrary as it is the case for more complicated in shape organs, the internal energy has an important role by adjusting the α and β coefficients, so the snake becomes more flexible.

4.5 3D Processing

Our approach is based on 2D processing in each slice of a CT scanner. It uses local information found in the current slice, and/or information from adjacent slices. The 3D structures are reconstructed from series of contours thus obtained in slices. This way is similar to the method used now by radiotherapists and radiologists to perform the radiation therapy planning. They detect the first slice where the anatomical

Algorithm 3 Modify a point on the snake

Require: Image I, the image gradient G, point i to be modified, snakes parameters α, β, γ, window size, contour v, nrPoints

Ensure: newX and newY for the i^{th} point

```
maxE_cont ← ComputeEcontMax(i, window)
maxE_curv ← ComputeEcurvMax(i, window)
maxGradient ← ComputeMaxGradient(i, window)
distance ← 1/nrPoints Σ_j ||v_j − v_{j+1}||
newX ← 0
newY ← 0
minE_total ← BIG_VALUE
for ∀ (k, l) ∈ windowXwindow do
    E_cont(i, k, l) ← |distance − ||v_i, I(k, l)||| / maxE_cont
    E_curv(i, k, l) ← ComputeCurvature(v_i, k, l)
    E_curv(i, k, l) ← E_curv(i, k, l) / maxE_curv
    E_image(i, k, l) ← −G(i, k, l)
    E_total ← α · E_cont(i, k, l) + β(i) · E_curv(i, k, l) + γ · E_image(i, k, l)
    if E_total < minE_total then
        newX ← k
        newY ← l
        minE_total ← E_total
    end if
end for
return newX and newY
```

structure of interest can be precisely identified. Than, they are navigating through the slices to delimitate the organ of interest, using the contours and information from adjacent slices. The algorithm we used is presented in 4. Let X the object to be determined. First we try to find the first contour of the object X in the medical exam. In this purpose we use a $2D$ general procedure based on ASM and PFT presented in 1. This procedure is used in all the slices until the contour found is reported to be correctly identified. This role of deciding either or not a contour is correctly identified, is played by the **VerifyCandidate** procedure. For each structure represented in ASM, a procedure is available. It classifies a region segmented as being or not a certain structure. Specific information about the size, intensity, position is used. A rule-based mechanism decides the correctness of identification algorithm. Once a contour is correctly identified in a slice k, the algorithm goes into the slices i, $i = \overline{k-1, 1}$. In a slice i, the contour from the slice $i+1$ is modified using a snake-based algorithm (lines $11-16$). The system continues analysis in the slices based on ASM and PFT (**IdentifyStructureUsingASM**) is used. Another procedure is used to determine if the contour thus segmented in a slice i ($i = \overline{k+1, nrTotalSlices}$) is correct or not. It uses also the contour well obtained in the slice $i-1$. The properties of the contour i should not be too different to the contour $i-1$. Again, when the **IdentifyStructureUsingASM** procedure fails, the snakes algorithm is used.

Depending on the type of structure shape, the snakes algorithms may do not always have a good performance. Finding the best energy parameters (the bias variance trade-off) is not obvious for very complicated shapes. That is why the contours obtained using the general scheme based on ASM are better than ones which are obtained using snakes. So, the first procedure is preferred to the second one. This is the order in which they are applied. The second method is used just in the cases where the first one fails.

Algorithm 4 Structure X 3D Identification

Require: medical exam 3D, nrTotalSlices
Ensure: the list with X contour identified in all the slices of the exam, $ListXContours$

SetActiveSlice(1)
$XC \leftarrow$ **IdentifyStructureUsingASM(X)**
$k \leftarrow 1$
while NOT VerifyCandidat(X) do
    $k \leftarrow k + 1$
    SetActiveSlice(k)
    $XC \leftarrow$ **IdentifyStructureUsingASM(X)**
end while
/**in the slice k, X is identified**/
$ListXContours(k) \leftarrow XC$
for $j = k - 1$ **to** 1 **do**
    SetActiveSlice(j)
    $XCNew \leftarrow$ **ModifyUsingSnake** (XC)
    $XC \leftarrow XCNew$
    $ListXContours(j) \leftarrow XC$
end for
$XC \leftarrow ListXContours(k)$
for $i = k + 1$ **to** $nrTotalSlices$ **do**
    SetActiveSlice(i)
    $XCNew \leftarrow$ **IdentifyStructureUsingASM(X)**
    if NOT VerifyCandidat$(X, XC, XCNew)$ **then**
        /**X not corectly identified with ASM, so use snakes**/
        $XCNew \leftarrow$ **ModifyUsingSnake** (XC)
    end if
    $XC \leftarrow XCNew$
    $ListXContours(i) \leftarrow XC$
end for

4.6 Implementing the ASM

The prototype we developed is implemented in C/C++. We adopt this solution because we need to obtain an unitary code, flexible and modular, object oriented, extensible, and easy to transform the prototype developed in this thesis into software packet which could be used as *Computer Aided Diagnostic* tool. Of course, we had to address the problem of the *AI* inference mechanism which is easier to use in *Lisp* [45, 49].

The *UML* classes diagram is presented in 4.6. The structures together with their relationships are represented as a graph oriented. Every structure has a segmentation type associated or his own scheme (as the case for *thorax contour*). Depending on it, different sub-tasks are performed, which just means that some of their neighbors might be also identified, which is a search of neighbors in the graph representation. A simple language describing *ASM* was created.

4.7 Materials used

The experimental data consists in 23 patient cases obtained with a Picker CT medical scanner. The slice thickness is 3 mm, and the interslice distance is 3 mm. The data was provided by *La Chaux de Fonds* Hospital (Switzerland). They also helped with the clinical interpretation of these images. The dataset contains images of patients of both gender (14 females and 9 males). Patients of different ages are also included (37-79 years). The minimum number of slices in a medical exam is 9 and maximum is 27. See the table 4.7 for more details, about the data we used. There is no clear delimitation of the dataset for learning (tuning the parameters in ASM) and the test dataset. This is due to the way the images have been obtained, in multiple sessions.

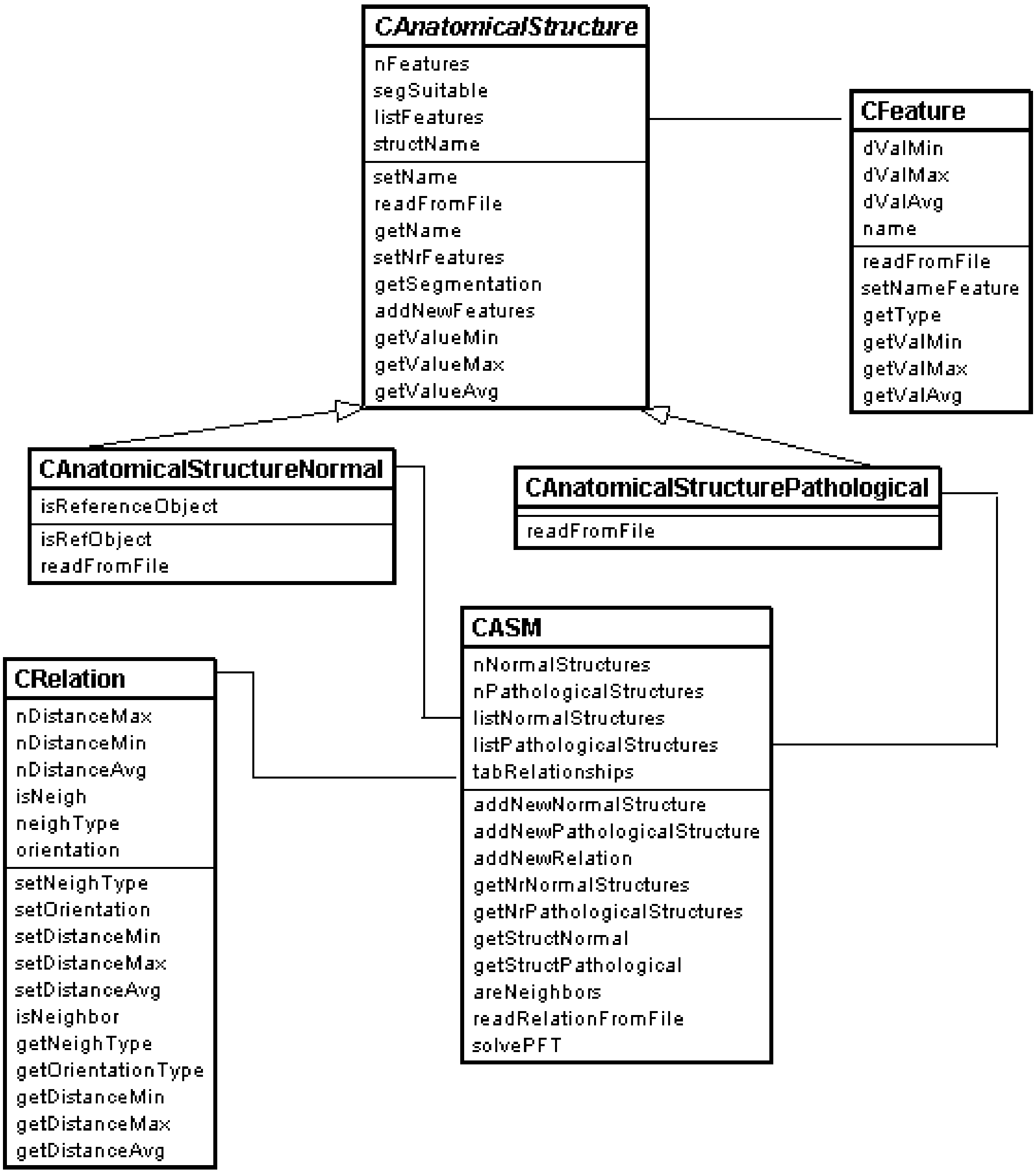

Figure 4.6: UML scheme, representing classes with the implementation of the Anatomical Structures Map

The training step was performed using the first seven CT scans listed in table 4.7. Then when all the other images were available, the algorithms developed were tested on all the 23 patients (the first seven patients included). This may be a limitation of the methodology used. We evaluated our approach according to two criteria: *accuracy* and *computational cost*. The accuracy is defined as the relative number of acceptable contours of a particular type that can be identified in an exam. The computational cost is the total execution time (in seconds) required to find all contours of a particular type in an exam (one contour per slice). Whereas the computational time is straightforward to compute, medical expertise is needed to assess the contours that were found by our system. A radiologist skilled in radiotherapy planning was asked to accept or reject each contour in each slice among all patients. In our case, evaluation was performed using a visual inspection of the contours projected on the CT image slices. The radiologist decides for each of the contours obtained with our system whether it is located precisely or not.

4.8 Problems solved

Two classes of problems has been solved using this approach. First one is identification of organs at risk (see previous chapter). We focused on spinal cord segmentation, one of the most common tasks performed in the oncology departments. Very few work have been done for its automatic segmentation [27], and at the time when the thesis started it was an unsolved problem. At our knowledge, the solution offered here, is one of the few existent. The second class of problems we solved, is the detection of **Gross Tumor Volume** (*GVT* see previous chapter). In our case, lungs have been choose for study because of the large number of patients having lung cancer.

Medical Exam ID	**No. of Slices**	**Age (years)**	**Sex**
Exam 1	37	68	F
Exam 2	87	60	M
Exam 3	27	58	F
Exam 4	70	62	M
Exam 5	87	59	F
Exam 6	15	61	M
Exam 7	31	50	F
Exam 8	9	54	F
Exam 9	22	51	F
Exam 10	97	53	F
Exam 11	38	48	F
Exam 12	22	68	F
Exam 13	20	52	F
Exam 14	75	63	M
Exam 15	22	66	F
Exam 16	50	37	F
Exam 17	18	43	F
Exam 18	55	62	M
Exam 19	83	70	M
Exam 20	45	64	M
Exam 21	40	56	F
Exam 22	44	79	M
Exam 23	37	55	M

Figure 4.7: The clinical cases in form of CT images used to test the algorithms presented in this thesis

Lung tumors detection on CT images is in the last years an active field. Most of the methods focus on nodules detection. Method developed here goes further and another type of metastases, situated at the lung borders is also detected. In figure 4.8, the contouring problems solved in this thesis are illustrated. Also some sub-problems have been solved: thorax, lamina, spinal canal, lungs, ribs segmentation.

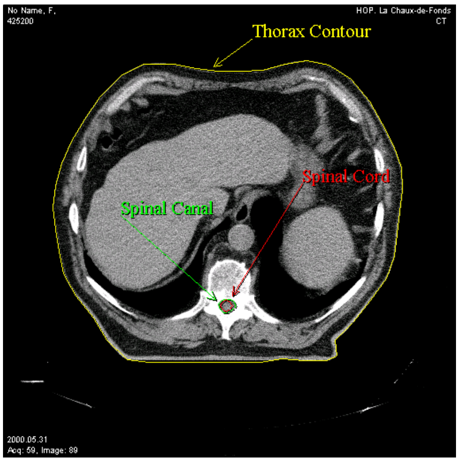

a

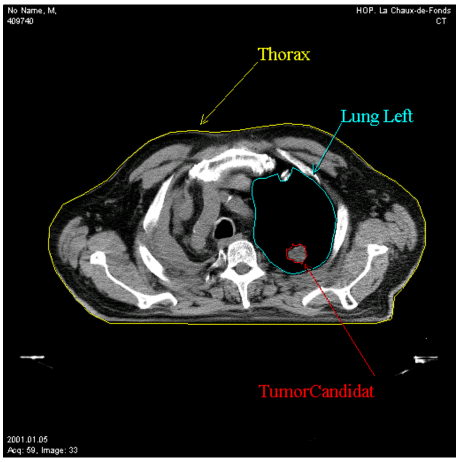

b

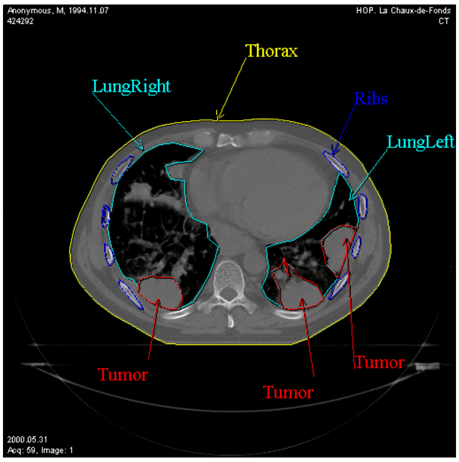

c

Figure 4.8: Contours of the detected structures by the approach. a. The spinal cord contour. b. The lung left together with a nodule. c. tumors detected at the lungs extremities.

Chapter 5

Spinal Cord Segmentation

In this chapter the developed method for automatic spinal cord segmentation is presented. The techniques introduced in the previous chapter are applied here to solve this particular problem. Meanwhile some other sub-problems are solved (like *spinal canal* or *lamina segmentation*). The way the algorithm is working for 3D identification of normal structures is presented. The chapter starts with a brief introduction, followed by anatomical considerations and the CT imaging of the spinal cord. Than, the algorithms used for 3D identification of spinal cord are presented. The chapter ends with experiments performed on real clinical image data and with some conclusions about the method introduced.

5.1 Introduction

The purpose of radiation therapy is to eradicate the tumor while minimizing the damage cause to the surrounding healthy tissues. The spinal cord is an extremely radiosensitive, vital organ which should be spared as much as possible. A certain amount of exposure to radiation can induce a number of undesired neurological complications in the spinal cord (paralysis) [13, 51, 72]. The risk of such serious complications implies much smaller dosage tolerances for the spinal cord than for the tumor. Successful radiotherapy relies on an precise planning and a thorough implementation of the radiation procedure. The problem of radiotherapy planning which is addressed here, requires that the different tissues of interest, including the tumor and the surrounding (vital) organs, be located with a high accuracy. The current planning procedure entails manual delineation of the spinal cord in each separate slice followed by an automatic reconstruction performed by the image analysis workstation that is connected with the CT-scanning device. Despite the existence of several semi-automatic approaches for planning of repetitive radiotherapy [19, 43], automatic identification of the spinal cord remains an unresolved problem. Being now performed manually, it is a very consuming time process. The goal, was to introduce a computer-based automatically method more efficient and faster than the one which is used now in the hospitals. A factor that complicates the analysis further is the occasional presence of the spine around the spinal canal (Fig. 5.2).

5.2 Spinal Cord 3D Identification

For spinal cord, the occasional presence of spine around the spinal canal complicates the delineation of its contour. The same $2D$ identification scheme cannot be used in all the slices. In this section, we first present the 2D segmentation of spinal cord, which is based on the anatomical structures map and the plan solver applied to the slices in which the spinal canal is completely surrounded by spine. Subsequently, the procedure responsible for identification of the 3D spinal canal contour segmentation process is described. Finally, the methods used in the case of failure of the standard procedures method (in the slices where the spinal canal is not surrounded by spine)

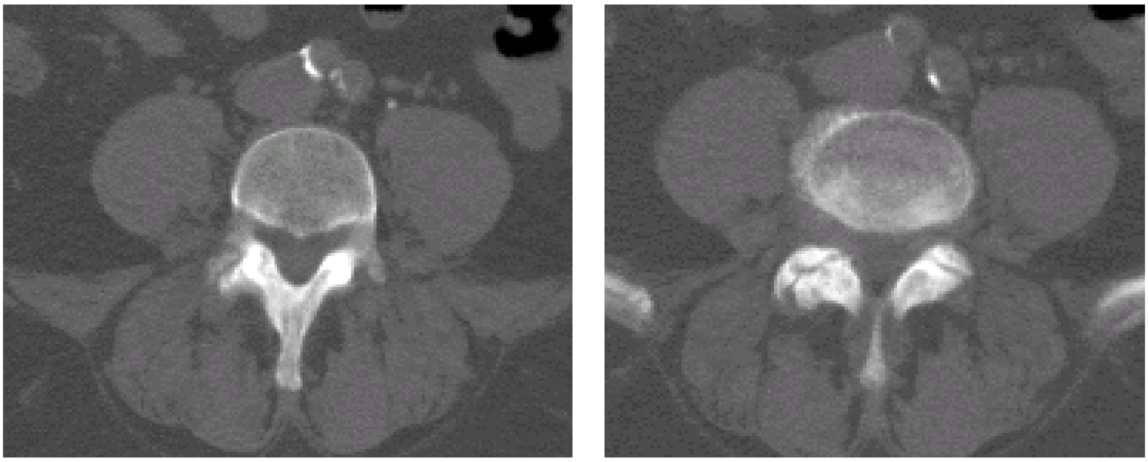

Figure 5.1: The two types of slices: **a** spinal canal completely surrounded by bone. **b** spinal canal partially surrounded by bone

are presented (e.g., snakes).

5.2.1 2D Spinal Cord identification based on the ASM

For the task of identifying the spinal cord contour in a slice, the *Plan Solver* is dispatched. Its sub-tasks rely on information from the *Anatomical Structures Map*. Fig. 5.3 illustrates how the spinal cord is being identified by our knowledge-based approach. The structures that aid the identification of the spinal cord are body contour, a region of the *spine* (called *lamina*), and the *spinal canal* (see also Fig. 6.2).

Body Contour Identification

The transition between the body (contour 1 in Fig. 6.2) and the outside air is very strong, which makes it rather straight-forward to find the contour around the thorax. Moreover, the body is generally the only object in the image. The pixels with a gradient exceeding threshold value ε are likely to form part of the border between

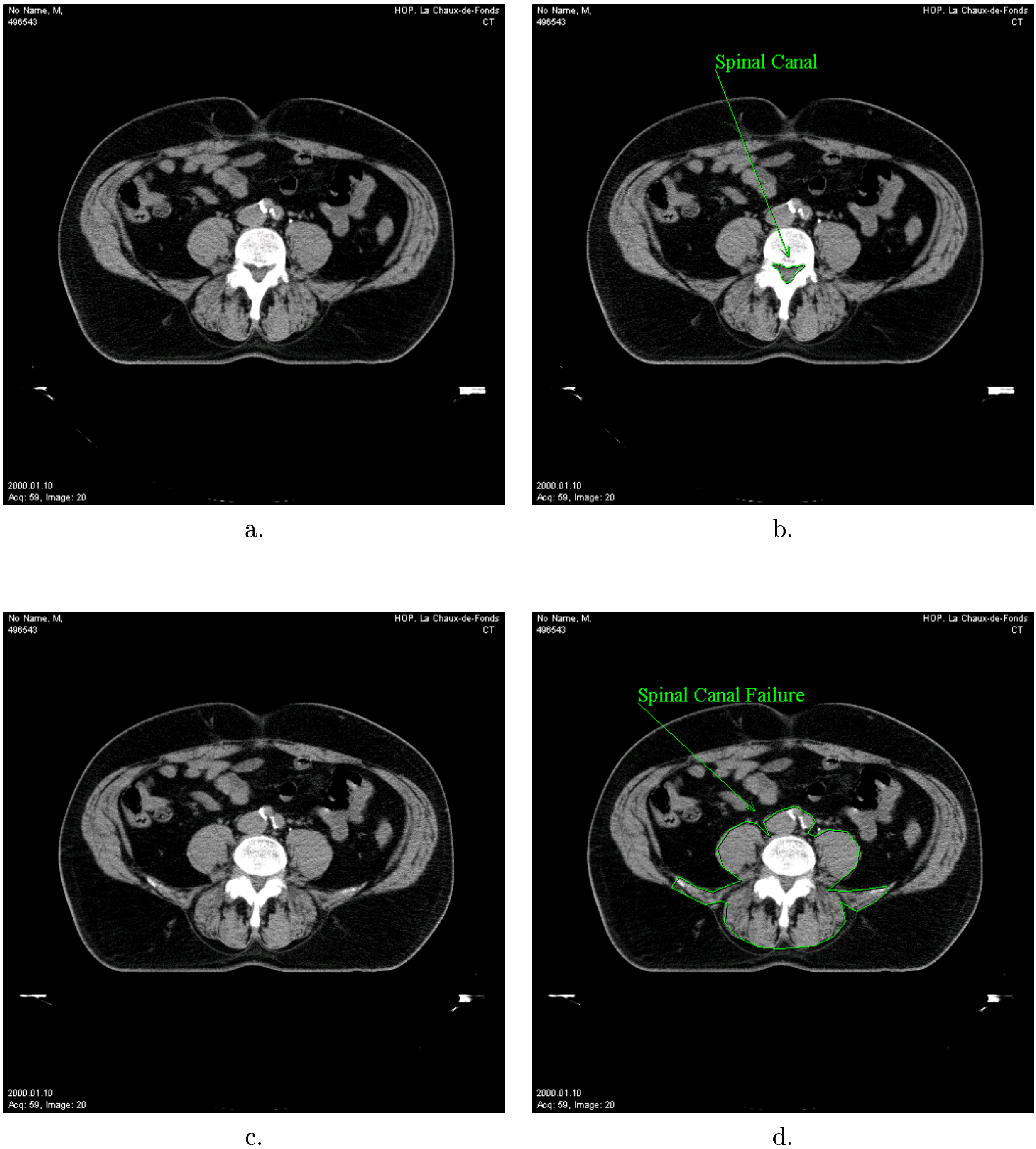

Figure 5.2: The two types of slices: *a*. spinal canal completely surrounded by bone; *b*. the method base on ASM works well for this type of slice; *c*.spinal canal partially surrounded by bone; *d*. the method based on ASM fails for this type of slice.

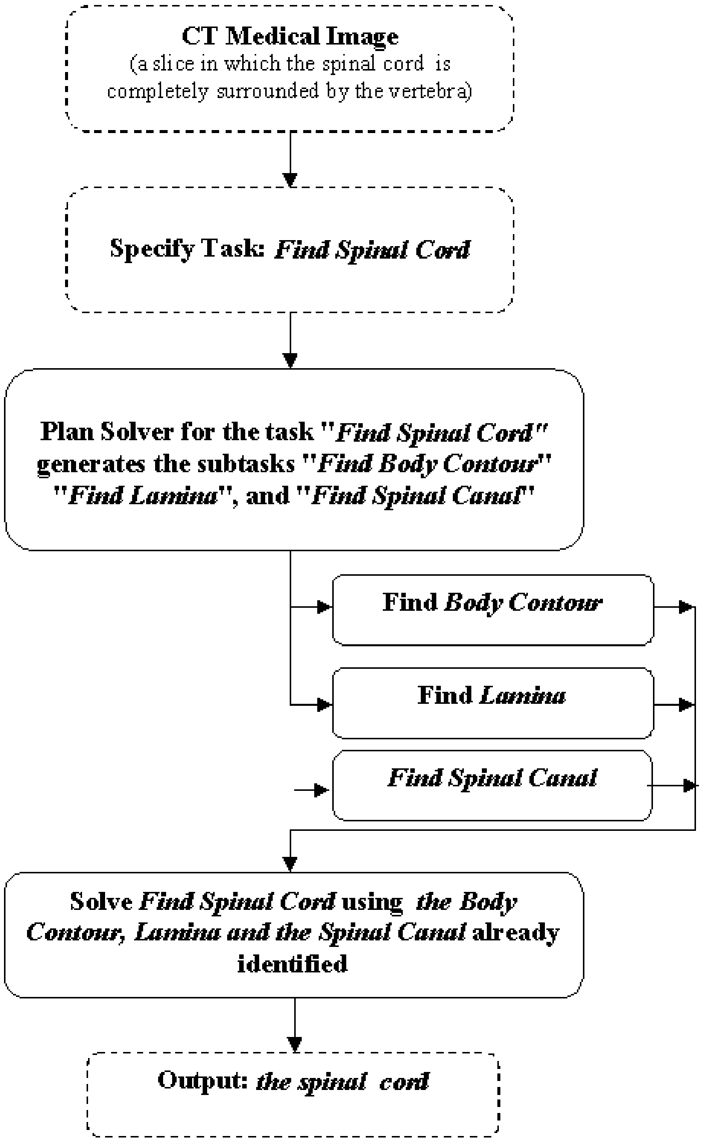

Figure 5.3: Plan for a task: the scheme used for spinal cord segmentation

body and air. Based on correlational analysis of the *HU* histograms of the body and air in a pilot study, the value of ε is found. The algorithm 5 is used to delineate the contour around the body.

Algorithm 5 Body Contour Identification

Require: Image I
Ensure: the abdomen contour

1: compute the gradient of the image using a Sobel-like operator;
2: in the middle column of the image, search the first pixel which has the gradient higher than a threshold ε;
3: this is the first point on the body contour;
4: starting from this point, follow in the clock-wise direction the high gradient, until it reaches the first point of the contour.

Because of its importance (all the other structures are *Inside* the body contour), the body contour identification is a sub-task which is performed for every main task.

Lamina identification

The lamina contour (contour 2 in Fig. 6.2) uses body contour as a reference object. In the ASM, the segmentation scheme associated with the lamina is a threshold operation. The threshold operator is applied to the pixels that occur inside the body contour. The lamina has a very high *HU* range (650-1200 *HU*). This is not the only structure with such a high intensity range. Other structures like the *sternum* and *scapula* might also be segmented by application of a threshold operator. By restricting threshold operator to a smaller region of the abdomen (centered at the medial axis), thresholding in most cases finds the lamina accurately. The algorithm 6 identify *lamina.* The bounding box of the abdomen (($left$, *top*), ($right$, *bottom*)) is used. As the spine is in the middle of the abdomen region and in its inferior half, the threshold

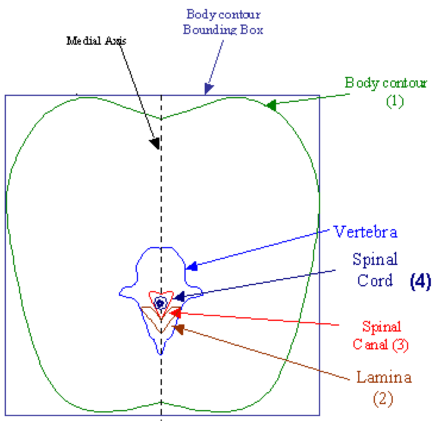

Figure 5.4: Contours identified for spinal cord task. First *Body contour*is identified, than *Lamina*, follow by *Spinal Canal* and finally *Spinal Cord*

.

window is: $((midlleAbdomen - wX, \frac{top+bottom}{2}), (midlleAbdomen + wX, bottom))$. All the pixels having the intensity value in *lamina* range interval, are selected (lines $5-11$). Multiple regions can be found. Those having the area bigger than a minimal threshold and being positioned on the vertical axis of the abdomen are considered as being candidates for *lamina* (lines $12 - 25$. Finally the lowest candidate situated in the abdomen is considered as being lamina, conform to the medical atlases [89] (lines $26 - 30$).

Spinal Canal segmentation in 2D

The contours of the lamina and thorax are used to identify the spinal canal (contour 3 in Fig. 6.2). There is a strong transition from lamina to the spine (large *HU* difference bone−tissue). Consequently, a region growing algorithm is used [4]. Two problems are related to the region growing algorithm. First, the homogeneity of the pixel intensities in the region may not be guaranteed. To cope with this problem,

Algorithm 6 Segment Lamina

Require: Image I, image size N, the abdomen contour

Ensure: $true$, if the lamina contour can be identified and in this case the lamina contour and $false$, otherwise;

$found \leftarrow false$
$R(i,j) = 0, \forall\ i,j = 1 \dots N$
$((left,\ top),\ (right,\ bottom)) \leftarrow$ the bounding box of the abdomen contour
$middleAbdomenX \leftarrow left + \frac{right-left}{2}$
for $i = middleAbdomenX - wX$ to $middleAbdomenX + wX$ **do**
  for $j = \frac{top+bottom}{2}$ to $bottom$ **do**
    if $I(i,j) \in [valMinLamina, valMaxLamina]$ **then**
      $R(i,j) = 1$
    end if
  end for
end for
for $i = middleAbdomenX - wX$ to $middleAbdomenX + wX$ **do**
  for $j = \frac{top+bottom}{2}$ to $bottom$ **do**
    if $R(i,j) = 1$ **then**
      build the contour of the region R_i starting from (i,j)
      $middleCandidate \leftarrow \frac{right(R_i)+left(R_i)}{2}$
      if $air(R_i) > air_\epsilon$ **AND** $|middleCandidate - middleAbdomenX| < \epsilon$ **then**
        add R_i *to the list* L *with candidates for the lamina*
      end if
      for $\forall (k,l) Inside R_i$ **do**
        $R(i,j) = 0$
      end for
    end if
  end for
end for
if $||L|| = 0$ **then**
  $found \leftarrow false$
else
  $found \leftarrow true$
  $LaminaContour = R_i \in L$ with $R_i.Y$ min.
end if
return $found$

a histogram based method [4] is combined with the a priori knowledge about the typical *HU* range of the spinal canal. A pilot experiment has been performed to find the optimal range of HU values (-70 - 110 HU). A second problem is how to set the seed point – the starting point of the region growing algorithm – automatically. This is accomplished by using the relative locations between body contour, lamina and in relation to the spinal canal. More specifically, the spinal canal and the spine have the same medial axis (represented by the relationship **isAtMedialAxis**). So, by identification of *lamina* (which is **isInside** the spine), the position of the seed point is obtained (being on the medial axis and upper than the top limit of *lamina*). The algorithm 7 is used. The seed point is found (lines $7 - 13$), using a smaller window inside the abdomen as search space (at the vertical axis of the abdomen, near *lamina*). The seed pixel intensity value should be in the tissue range. The gradient information is used to detect the border between bone (*lamina*) and tissue (*spinal canal*) which is very high. Finally a region growing algorithm is used.

Spinal Cord segmentation in 2D

The problem of spinal cord segmentation (contour 4 in Fig. 6.2) reduces to finding the maximal inscribed circle in the polygon that represents the spinal canal (see also Fig. 5.2). The problem is solved by computing the medial axis of the polygon using an efficient algorithm (complexity $O(n \ \log \ n)$), which was presented in [52, 70].

5.2.2 Spinal Canal identification in 3D

The problem of 3D spinal canal identification is based directly on procedure for spinal canal identification in 2D presented in Section 5.2.1. However, this scheme cannot be applied successfully to all slices because the spinal canal is notalways surrounded

Algorithm 7 Spinal Canal Segmentation

Require: Image I, the body contour BC, LC the lamina contour
Ensure: $true$, if the SC can be identified and in this case the SC contour and $false$, otherwise;

ComputeGradient G of the image I
$((left, top), (right, bottom)) \leftarrow$ **the bounding box of the** LC
$((la, ta), (ra, ba)) \leftarrow$ **the bounding box of the abdomen**
$XS_i = la + \frac{ra+la}{2}$
$YS_i = \frac{top+bottom}{2}$
$found \leftarrow false$
for $SearchX = XS_i - wX$ **to** $XS_i + wX$ **AND not** $found$ **do**
    for $SearchY = YS_i - wY$ **to** $YS_i + wY$ **AND not** $found$ **do**
        if $I(SearchX, SearchY) \in [valMinSC, valMaxSC]$ **AND** $G(SearchX, SearchY) < \epsilon$ **then**
            $found \leftarrow true$
        end if
    end for
end for
if NOT *found* ***then***
    return *false*
else
    $SCContour \leftarrow \mathbf{StartRG(SearchX, SearchY)}$
    return *true* **AND** $SCContour$
end if

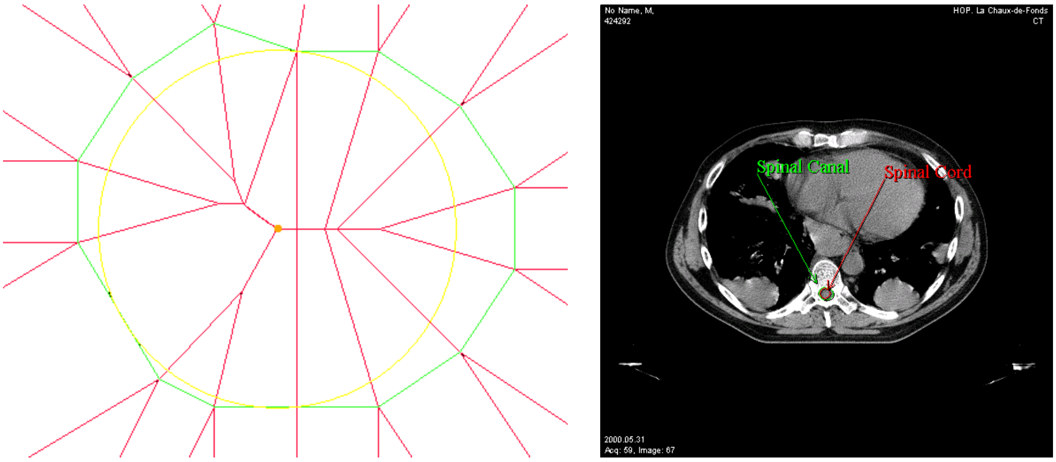

Figure 5.5: Maximum inscribed circle in the spinal canal polygon

by the spine. Instead, the algorithm for 3D spinal canal segmentation first identifies the spinal canal each slice using the algorithm 8. The first step is to apply the 2D algorithm presented in the previous section, to identify the spinal canal in the first slice. It uses no information about whether the spinal canal is surrounded completely by bone. A procedure verifies (line 4) whether the spinal canal was identified correctly. This procedure uses information about the position, the intensity and the area of the region segmented by the 2D algorithm. If the algorithm failed to identify the spinal canal correctly in the first slice, the same 2D algorithm is applied to the next slices (lines 4–8), until it succeeds finding the contour of the spinal canal in as many slices as possible. Once a contour around the spinal canal has been found, the algorithm uses it as reference in neighboring slices in two ways: First it might be used to verify the candidate contour for spinal canal in the adjacent slices (lines 14,28; assuming a small difference between the contours of the spinal canal in two consecutive slices). The second way is to use a spinal canal contour as an information to guide the identification scheme in the adjacent slice (in case the 2D algorithm fails to identify correctly the spinal canal – lines 13,27). These two modalities of using a contour already identified are presented in the next section. In the k'th slice, the contour of the spinal canal is identified (line 10). The 3D algorithm proceeds from the $k-1 \rightarrow 1$ and $k+1 \rightarrow nrTotalSlices$ slices, applying the 2D identification algorithm. In case of failure, it chooses one of the alternative methods presented in the next section. The evolution of the algorithm in two consecutive slices is illustrated in Fig. 5.8.

Two procedures are used to check the results of the spinal cord identification algorithms. In the first slice k where the spinal canal is identified, the procedure *VerifyCandidateSpinalCanal*(SCC) uses the *a priori* knowledge about the spinal canal region: expected *position*, *area*, *intensity* and *shape* (line 4). If these properties of the candidate fall within the predefined rabges in our model, the region is recognized as *spinal canal*, otherwise it is rejected. When at least the spinal canal contour is correctly identified, a second procedure (line 14) *VerifyCandidateSpinalCanal*(SCC, SCCNew) is used to verify the new region candidate. For each of these regions, different features are computed - *area*, *position*, *intensity* and *shape descriptor* resulting in a vector. The Euclidean norm is used to obtain the difference between a candidate for spinal canal vector and the vector of the spinal canal situated in an adjacent slice. Based on this difference, the candidate is accepted or not as being the searched region.

5.2.3 When segmentation scheme of the Spinal Canal fails

The misidentification based on ASM of the spinal canal within one slice is due to the misidentification of one of its reference objects. In the Figure 5.1 the two type of slices have been presented. Still, the region based method works fine the slices where the spinal canal is completely surrounded by the spine, due to gradient high

Algorithm 8 Spinal Canal 3D identification

Require: medical exam 3D, nrTotalSlices

Ensure: the list with spinal canal contour identified in all the slices of the exam, $ListSCContours$

```
SetActiveSlice(1)
SCC ← IdentifySpinalCanalContourUsingASM()
k ← 1
while NOT VerifyCandidateSpinalCanal(SCC) do
    k ← k + 1
    SetActiveSlice(k)
    SCC ← IdentifySpinalCanalContourUsingASM()
end while
/*in the slice k, spinal canal is identified*/
ListSCContours(k) ← SCC
for j = k − 1 to 1 do
    SetActiveSlice(j)
    SCCNew ← IdentifySpinalCanalContour(SCC)
    if NOT VerifyCandidateSpinalCanal(SCC, SCCNew) then
        /*spinal canal not corectly identified so use snakes*/
        SCCNew ← ModifyUsingSnake (SCC)
    end if
    SCC ← SCCNew
    ListSCContours(j) ← SCC
end for
SCC ← ListSCContours(k)
for i = k + 1 to nrTotalSlices do
    SetActiveSlice(i)
    SCCNew ← IdentifySpinalCanalContourUsingASM()
    if NOT VerifyCandidateSpinalCanal(SCCNew,SCC) then
        /*spinal canal not corectly identified with ASM*/
        SCCNew ← IdentifySpinalCanalContour(SCC)
        if NOT VerifyCandidateSpinalCanal(SCC,SCCNew) then
            /*spinal canal not corectly identified so use again snakes*/
            SCCNew ← ModifyUsingSnake (SCC)
        end if
    end if
    SCC ← SCCNew
    ListSCContours(i) ← SCC
end for
return ListSCContours
```

magnitude at its border (the HU difference bone-tissue). This method it will fail in the slices where the spinal canal is not completely surrounded by spine. Meanwhile it gives better results, referring to contour quality than the snakes. That is why this algorithm has a higher priority than the snakes. The snakes are used just in case the region based method fails. Both methods use the (already approved) contour around the spinal canal identified in an adjacent slice as an input parameter.

Finding the Spinal Canal by Region Growing

Occasionally, the general scheme for identification of the spinal canal fails because it cannot identify the *lamina* region, even when the spinal canal is completely surrounded by bone cortex. In these cases, a region based segmentation technique works well and is applied to the slice (lines 13, 27). The problem is to find the seed point for the region growing process. We use the center of gravity of the spinal canal region identified in an adjacent slice, thereby assuming spatial continuity of the spinal canal. To compute the center of gravity of a region given by a function f, the moments are used which are defined for the continue case as:

$$m_{pq} = \int_{-\infty}^{\infty} \int_{-\infty}^{\infty} x^p y^q f(x,y) dx dy \quad with \ p,q = 0,1,2,... \tag{5.1}$$

and for the discret case:

$$m_{pq} = \sum_i \sum_j i^p j^q f(i,j) \quad with \ p,q = 0,1,2,...$$

Thus the center of gravity is defined as:

$$\overline{x} = \frac{m_{10}}{m_{00}} \quad and \ \overline{y} = \frac{m_{01}}{m_{00}}$$

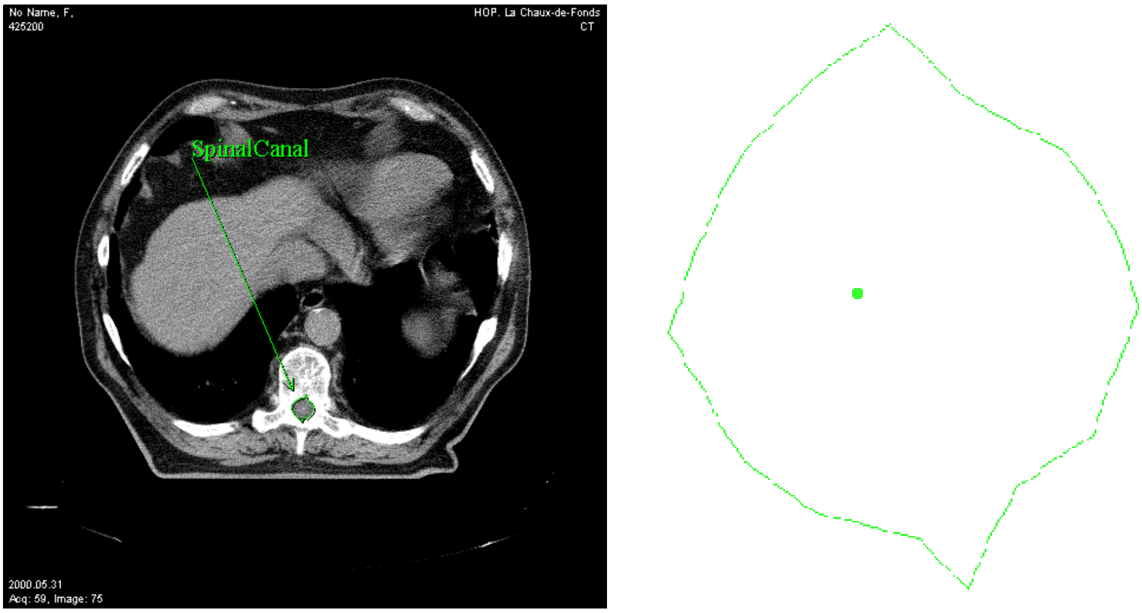

Figure 5.6: The spinal cord contour and its gravity center

The use of snakes

In case where the general schema fails to identify the spinal canal, e.g., because the spinal canal is not completely surrounded by spine, the system uses a snake based method [60].

5.3 Experimental results

The knowledge-based approach for spinal cord identification problem is evaluated by applying the system consisting of the *Anatomical Structures Map* and the *Plan Solver* on 3D CT datasets of 23 real patients. After the CT examination, each patient underwent radiotherapy in the hospital. Our population consisted of 9 male and 14 female patients. Their age varied from 37 to 79 years with a mean of 58 years and a median of 59 years. The number of CT slices per exam varied from 9 to 97 with a mean of 45 slices and a median of 38 slices. The images were obtained from a CT scanner from Picker and were acquired with a slice thickness of 3 mm and an inter-slice distance of 3 mm. We distinguished four types of contour: *Spinal cord*, *Spinal canal*, *Lamina* and (outer) *Thorax*. Whereas the computational time is straight-forward to compute, medical expertise is needed to assess the contours that were found by our system. A radiologist skilled in radiotherapy planning was asked to accept or reject each contour in each slice among all 23 patients. In our case, evaluation was performed using a visual inspection of the contours projected on the CT image slices. The radiologist decides for each of the contours obtained with our system whether it is acceptable or not.

5.3.1 Accuracy

In table 7.1, results of the experiments on the real clinical data are shown. The accuracy is defined as the number of slices in the exam in which the particular type of contour was located correctly. In Exam 1, for example, 91.8% of the contours were located around the spinal cord with a sufficient accuracy. The average accuracy of the spinal cord contours among all patients is 91.7%, the average accuracy per slice lies within the range 80% to 100%. The spinal canal is more difficult to identify. The average identification accuracy among all patients is 85.3%, the average accuracy per slice lies within the range 60% to 100%. The lamina is the most difficult structure to identify for our approach. The average accuracy among the 23 patients is 72.1% and the range is 33% – 100%. The thorax is correctly located in all slices among all 23 patients. The body is easy to segment because of the sharp transition from the surrounding air to human tissue. Among these four structures, the accuracy of each contour is rather correlated for the spinal canal and spinal cord, 0.594, the correlation coefficients between the other types of contours are all below 0.15. The results presented in the Figure 7.1 reflect the validation of the spinal cord segmentation module. As explained in the previous section, different other structures are also identified (reference objects). That is why even if for some cases the accuracy is very low (e.g. lamina), still the accuracy of the spinal cord is high, due to the 3D identification process. Failure within a slice of a reference object identification, does not mean that the whole identification step is compromised. An alternative method is just used, together with a contour correctly identified in an adjacent slice. This capability of failure response is one of the qualities of our approach. The ideal case is when the 2D identification schema based on ASM works in every slice of the CT scan. Identifying correctly the thorax contour in all the slices helps it further during the segmentation process. For a good approximation of the spinal cord, the spinal canal identification is crucial. Due to the nature of this approximation (by the use of MIC), there are cases when the spinal cord accuracy is higher than the spinal canal ones. The explanation is very simple: some false positive spinal canal detections, will not affect the geometrical problem of finding the maximum inscribed circle in a polygon. In general, when contours were identified wrongly, the major cause was the mislabeling of the neighboring *reference objects* such as the spinal canal. The problems in most cases arise in CT exams where the standard acquisition protocol had not been followed such that one or more unexpected objects (e.g., arms) were present in the slice. The presence of such objects affects the symmetry of the body. This is one of the weaknesses of a frame-based representation of anatomical knowledge.

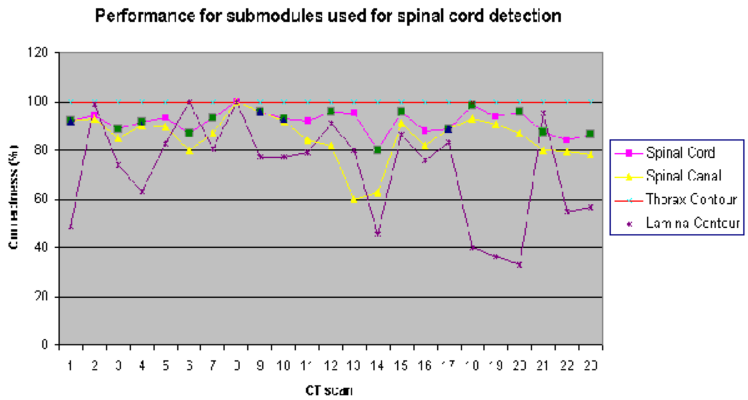

Figure 5.7: Graphical performance of the algorithms involved in spinal cord identification

5.3.2 Computational cost

Our algorithms are implemented on a PC Windows machine, with processor Pentium III 500 MHz, 512 MB RAM. As presented in the table 7.1, the spinal cord identification is done practically in real time. The worst case is when the snakes are used in all the slices. The interactivity is minimum and might consists just in human correction of the errors in a couple of slices. In the *Anatomic Structures Map*, about 10 different structures are represented so the query process performed by the *Plan Solver* terminates quickly. The most time consuming routine is the Snake algorithm which optimizes the location of the contour by minimizing the total energy. All other routines are performed in less than a second per slice ($0.3 - 0.5$ seconds) in our current application. The snake algorithm is only applied to slices where the spinal cord is not surrounded by the spinal canal, which boils down to about half of the slices.

Medical Exam ID	**No. of Slices**	**Age (years)**	**Sex**	**Sp. Cord**		**Sp. Canal**		**Lamina**		**Thorax**	
				Succ.	*Texec*	*Succ.*	*Texec*	*Succ.*	*Texec*	*Succ.*	*Texec*
Exam 1	37	68	F	91.9%	65s	91.89%	62s	48.64%	42s	100%	34s
Exam 2	87	60	M	94.26%	153s	93.10%	148s	98.85%	92s	100%	73s
Exam 3	27	58	F	88.89%	40s	85.18%	39s	74.07%	25s	100%	18s
Exam 4	70	62	M	91.43%	108s	90%	105s	62.85%	68s	100%	52s
Exam 5	87	59	F	93.11%	177s	89.65%	173s	82.75%	112s	100%	90s
Exam 6	15	61	M	86.7%	31s	80%	30s	100%	16s	100%	13s
Exam 7	31	50	F	93.55%	62s	87.09%	59s	80.64%	25s	100%	18s
Exam 8	9	54	F	100%	12s	100%	12s	100%	7s	100%	5s
Exam 9	22	51	F	95.45%	55s	95.45%	55s	77.27%	17s	100%	13s
Exam 10	97	53	F	92.78%	135s	91.75%	132s	77.31%	83s	100%	61s
Exam 11	38	48	F	92.10%	61s	84.21%	57s	78.94%	38s	100%	32s
Exam 12	22	68	F	95.45%	34s	81.81%	33s	90.90%	18s	100%	14s
Exam 13	20	52	F	95%	38s	60%	38s	80%	16s	100%	11s
Exam 14	75	63	M	80%	125s	62.66%	122s	45.33%	78s	100%	60s
Exam 15	22	66	F	95.45%	35s	90.90%	35s	86.36%	20s	100%	14s
Exam 16	50	37	F	88%	99s	82%	98s	76%	48s	100%	37s
Exam 17	18	43	F	88.88%	28s	88.88%	27s	83.33%	17s	100%	13s
Exam 18	55	62	M	98.18%	94s	92.72%	93s	40%	45s	100%	32s
Exam 19	83	70	M	93.97%	141s	90.36%	139s	36.14%	86s	100%	69s
Exam 20	45	64	M	95.55%	72s	86.67%	70s	33.33%	45s	100%	35s
Exam 21	40	56	F	87.5%	69s	80%	68s	95%	43s	100%	34s
Exam 22	44	79	M	84.09%	77s	79.54%	76s	54.54%	43s	100%	33s
Exam 23	37	55	M	86.48%	66s	78.37%	64s	56.75%	44s	100%	35s

Table 5.1: Experimental results for spinal cord segmentation and the structures involved in solving this task

5.4 Discussion

Radiotherapy of malignant tumors located in the vicinity of the is spinal cord requires a very accurate planning to avoid causing unnecessary damage in this vital organ. The spinal cord is a highly radiosensitive; even moderate doses of radiation can cause different complications such as paralysis of the patient. In this chapter, we present the knowledge-based approach described in the previous chapter for spinal cord segmentation. The approach is based on two closely linked knowledge bases: the *anatomical structures map* and the *plan solver*. The former represents structural (static) knowledge of the macro anatomy in the human thorax. The latter represents the procedural knowledge - the scripts - that are used for identification of the different objects of interest. The plan solver combines atomic and composite image processing operators using an inheritance scheme. Which (composite) operators inherit an atomic operator, say a snake algorithm, is derived from the anatomical structures map, which contains the structural knowledge. The method was implemented on a standard PC. The system was subsequently validated on CT image data from 23 patients who were to undergo radiotherapy. The plan solver was used to locate the following four kinds of objects: the spinal cord, the spinal canal, the lamina and the body (outer thorax). The highest accuracy was obtained for the body, which was located correctly in all slices among the 23 patients. The spinal canal was located with an accuracy of 92%, the spinal canal with an accuracy of 85% and the lamina with an accuracy of 72%.

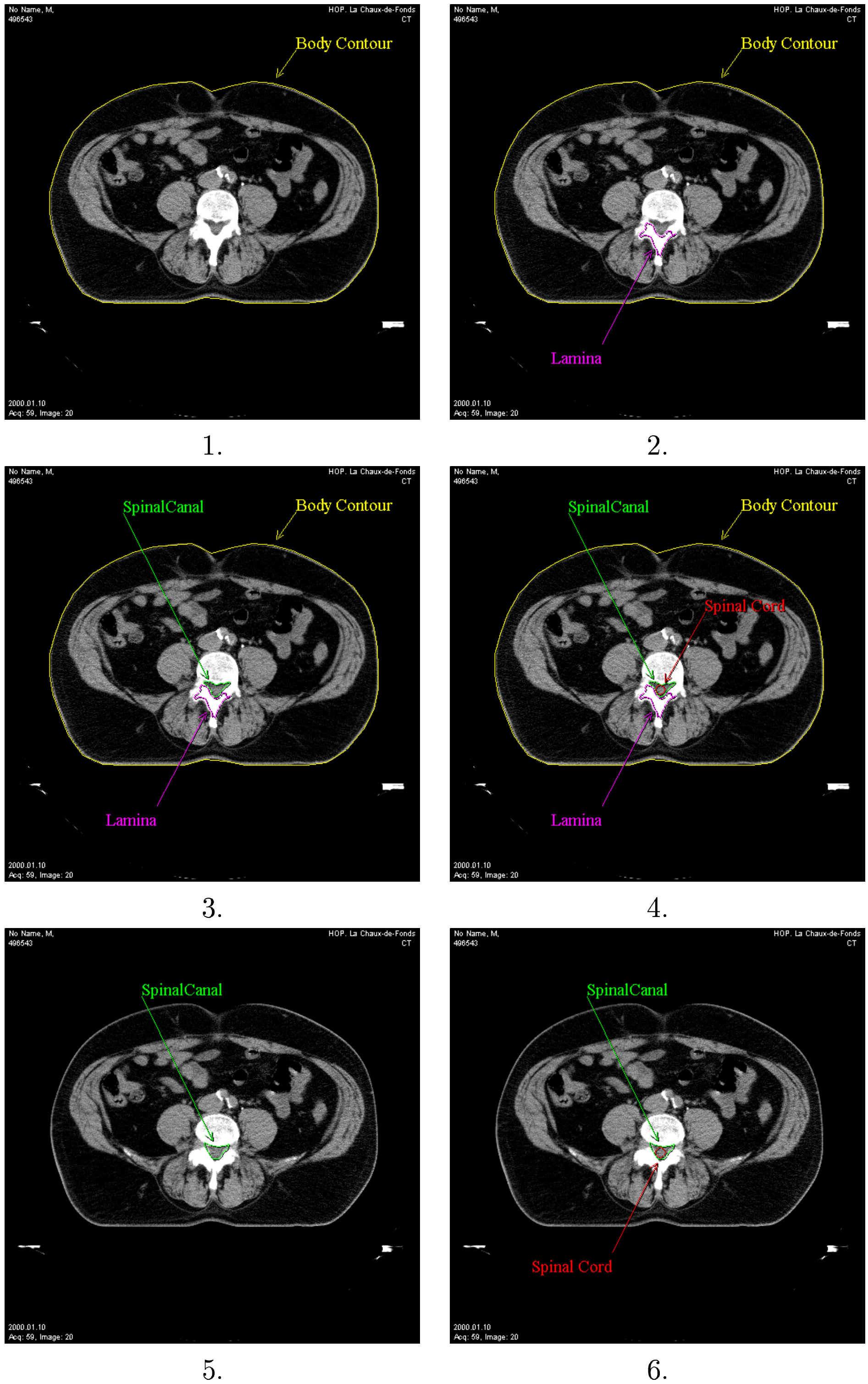

Figure 5.8: The algorithm for spinal cord identification 1. in the first slice identify the body contour 2. find a *spine part* 3. using the bone part identified, find the seed for the Region Growing, which identifies the spinal canal 4. apply MIC to find the spinal cord 5. propagate the spinal canal contour in the next slice and improve it using snakes 6. apply again MIC to find the spinal cord

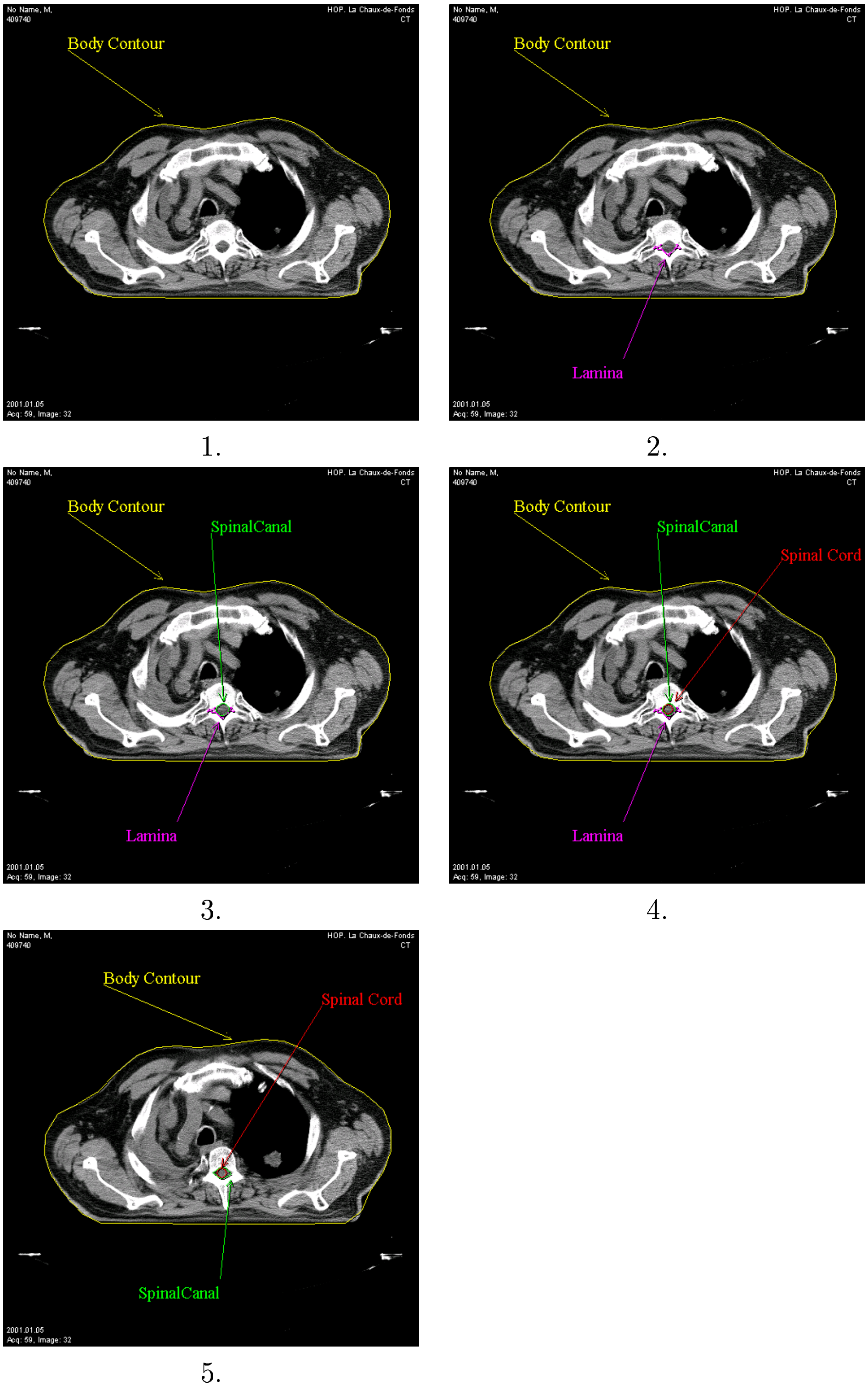

Figure 5.9: The algorithm for spinal cord identification in the case when the images are affected by abnormalities (right lung not visible) 1. in the first slice identify the body contour 2. find a *spine part* 3. using the bone part identified, find the seed for the Region Growing, which identifies the spinal canal 4. apply *MIC* to find the spinal cord 5. The process continues in the next slice.

Chapter 6

Lung Tumor Detection

In this chapter the solution to the problem of lung, lung nodules and lung tumors detection is presented. The method is based on the approach introduced in Chapter 4. The knowledge base in form of ASM and the plan solver PFT are used. Experiments, validating the method are finally presented on 20 patients CT image data set.

6.1 Introduction

Early detection of suspicious metastases is effective to reduce the number of death caused by lung cancer. Although a conventional chest radiogram has been used for the screening of lung cancer, mass screening by helical CT is used with a very good performance for the diagnosis. However numerous scans have to be interpreted by a radiologist for each case. Therefore, development of computer-aided diagnosis system which can assist the radiologists decision is required.

Tumors are heterogeneous lesions that exhibit growth patterns which are unique for each patient. As a consequence, the CT images cannot be acquired according to a standardized protocol but are subject to much inter-patient variation. This rather high amount of variation in our image material impedes the application of a standard low level image processing technique, when radiation therapy planning is performed. That is why the previous general identification method presented in the chapter 4 is used for the detection of **Gross Tumor Volume (GTV)**.

For the $2D$ case, based on the plan solver scheme, and on the information stocked in ASM the task of finding lung metastases is divided in the sub-tasks *find thorax contour*, *find lungs* and *find ribs.* A 3D segmentation algorithm is applied using the general scheme presented previously. Two type of lung tumors are detected: the nodules and the metastases situated at the lung borders.

The chapter is structured as follow: first, the knowledge-based image processing approach is presented, with different types of knowledge that we used. Than lesions detection algorithms are described, including the identification of normal structures (thorax, lungs, ribs) used to segment easily the others. The chapter ends with the experiments performed on 20 patients and the conclusions on the method presented here. The results show that the modules presented in this chapter, could be used with success in an oncology department for *Computer Aided Diagnostic*, for clinical purpose.

6.2 Lung tumor detection

Applying the general procedure presented in the chapter 4, for the task *Find lung metastases*, the scheme obtained in the Fig. 6.1 is obtained. The sub-tasks which should be performed are *Find thorax contour*, *Find lungs*, *Find ribs.* The two types of tumors represented in our knowledge-base ASM, are *the nodules* and *the extremity lung tumors.* The region founded correspond to *Gross Tumor Volume*, the clinical term used in radiotherapy planning (see the Chapter 4). The algorithms for each of the normal structures is further presented.

6.2.1 Lung Contouring

For lungs, a threshold based procedure is used for segmentation. The threshold area should be specified. As the lung **isInside** the thorax, first step is to segment the thorax contour.

Thorax Contour Segmentation

The first contour obtained is the thorax, as all the structures of interest are inside it. The algorithm used is presented in the previous chapter (alg. 5).

2D Lung Segmentation

The lungs (contours 2 on the scheme 6.2) have a typical intensity graphic representation on the CT images, due to their *HU* level.

The algorithm 9 segments the lung right within a slice. For the left lung, a symmetrical algorithm is used. The graphic has the form represented in the Fig. 6.3. Two valleys are presented on the images, representing the two lungs. The gradient value at the lungs border is high. That is why a threshold-based algorithm is used. To restrict the threshold area the thorax contour is identified too (cf. identification scheme Fig 6.1). Due to their position in the abdomen (in the each half of the thorax) which are represented in *ASM* (see the Chapter 4), the area where the threshold algorithm is performed is clear delimited (line 4 in the algorithm 9). The air which fills the lungs, give rise to a low HU values. There are the only objects having these values inside the abdomen. In the slices where the lung contours are not present the threshold operation gets just a small region representing the noise present on the image. Using

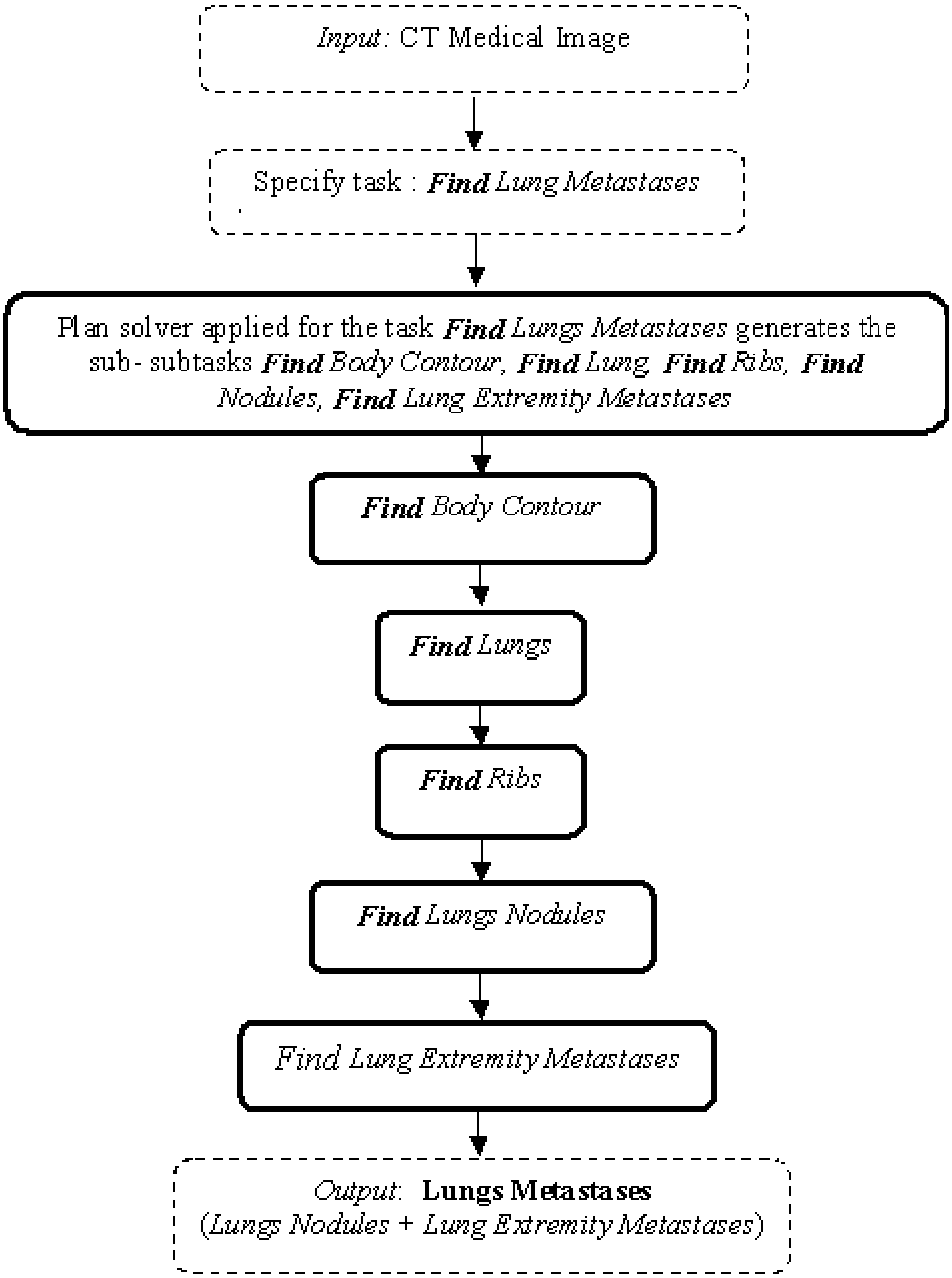

Figure 6.1: General scheme for lung tumor detection task, based on plan solver and anatomical structures map

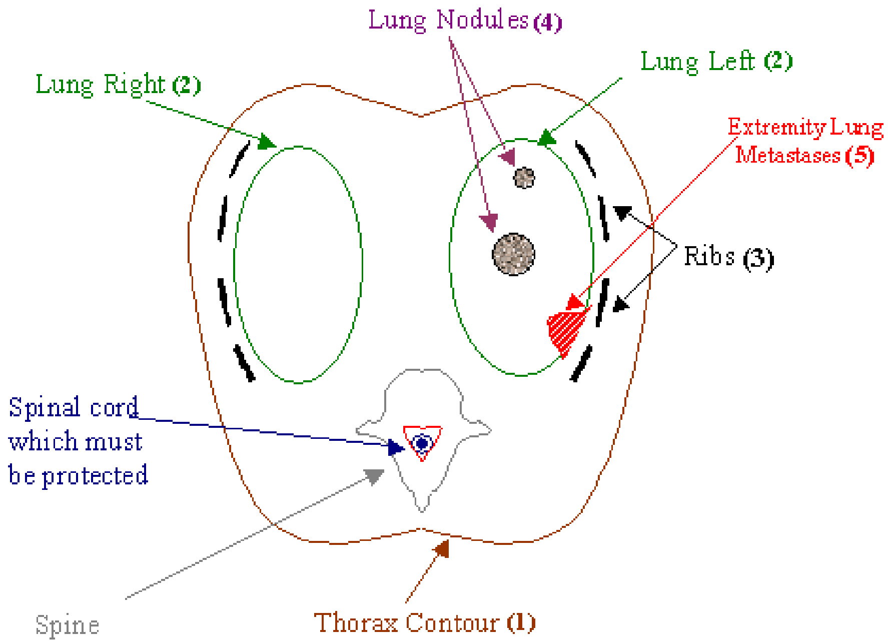

Figure 6.2: Structures involved in lung lesions detection

this information the test in the line 6 is used to decide if the contour found represents the lung or not.

As the right lung **isAtRight** in relationship with the thorax contour, the threshold procedure is performed in the right half of the body region. Its bounding box is used to restrict the area (line 2).

For the slices which do not contain the lung, the results of the threshold will be a small (or empty) region. That is why (line 5) the area size of the candidate is checked.

3D Lung Identification

The identification scheme described in previous section is applied through all the slices of the CT scan. There are slices where this scheme fails. That is why two procedures are used to classify the results of the general scheme based on ASM.

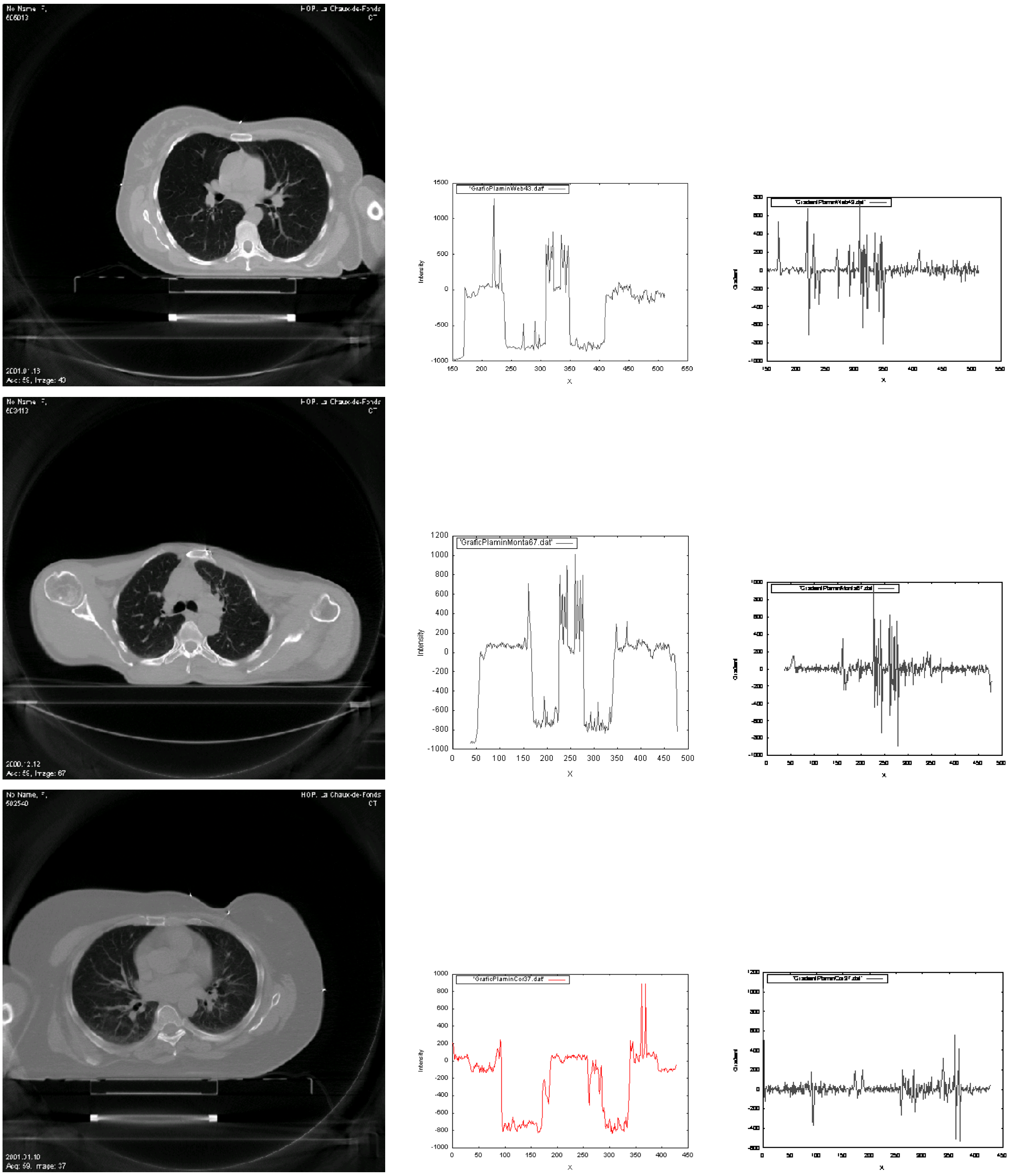

Figure 6.3: Lung intensities graphics. On each of the three images two valleys are present, corresponding to the lungs.

Algorithm 9 Right Lung Identification

Require: Image I and the abdomen contour
Ensure: $true$, if it is possible to segment the right lung and in this case the contour of the right lung and $false$, otherwise
1: compute the image gradient G
2: $((left, top), (right, bottom)) \Leftarrow$ the bounding box of the abdomen contour
3: $middle \Leftarrow \frac{right+left}{2}$
4: $\forall(x, y) \in ((middle,top),(right, bottom))$
5: with $I(x, y) \in [minAbdomenBrightness, maxAbdomenBrightness]$, **add** (x, y) to R_{Lung}
6: **if** $Air(R_{Lung}) > \epsilon_{Aria}$ **then**
7: /*the whole image is not filled, as the threshold area is restricted
8: to the region where the lung is expected to be inside the abdomen */
9: $found \Leftarrow true$
10: **else**
11: $found \Leftarrow false$
12: **end if**
13: **return** $found$

First *VerifyCandidateLung(LungContourCandidate)* (line 5) uses a rule-based system with information about lung represented in ASM - intensity of lungs, standard deviation, the rapport surface lung/surface thorax, position within the thorax (see the algorithm 11). The second one, *VerifyCandidateLung(LungContour, LungContour-Candidate)* (lines 15,24), uses the contour, *LungContour*, obtained in a adjacent slice. The procedure verifies the differences between the two regions concerning morphological and intensity features. In the slices where the scheme based on ASM fails, a snake algorithm is used to improve the contour from an adjacent slice. One point should be noticed here, related to the transfarability of this algorithm to another scanner. The parameter values used to for the rule-based system, are obtained from medical images acquired with the Picker scanner. To transfer the technique into another clinic using a CT scanner produced by another manufacturer, another pilot test needs to

Algorithm 10 Lung 3D identification

```
Require: medical exam 3D, nrTotalSlices
Ensure: the list with lung contour identified in all the slices of the exam, ListLungContours
SetActiveSlice(1)
/*find the first slice k, where the lung contour is correctly identified*/
LC ← 2DLungIdentUsingASM()
k ← 1
while NOT VerifyCandidateLung(LC) do
   k ← k + 1
   SetActiveSlice(k)
   LC ← 2DLungIdentUsingASM()
end while
/*in the slice k, lung contour is identified*/
ListLungContours(k) ← LC
for j = k − 1 to 1 do
   SetActiveSlice(j)
   LCNew ← 2DLungIdentUsingASM(LC)
   if NOT VerifyCandidateLung (LC, LCNew) then
      /*lung not corectly identified so use snakes*/
      LCNew ← ModifyUsingSnake (LC)
   end if
   LC ← LCNew
   ListLungContours(j) ← LC
end for
LC ← ListLungContours(k)
for i = k + 1 to nrTotalSlices do
   SetActiveSlice(i)
   LCNew ← 2DLungIdentUsingASM()
   if NOT VerifyCandidateLung(LC, LCNew) then
      /*lung not corectly identified with the ASM scheme, so use again snakes*/
      LCNew ← ModifyUsingSnake (LC)
   end if
   LC ← LCNew
   ListLungContours(i) ← LC
end for
```

be performed in order to find the right values.

Algorithm 11 Verify Candidate Lung Left

Require: the abdomen contour, the contour of the candidate for lung left R_i
Ensure: $true$, if the contour candidate is the left lung and $false$, otherwise;

$AirCandidate \leftarrow$ *the air of the* R_i
$AirAbdomen \leftarrow$ *the air of the abdomen*
$midlleCandidate \leftarrow \frac{leftCandidate+rightCandidate}{2}$
$midlleAbdomen \leftarrow \frac{leftAbdomen+rightAbdomen}{2}$
$DensityCandidate \leftarrow$ *the average density of the* R_i
if $AirCandidate \leq \frac{AirAbdomen}{2}$ **AND** $midlleCandidate > midlleAbdomen$ **AND** $DensityCandidate \in [valMinLung, valMaxLung]$ **then**
    return true
else
    return false
end if

6.2.2 Ribs Identification

The ribs (contours 3 on the scheme 6.2) are bones structures with a high HU value, and their identification is based on a threshold algorithm. The problem which must be solved is to restrict the region where threshold is performed, to avoid identification of other bones like the stern or the spine. That is why the thorax contour and lungs are used, following the identification scheme generated by the plan solver.

The ribs left identification is presented in the algorithm 12. Let be $(leftThorax, topThorax)$ and $(rightThorax, bottomThorax)$ the thorax bounding box.
We denote by $(leftLung, topLung)$ and $(rightLung, bottomLung)$ the bounding box of the left lung. The area where the threshold is performed is given by $(leftLung + d'_\epsilon(leftLung, rightLung),\ topLung - d''_\epsilon(topLung, topThorax))$ and $(rightLung+d'_\epsilon(leftLung, rightLung), bottomLung+d''_\epsilon(bottomLung, bottomThorax))$.

By d'_ϵ and d''_ϵ are denoted two functions which gives a neighborhood of the lungs, depending on their bounding boxes.

6.2.3 Lungs metastases detection

Two types of lung tumor are represented in the knowledge-base ASM: nodules and metastases situated at lung extremity, like the one presented in the figure 6.5. The identification scheme generated by the plan solver is presented in the figure 6.1. The system has already obtained the thorax contour, the lungs and the ribs in the CT scan. It uses them further for detection of two types of lesions. This gives rise to the algorithm 13.

Nodules Detection

Pulmonary nodules (contour 4 on the scheme 6.2) may be either solitary or multiple. A solitary nodule is one of the most common radiological findings and characterized as single well-defined, round within the lung up to 3 cm in diameter. Among the many diseases which may give rise to multiple nodules, hematogenous pulmonary metastases are the most common cause of multiple nodules. The typical radiological appearance of hematogenous pulmonary metastases is multiple variable sized, round, smooth and well circumscribed.

The intensity graphic of a lung having a nodule inside is represented in figure 6.4. The intensity difference lung - tissue is important. Moreover, lung being already identified, a multi-threshold procedure offers us the 3D candidates for nodules. The algorithm 14 is used.

A number of candidates for tumor regions is obtained. A number of three dimensional nodules features is used to eliminate the false-positive candidates: circularity,

Algorithm 12 Identify Left Ribs

Require: Image I, thorax contour, left lung contour;
Ensure: The list with ribs contours
$R(i,j) = 0, \forall\, i,j = 1 \dots N$
$((leftThorax,\ topThorax),\ (rightThorax,\ bottomThorax)) \Leftarrow$ the bounding box of thorax
$((leftLung,\ topLung),\ (rightLung,\ bottomLung)) \Leftarrow$ the bounding box of the lung left contour
$neighLeftLung \Leftarrow leftLung + d'_{\epsilon}(leftLung, rightLung)$
$neighRightLung \Leftarrow rightLung + d'_{\epsilon}(leftLung, rightLung)$
$neighTopLung \Leftarrow topLung - d''_{\epsilon}(topLung, topThorax)$
$neighBottomLung \Leftarrow rightLung + d'_{\epsilon}(leftLung, rightLung)$
for $i = neighLeftLung$ to $neighRightLung$ **do**
for $j = neighTopLung$ to $neighBottomLung$ **do**
if $I(i,j) \in [valMinRibs, valMaxRibs]$ **then**
$R(i,j) = 1$
end if
end for
end for
for $i = neighLeftLung$ to $neighRightLung$ **do**
for $j = neighTopLung$ to $neighBottomLung$ **do**
if $R(i,j) = 1$ **then**
build the contour of the region R_i starting from (i,j)
if **VerifyCandidateRibs**(R_i) **then**
Add R_i to the list of Ribs
end if
for $\forall (k,l)$ *Inside* R_i **do**
$R(i,j) = 0$
end for
end if
end for
end for
return ribs list

Algorithm 13 Identification of Lung Right Regions Candidate for Tumor

Require: medical exam to be analysed
Ensure: *true*, if it is possible to identify lung right tumors candidates and in this case these regions; *false* otherwise.

```
boundaryContrastAbdo ← ASM.Abdomen.boundaryContrast
brightTreshAbdo ← ASM.Abdomen.brightThreshold
IdentifyAbdomen(boundaryContrastAbdo, brightTreshAbdo, ...)
if error then
   return false
else
   meanBrightnessL ← ASM.RightLung.MeanBrightness
   boundaryContrastL ← ASM.RightLung.boundaryContrast
   toleranceL ← ASM.RightLung.ToleranceRate
   IdentifyRightLung(meanBrightnessL, boundaryContrastL, toleranceL,
   AbdomenContour)
   if error then
      return false
   else
      minMeanBrightnessN ← ASM.Nodul.MeanBrightness.Min
      maxMeanBrightnessN ← ASM.Nodul.MeanBrightness.Max
      NodulDetection(minMeanBrightnessN, maxMeanBrightnessN,
      AbdomenContour, RightLungContour)
      BorderTumorDetection()
      if error then
         return false
      else
         return true and regions obtained
      end if
   end if
end if
```

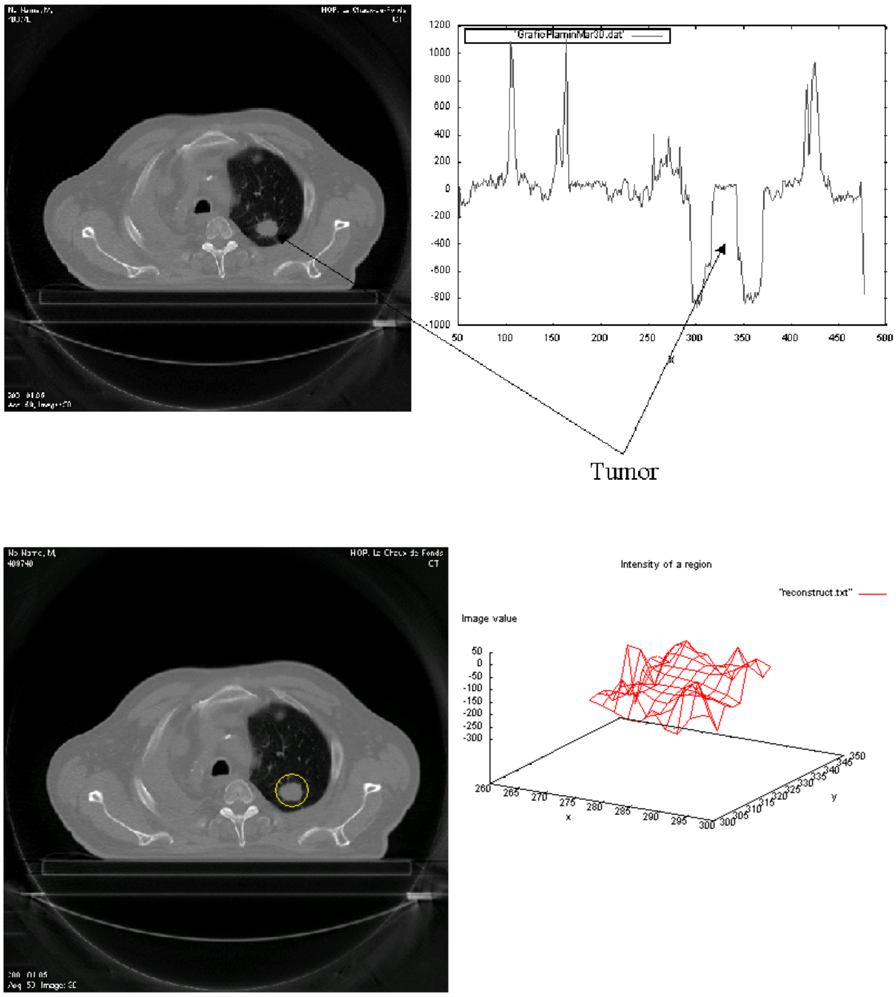

Figure 6.4: Lung Tumor. The graphic is changed, due to the presence of nodule.

sphericity, compactness, volume, mean gray level. These features ensure a delimitation of tumors from vessels which have a different shape and size (see algorithm 15).

Algorithm 14 Nodules Inside Right Lung Detection

Require: Image I, image size N, the abdomen contour and the right lung contour;
Ensure: $true$, if there are region candidates for nodules and in this case the regions contour and $false$, otherwise;

$foundTumor \Leftarrow false$
$R(i,j) = 0, \forall\ i,j = 1 \ldots N$
$((left,\ top),\ (right,\ bottom)) \Leftarrow$ the bounding box of the lung right contour
for $i = left$ to $right$ **do**
  for $j = top$ to $bottom$ **do**
    if $I(i, j+k) \in [valMinTumor, valMaxTumor]$ AND $(i,j) IsInside$ LungRight **then**
      $R(i,j) = 1$
    end if
  end for
end for
for $i = left$ to $right$ **do**
  for $j = top$ to $bottom$ **do**
    if $R(i,j) = 1$ **then**
      build the contour of the region R_i starting from (i,j)
      if VerifyCandidatNodul(R_i) **then**
        $foundTumor \Leftarrow true$
      end if
      for $\forall (k,l)$ $Inside$ R_i **do**
        $R(i,j) = 0$
      end for
    end if
  end for
end for
return found

Algorithm 15 Verify Candidate Nodule

Require: contour of the region candidate
Ensure: *true* if the region contour is nodule and $false$ otherwise
$((left,\ top),\ (right,\ bottom)) \Leftarrow$ the bounding box of the contour of the region candidate
$diamLenght \leftarrow right - left$
$diamHeight \leftarrow bottom - top$
$r \leftarrow \frac{2 \cdot AirRegionCandidate}{PerimeterRegionCandidate}$
$circularity \leftarrow \frac{PerimeterRegionCandidate}{2 \cdot r}$
if $(\frac{diamLenght}{diamHeight} \leq \epsilon_1)$ **AND** $(\frac{diamHeight}{2 \cdot r} \leq \epsilon_2)$ **AND** $(\frac{circularity}{\pi} \leq \epsilon_3)$ **then**
    return true
else
    return false
end if

Detection of metastases located at lungs extremities

In the literature, most of the work is done for nodules detection on CT images. At our knowledge, there is no work consecrated on the detection of peripherical tumors of lungs as the one seen in the fig. 6.5. In a normal CT scan, the distance lungs-ribs is approximately constant. The lung curvature is also the same as the ribs curvature.

An affected lung has these parameters changed. Detecting these changes on the lungs is equivalent with peripherical lesions detection (see algorithm 17). In the figure 6.6 the lungs and the ribs contours have been detected in the previous steps. For the left side of the patient, for each ribs we consider the gravity center. Let it be R_i with $i = \overline{1,m}$. On the lung contour we consider the points which are under the second diagonal. Let them be L_i with $i = \overline{1,n}$. For each point L_i, we found R_j and R_{j+1} with $R_j(Y) <= L_i(Y)$ and $R_{j+1}(Y) >= L_i(Y)$ (algorithm 16).

The distance $d(L_i)$ from each L_i to $[R_j, R_{j+1}]$ is computed. Also the curvatures in every L_i, R_j is computed. The peripherical lesions are the contours $L_k, L_{k+1}, .., L_p, L_k$, with

$d(L_j) > \varepsilon_1$,

$|curvature(L_k) - curvature(R_{j_k})| > \varepsilon_2$ and

$|curvature(L_p) - curvature(R_{j_p})| > \varepsilon_2$

The process is repeated in 3D, slice by slice. Symmetrically the same algorithm is applied for the right lung.

6.3 Experimental results

The experimental data consists in 20 patient cases (988 total images). The images used for these experiments have been also provided by the hospital in *La Chaux de Fonds* (Switzerland). They also helped with the clinical interpretation of images. The slice number per scan varies between 31 and 73. The experiments are done on images of patients of both gender (11 females and 9 males). Patients of different ages are also included (37-79 years). Not all the images had the lungs affected by tumors. Some patients have breast cancer or the prostate is affected. The smallest nodule detected in the test images has a 7 mm diameter. The solution for detecting even smaller nodules would be to use texture information about the nodules. A database with lung cancers would be necessary to obtain statistical information about the textural properties. In the current status of our research, such a database was unavailable. A more efficient classifier needs more data for training. The tumor contours obtained can be further improved using a technique like the snake algorithm.

With the images dataset available, for the nodules the accuracy is 91%, the rest of 9% being false negative. There were no false positive regions founded.

Algorithm 16 Detect points on the left lung to be examined for tumor candidate at the border

Require: ribs contours, the right lung contour ContourLung, number of points on the lung contour $nbLungPoints$;

Ensure: the list L with the selected points

```
minYRibs ⇐ top of the ribs
maxYRibs ⇐ bottom of the ribs
((left, top), (right, bottom)) ⇐ the bounding box of the lung right contour
a ⇐ (bottom−top)/(right−left)
b ⇐ left + (top−bottom)/(right−left) − bottom
for i = 1 to nbLungPoints do
   L_iY ⇐ ContourLung(i).Y
   L_iX ⇐ ContourLung(i).X
   if (L_iY + a · L_iX + b ≥ 0) AND (L_iY ∈ [minYRibs, maxYRibs]) then
      add(L_iX, L_iY))toL
   else
      if L not empty then
         j ⇐ i + 1
         finish ⇐ false
         while NOT finish do
            if j > nbLungPoints then
               finish ⇐ true
            else
               if (L_iY + a · L_iX + b ≥ 0) AND (L_iY ∈ [minYRibs, maxYRibs])
               then
                  finish ⇐ true
               else
                  j ⇐ j + 1
               end if
            end if
         end while
         if j ≤ nbLungPoints then
            for k = i + 1 to j do
               add(L_kX, L_kY))toL
            end for
         end if
      end if
   end if
   i ⇐ j + 1
end for
return L
```

Algorithm 17 Identification of Peripherical Lung Left Metastases Candidates

Require: the lung left contour, the left ribs contours *ListLeftRibs*

Ensure: *true*, if there is at least one candidate and in this case the list with regions candidate
$false$, otherwise

for $\forall$ ribs region i being in the list *ListLeftRibs*, compute the gravity center R_i, $i = \overline{1, m}$
select the points on the lung contour, L_i, $i = \overline{1, n}$
for $i = 1$ to n **do**
  find j which respect $R_j(Y) \leq L_i(Y)$ and $R_{j+1}(Y) \geq L_i(Y)$
  compute distance $d_i = d(L_i(Y), [R_j(Y), R_{j+1}(Y)])$
  compute $curvature(L_i)$
end for
if exist k, p with $d_j > \varepsilon_1$, and $|curvature(L_k) - curvature(R_k)| > \varepsilon_2$ and $|curvature(L_p) - curvature(R_p)| > \varepsilon_2$ **then**
  return *true* and all the contours $[L_k, L_{k+1}, .., L_p, L_k]$
else
  return *false*
end if

For the other type of metastases located at the lung extremities, all tumors present on the images are detected.

There is still a type of metastases that can not be detected with our method. There are the tumors located near aorta, esophagus or mediastinal lymph node, because these irregularities are less visible on CT images without the administration of a contrast product, even for a radiologist. Another imaging modality should be used, to highlight this tumors (like PET).

Our algorithms are implemented on a PC Windows machine. The worst execution time is 105 seconds for an 60 slices CT scan. The interactivity is minimum and might consists just in human correction of the errors in a couple of slices.

6.4 Discussion

In this chapter the top down approach presented in the Chapter 4 is applied for lung metastases detection. To detect the metastases which correspond to *Gross Tumor Volume*, several normal structures are first identified: the thorax contour, the lungs and the ribs. Further two types of metastases are detected: the nodules and the tumors located at the lungs periphery. The volume structures thus obtained are visualized using a method we have developed. The validation of the method has been performed on 20 real patient data, obtained from our clinical partner *La Chaux de Fonds Hospital* - Switzerland. The accuracy is higher of 90%. The analysis is done in real time. The main advantages of our method are the very high degree of precision, the speed of the algorithms, and the user interactivity which offers to the human operator a total control on the results, and thus the possibility to correct local errors of the contours. These advantages show that the system might work with success in an oncology department, as a tool for *Computer Aided Diagnostic*.

There is still a type of metastases that can not be detected with our method. There are the tumors located near aorta, esophagus or mediastinal lymph node, beacuse on CT images these irregularities are less visible without the administration of a contrast product.

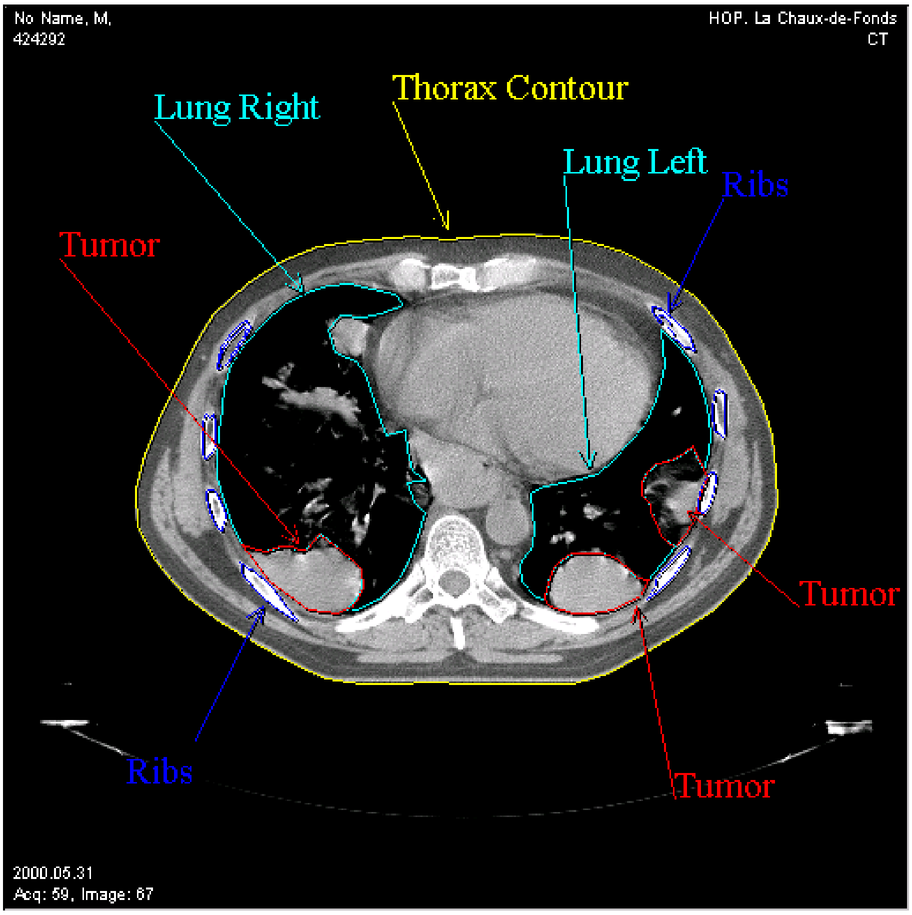

Figure 6.5: The type of metastases situated at the lung borders detected with our algorithms.

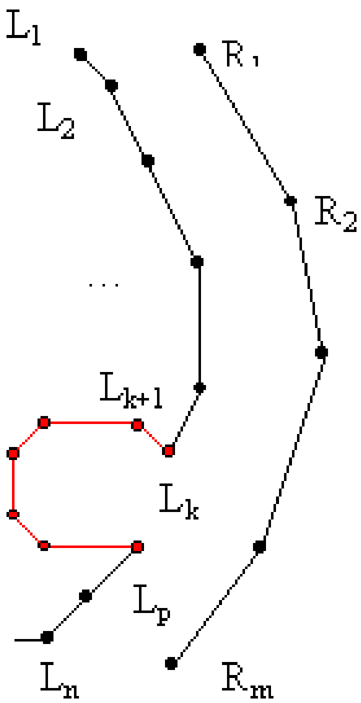

a.

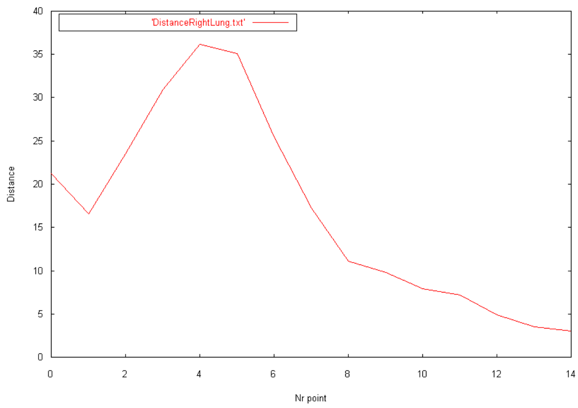

b.

Figure 6.6: a. Parts of the lung and ribs contours. With red the lesion is represented. b. distance graphic from ribs to lungs for this lesion.

Chapter 7

Visualization of Anatomical Structures

In this chapter a method to visualize the anatomical structures obtained with the method presented in previous chapters. Using a set of contours, on parallel slices, the surface and volume model of the object are created, using a $3D$ Delaunay triangulation algorithm. The method can be applied in radiotherapy planning to view in $3D$ the distribution of tumors inside the normal organs. Also it can be used in *Computer Assisted Surgery* where precise models of bones are needed.

7.1 Introduction

The 3D reconstruction of volumes from a set of points is a common problem for medical applications. The case when the object has a convex shape is easier to solve, and there are already some approaches [24, 39, 40, 61]. The problem arises for complicated structures like skull, spine or pelvis. The drawbacks of existent approaches consist mainly in time execution and quality of the surface. This problem might be reduced to the problem of mesh generation, a know problem in finite analyze element and in CAD. A certain number of methods of solution are given to this problem of mesh generation.

Three types of method are most popular:

- Delaunay triangulation;
- octree based techniques;
- advanced front.

The $3D$ Delaunay method is used to generate the volume meshes for it low cost computational time and for the quality of meshes obtained. To reconstruct anatomical structures with complicated shapes the solution chosen was to use a 3D Delaunay triangulation, obtain a convex hull and than eliminating the tetrahedral which are not inside the object.

The steps performed by our algorithm are:

- contour improving by the use of smooth techniques [92] and an *b-spline* interpolation;
- generation of tetrahedral meshes of the convex hull using 3D Delaunay triangulation;
- sculpting the convex hull, removing the non-organ tetrahedral, using the distance map and bit volume information.

7.2 Input data

The input consists in a set of parallel contours obtained with a classical segmentation algorithm (e.g. threshold) applied to a set of CT data. Usually because of the CT images properties, the bones are segmented (high HU level intensity). A set of contours corresponds for each slice of the CT scan. The object is non-convex, multiple contours might exists on a slice, generating ramifications and holes. Due to the presence of noise, additional points might be obtained with the segmentation algorithm. Also the contours are not always smoothed, even when we have to deal with smoothed surfaces like the bones. This is the reason why a simplification procedure is performed on the contours.

7.3 Contours simplification

Image noise can affect directly the quality of contours obtained with a segmentation algorithm. Of course, the quality of the 3D reconstruction algorithm will be affected as well. That is why, the contour simplification has an essential role in the quality of the 3D reconstruction algorithms, from two points of view. The first one is that the surface obtained with noisy contours is very fuzzy and not conform to the real object. The second problem with the noisy contours is the execution time, because of 3D triangulation which is very time consuming.

To avoid these problems, the contours obtained with the segmentation algorithms are modified in two ways: by applying a smoothing method and then by an interpolation algorithm.

7.3.1 Contour smoothing

The original CT images contain a lot of noise, and thus the quality of contours obtained with the segmentation algorithms is not always optimal (see the Figure 7.1.a). That is why a technique which will improve and correct the contours is needed (like in Figure 7.1.b). The problem is to not loose important information by their modification. Let be the original contour P,

$$P = (x_1, y_1), (x_2, y_2), ..., (x_n, y_n) \tag{7.1}$$

with n being the number of vertices of the P. Its modification consists in application of three steps:

1 use mid-point algorithm;

2 points removal based on inter-points distance;

3 points removal based on curvature information.

Mid point algorithm

The idea behind this algorithm is very simple, but still the results are very good. Given an input polygon, a mid-pointed smoothed version of the polygon is constructed, by joining the midpoints of the edges of the original polygon in the order in which they are encountered. The new polygon smoothed obtained is:

$$M = ((x_1 + x_2)/2, (y_1 + y_2)/2), ((x_2 + x_3)/2, (y_2 + y_3)/2), ..., ((x_n + x_1)/2, (y_n + y_1)/2)$$

The main advantage of the algorithm is its speed, the complexity being $O(kn)$, where k is the number of iterations. In our case just one iterations is performed, because multiple applications may deform considerably the initial contour, and thus information might be lost.

Points removal based on inter-points distance

There are points on the contour which are very close to each other and which does not influence the contour topology. That is why, these points might be removed, without a lost of information about the contour. For each point P_i and P_{i+1} (with $P_{n+1} = P_1$), we compute $d_i = ||P_{i+1} - P_i||$, where $||||$ is the Euclidian norm. The points P_i having $d_i < \varepsilon$ are removed.

Points removal based on curvature information

The third step performed is the removal of the points on the contour which have a high curvature. The curvature of the curve given by the position vector $r(t)$ is:

$$K(t) = \frac{|r^{'}(t) X r^{''}(t)|}{|r^{'}(t)|^3}$$

We approximate the curvature in each point of the contour P. Thus, for each point P_i (with $P_{n+1} = P_1$), we compute:

$$\Delta X_i = P_i^x - P_{i-1}^x$$
$$\Delta Y_i = P_i^y - P_{i-1}^y$$

and respectively:

$$\Delta X_{i+1} = P_{i+1}^x - P_i^x$$

$$\Delta Y_{i+1} = P^y_{i+1} - P^y_i$$

Than:

$$\Delta S_i = \sqrt{\Delta X_i^2 - \Delta Y_i^2}$$
$$\Delta S_{i+1} = \sqrt{\Delta X_{i+1}^2 - \Delta Y_{i+1}^2}$$

which leads to:

$$K_i = (\frac{\Delta X_i}{\Delta S_i} - \frac{\Delta X_{i+1}}{\Delta S_{i+1}})^2 + (\frac{\Delta Y_i}{\Delta S_i} - \frac{\Delta Y_{i+1}}{\Delta S_{i+1}})^2$$

The points having the K_i higher than a threshold ε are removed from the contour.

7.3.2 B-spline interpolation

Given $n+1$ points $d_0, ..., d_n$ to be interpolated by a B-spline curve of degree p, where $p <= n$. A set parameter values $t_0, ..., t_n$ can be selected (each t_k corresponds to d_k). From these parameters, a knot vector of $m+1$ knots is computed where $m = n+p+1$. The B-spline curve is defined as:

$$p(u) = \sum_{i=0}^{n} N_{i,p}(u) p_i \tag{7.2}$$

where $N_{ip,p}(u)$'s are *B-Spline* basis functions of degree p. The i-th *B-Spline* basis function of degree p, written as $N_{i,p}(u)$, is defined recursively as follows:

$$N_{i,0}(u) = \begin{cases} 1 & \text{if } u_i \le u < u_{i+1}, \\ 0 & \text{otherwise.} \end{cases}$$

and:

$$N_{i,p}(u) = \frac{u - u_i}{u_{i+p} - u_i} N_{i,p-1}(u) + \frac{u_{i+p+1} - u}{u_{i+p+1} - u_{i+1}} N_{i+1,p-1}(u) \tag{7.3}$$

7.3 is usually referred to as the Cox-de Boor recursion formula.

The curve p has $n+1$ unknown control points. Since parameter t_k corresponds to data point d_k, plugging t_k into the equation **??** yields the following:

$$d_k = p(t_k) = \sum_{i=0}^{n} N_{i,p}(t_k) p_i \tag{7.4}$$

for $0 <= k <= n$.

In equation 7.4 each data point d_k, as well each p_i are vectors in s-dimensional space(i.e. $d_k = [d_{k1}, ..., d_{ks}]$ and $p_i = [p_{i1}, ..., p_{is}]$). We denote by:

$$\mathbf{N} = \begin{pmatrix} N_{0,p}(t_0) & N_{1,p}(t_0) & \cdots & N_{n,p}(t_0) \\ N_{0,p}(t_1) & N_{1,p}(t_1) & \cdots & N_{n,p}(t_1) \\ \vdots & & \ddots & \vdots \\ N_{0,p}(t_n) & N_{1,p}(t_n) & \cdots & N_{n,p}(t_n) \end{pmatrix} \tag{7.5}$$

$$\mathbf{D} = \begin{pmatrix} d_{01} & d_{02} & \cdots & d_{0s} \\ d_{11} & d_{12} & \cdots & d_{1s} \\ \vdots & & \ddots & \vdots \\ d_{n1} & d_{n2} & \cdots & d_{ns} \end{pmatrix} \tag{7.6}$$

$$\mathbf{P} = \begin{pmatrix} p_{01} & p_{02} & \cdots & p_{0s} \\ p_{11} & p_{12} & \cdots & p_{1s} \\ \vdots & & \ddots & \vdots \\ p_{n1} & p_{n2} & \cdots & p_{ns} \end{pmatrix} \tag{7.7}$$

With these notations a linear system is obtained:

$$D = N \cdot P \tag{7.8}$$

In which D and P are both known and P is unknown. Solving this system the equation of the B-spline curve is found, and thus interpolation problem is solved.

In our case p was choose to be 4. The final problem is to determine the number of points which is keep from initial contour. Different number of points have been used to generate models of bones. For more details, see the Section 7.6.

Algorithm 18 Contour simplification

Require: m data points $d_0, \dots d_{m-1}$ and a degree p

Ensure: a B-spline curve of degree p that contains all data points in the given order

```
delete all points d_i with ||d_{i+1} - d_i|| < ε
delete all points d_i with curvature(i) > ε
let be d_0, ... d_n, remaining points
Select a method for computing a set of n + 1 parameters t_0, ... t_1
for i = 0 to n do
   for j = 0 to n do
      Evaluate N_{j,p}(t_i) into row i and column j of matrix N
   end for
end for
for i = 0 to n do
   Place data point d_i on row i of matrix D
end for
Use a linear system solver to solve for P from D = N · P
/* row i of P is control point p_i */
return control points p_0, ··· p_n, and matrix N
```

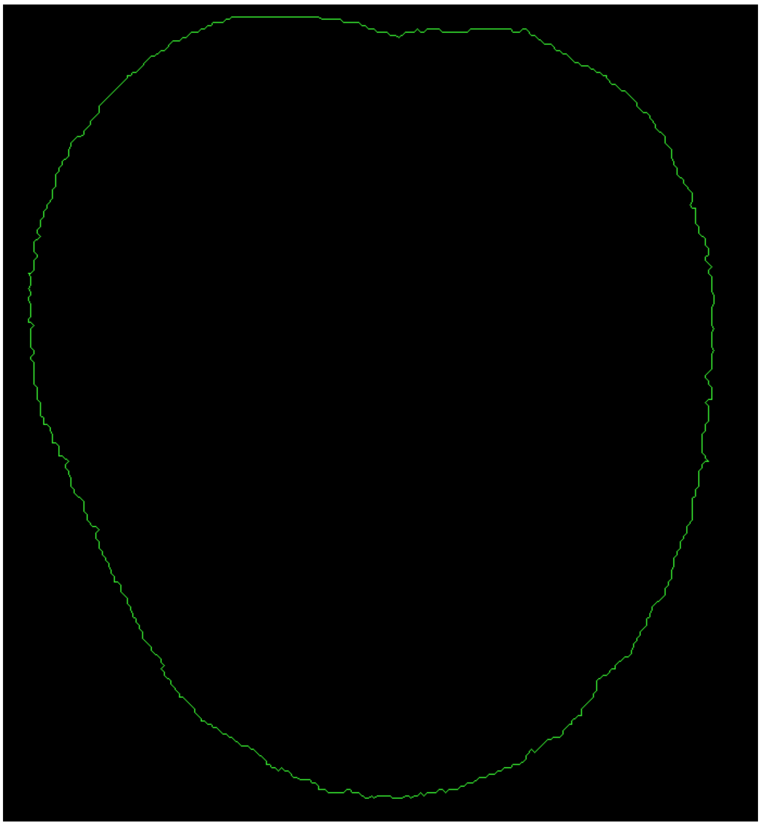

a.

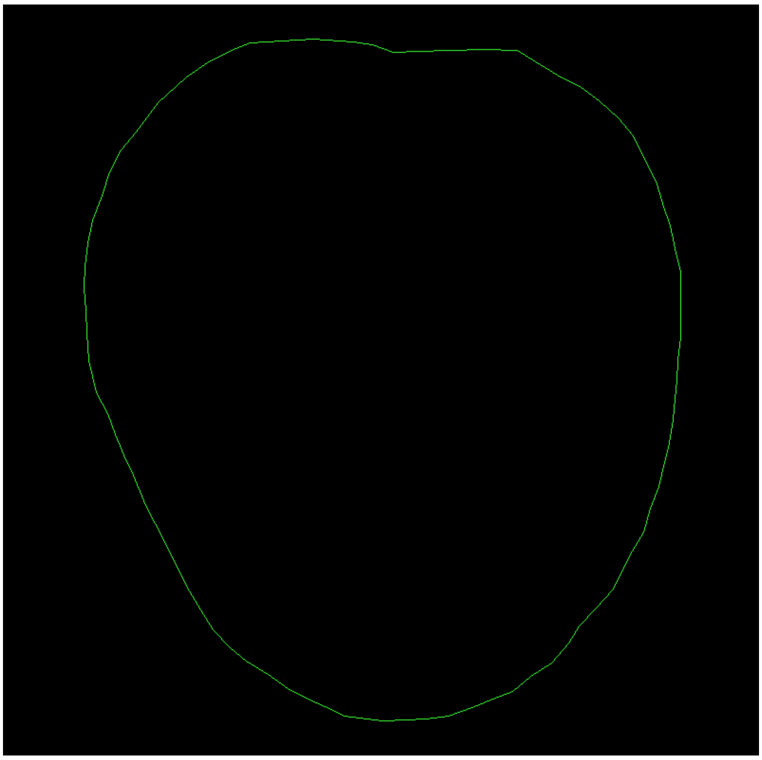

b.

Figure 7.1: a. An initial contour obtained with a segmentation algorithm. b. Its improving with the simplification algorithm.

7.4 Delaunay 3D triangulation

Our approach makes extensive use of Voronoi diagram and its dual Delaunay triangulation. Given a set of points $U \in R^2$, a Voronoi face v_p for a point $p \in U$ is the set of all points in plane that are closer to p than any other point in U. Closure of each Voronoi face is a convex polygon. The boundaries of Voronoi faces consist of vertices and edges called *Voronoi vertices* and *Voronoi edges* respectively. In the absence of degeneracy, every Voronoi vertex has degree 3. Voronoi vertexes, Voronoi edges and Voronoi faces form a planar subdivision of R^2 which is called *Voronoi diagram.*

A dual planar subdivision called *Delaunay triangulation* can be defined from Voronoi diagram as follows. Dual of a Voronoi face v_x is the vertex x. Dual of a Voronoi edge shared by two Voronoi faces v_x and v_y is the *Delaunay edge* defined as the line segment connecting x and y. Dual of a Voronoi vertex where three Voronoi faces v_x, v_y, v_z meet, is a *Delaunay triangle* xyz with vertices x, y and z. For each Delaunay triangle xyz, the Voronoi vertex is the circumcenter and thus, the circumcircle of xyz does not contain any fourth point in U. Equivalently, a $2D$ Delaunay triangulation of U can be defined as the collection of triangles with vertices in U whose circumcircles are empty. Essential is the Delaunay criterion respected by the triangles generated. It states that any node must not be contained within the circle of any triangle within the mesh.

The $2D$ case can be extended easily to the $3D$ case for tetrahedrical meshes which are used in this application.

7.5 Volume Sculpting

A convex hull is obtained with the triangulation process. Depending on the anatomical structure, up to 40% tetrahedral must be removed. Of course it is essential the decision about which tetrahedral to be removed. In [20], a method based on the external medial axis of each polygon is used, which gives good results, but for simple polygons where the skeleton might be computed without numerical approximation errors. That is why we choose a method which use information from segmentation algorithms in the form of *Bit Volume* and *Distance Map*. These structures are used originally in surface matching methods, and are adapted to be used in our problem.

7.5.1 Bit Volume

The bit volume is obtained with a segmentation algorithm. Each voxel of original data set, receives an label *inside/outside* the object.

7.5.2 Distance Map

In this data structure, for each voxel of an object volume, the distance to the closest point on the surface is stored. The method used to compute it is based on a chamfer [14, 41].

Moreover, for the surface matching purpose for the voxels which are inside the object, the distance is multiplied by a so-called *penalty factor*. That is why, just the distance map cannot be used, and the bit volume is also needed for the sculpting process. Moreover the distance map is shrunk, by a factor 2. A border is also added around the whole volume (see the figure 7.2).

7.5.3 Correlating all the information sources

Let be a voxel (x, y, z) in the original bit plane. Its corresponding x_{dm}, y_{dm}, z_{dm} voxel inside the distance map is given by:

$$x_{dm} = \frac{x - x_{OrigBv}}{2} + BORDER;$$
$$y_{dm} = \frac{y - y_{OrigBv}}{2} + BORDER;$$
$$z_{dm} = z_{dimDM} - BORDER - \frac{z_f - z_{OrigBv}}{2}.$$

where:

- $x_{OrigBv}, y_{OrigBv}, z_{OrigBv}$ is the origin of the contours bounding box;

- $BORDER$ is the size of the border present in the distance map;

- z_{dimDM} is the size of the distance map on the z axis.

The corresponding bit plane voxel x_{BV}, y_{BV}, z_{BV} is obtained using the formulas:

$$x_{BV} = x - xOrigBv;$$
$$y_{BV} = y - yOrigBv;$$
$$z_{BV} = z_{dimBV} - z - zOrigBv.$$

where:

- z_{dimBV} is the size of the bit volume on the z axis.

The relationships existent between the sizes of the bit planes, bit volume and distance map are:

$$bpLength - 2 \cdot y_{dimDM} = 4 \cdot BORDER;$$

$$bpWidth - 2 \cdot x_{dimDM} = 4 \cdot BORDER;$$

$$bpHeight - 2 \cdot z_{dimDM} = 4 \cdot BORDER;$$

where

- $bpLength$, $bpWidth$ and $bpHeight$ are the sizes of the bit planes on the three axes x, y and z respectively.

7.5.4 Removing tetrahedrons

A number of points inside each tetrahedral are examined to decide if the tetrahedral lies inside or outside the volume. Due to the initial modification of the contours, tetrahedral, which are not completely inside the object are also added. Considering all the points inside a tetrahedral is very time consuming, that is why the decision if a tetrahedral is inside the volume or not, is taken by examination of a number of key points (see the figure 7.3). Different criteria have been used to choose these points and thus different elements of the tetrahedral:

- number of faces which are inside;
- number of edges;
- number of gravity centers on each face.

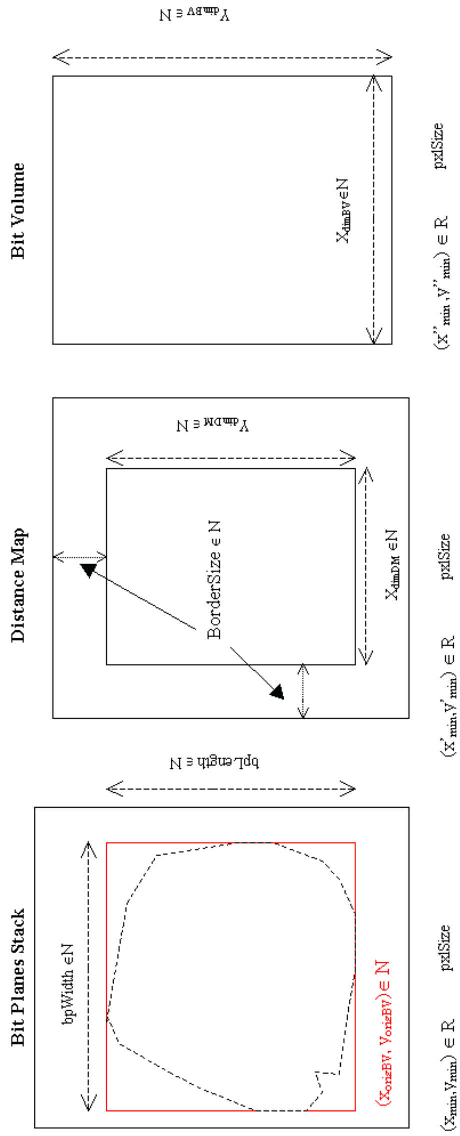

Figure 7.2: Relationships bit volume, distance map, bit planes. Correlating the information from all 3 sources, the sculpting process is performed.

Finally after experiments, given a tetrahedral $ABCD$, it is considered to be inside the volume if at least three faces are inside the original object volume. A face is considered to be on the volume if four elements are on volume. To give an example, the face ABC is inside the volume, if its edges middles (M_1, M_2, M_3) and its gravity center (C_1) have either the bit volume corresponding 1 or the distance from these points to a the closest points on the surface is less than a threshold distance d_ϵ (after experiments the value $d_\epsilon = 2$ has been used).

Surface model is obtained from volume model. Using the set of tetrahedrons, the set of triangles lying on the surface is generated.

7.6 Experimental results

Several tests have been performed. Models for hip, skull, and spine have been generated. Time needed to obtain a model with about 100000 tetrahedrons is less than 3 minutes, for a skull defined by a CT scan with 55 slices, on a Sun Ultra Sparc Workstation, 256 MB RAM, 450 MHz processor (see the Table 7.1 and the Figure 7.4 for more information). The most important problem is to find a balance between execution time and surface quality. Increasing the number of points on the surface will increase the execution time, but also the surface quality. This parameter is tuned by contour simplification procedure. The quality was judged by visual inspection. It was noticed that, from $25\% - 100\%$ of initial point kept, the surface quality is not changed. The quality surfaces has been judged satisfactory for display purposes in medical applications. Small problems occur in the case of concavities, the surface obtained is not smooth enough. Models which can be used in radiotherapy planning are presented in the Figures 7.6 and 7.7. Some bone models are presented in the

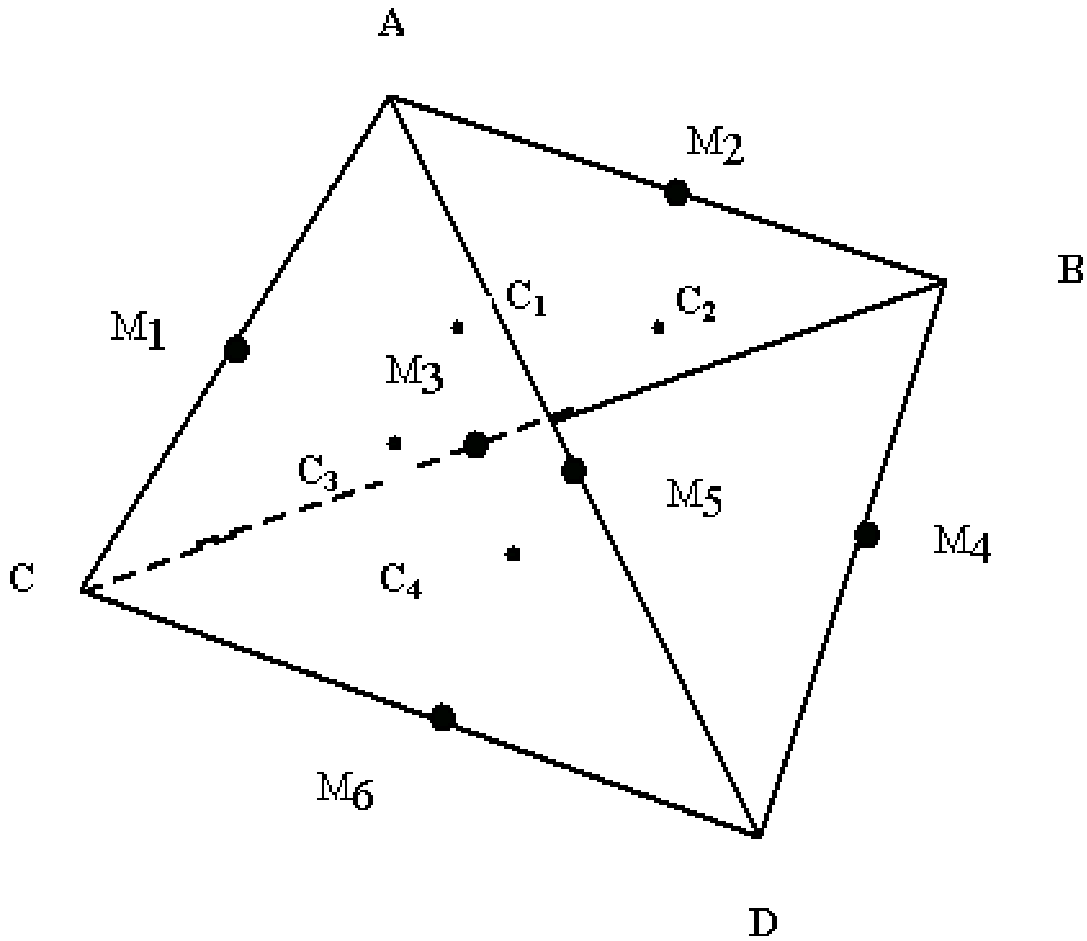

Figure 7.3: Points on the tetrahedral which are considered for elimination process. The face ABC is on the volume is edges middles M_1, M_2, M_3 and its gravity center C_1 are on the volume. The tetrahedral $ABCD$ is keep on the volume if at least 3 faces are on the volume.

Figure 7.8 with application in *Computer Assisted Surgery*. The numerical results are shown in the Table 7.1.

7.7 Discussion

In this chapter, a method for reconstruction of 3D surface and volume models of anatomical structures is presented. Initial data, in form of contours on parallel slices is simplified using smoothing techniques and B-spline interpolation. Than, the convex hull is obtained applying a $3D$ Delaunay triangulation. A sculpting process of non-object tetrahedron is performed, using original image information. The only problems concerning the surface quality remain in the concavities. There are no surface smoothing or decimation techniques used. But still, the surface quality was judged to be satisfactory for displaying purposes in medical applications. The execution time, another important issue is also reasonable. Several improvements might be still possible to improve the surfaces quality in the concavities. Also the execution time could be further reduced. For different structures different parameters (for triangulation and sculpting) should be found by statistical experiments.

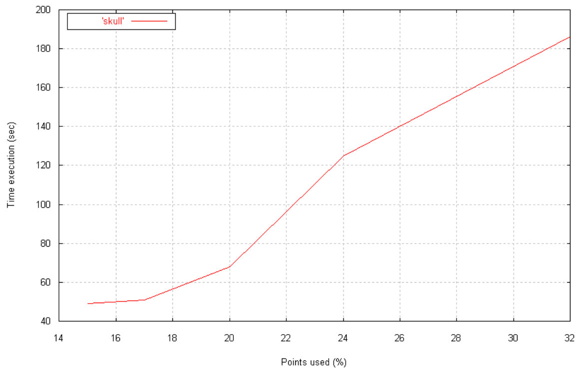

a.

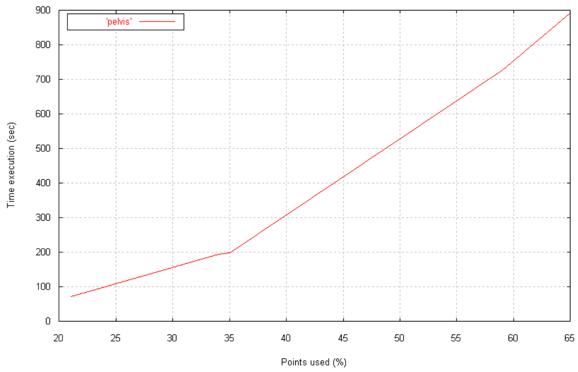

b.

Figure 7.4: Graphic of time execution for different number of data points: a. Skull model; b. Pelvis model

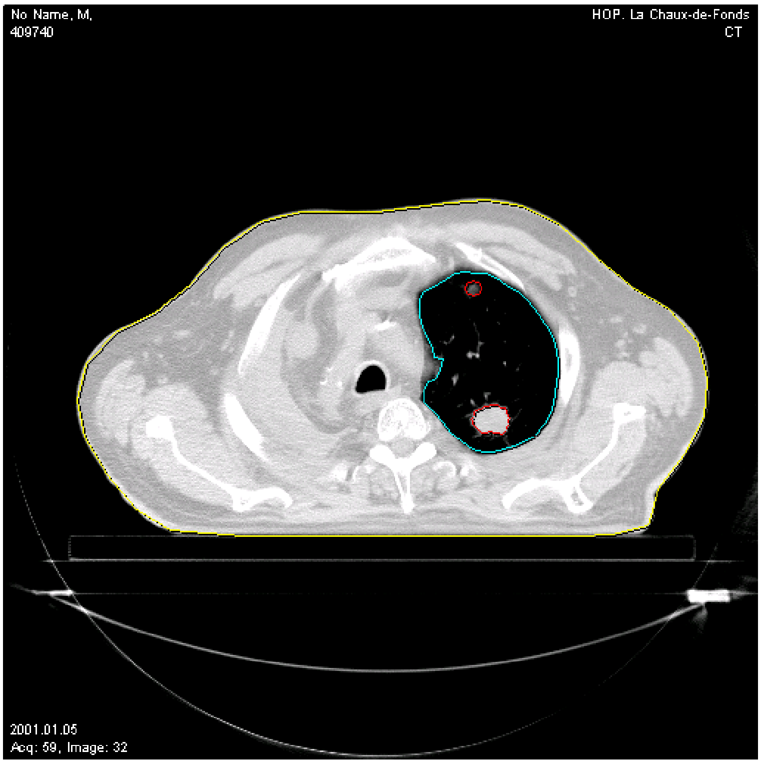

Figure 7.5: 2D Slice containing two nodules detected with our algorithms. In the next figure the lung is reconstructed in 3D together with its nodules.

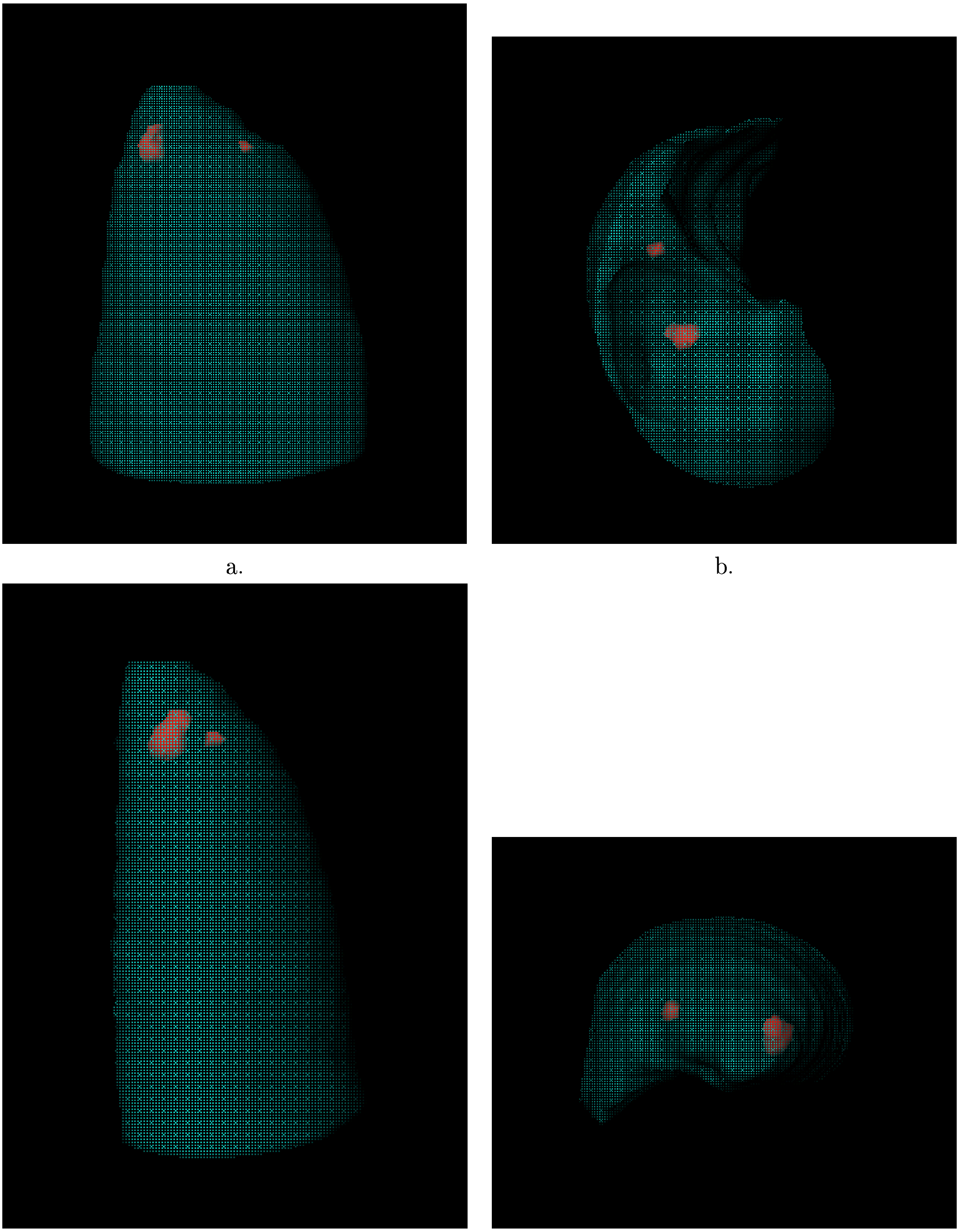

a. b. c. d.

Figure 7.6: Lung reconstructed. A slice from the original CT scan, is presented in the previous figure. With red the nodules are represented. a., b., c. and d. present different views of the same object.

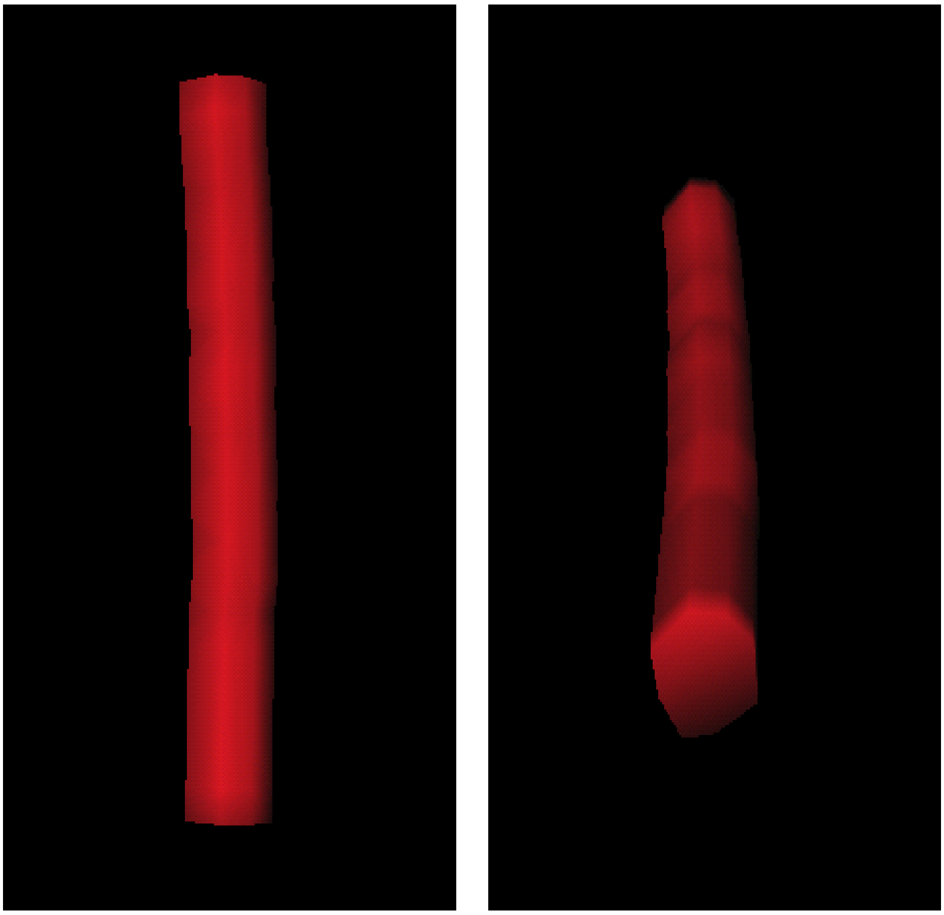

a. b.

Figure 7.7: Spinal Cord reconstructed from 22 slices. a. and b. present two different views of the same object.

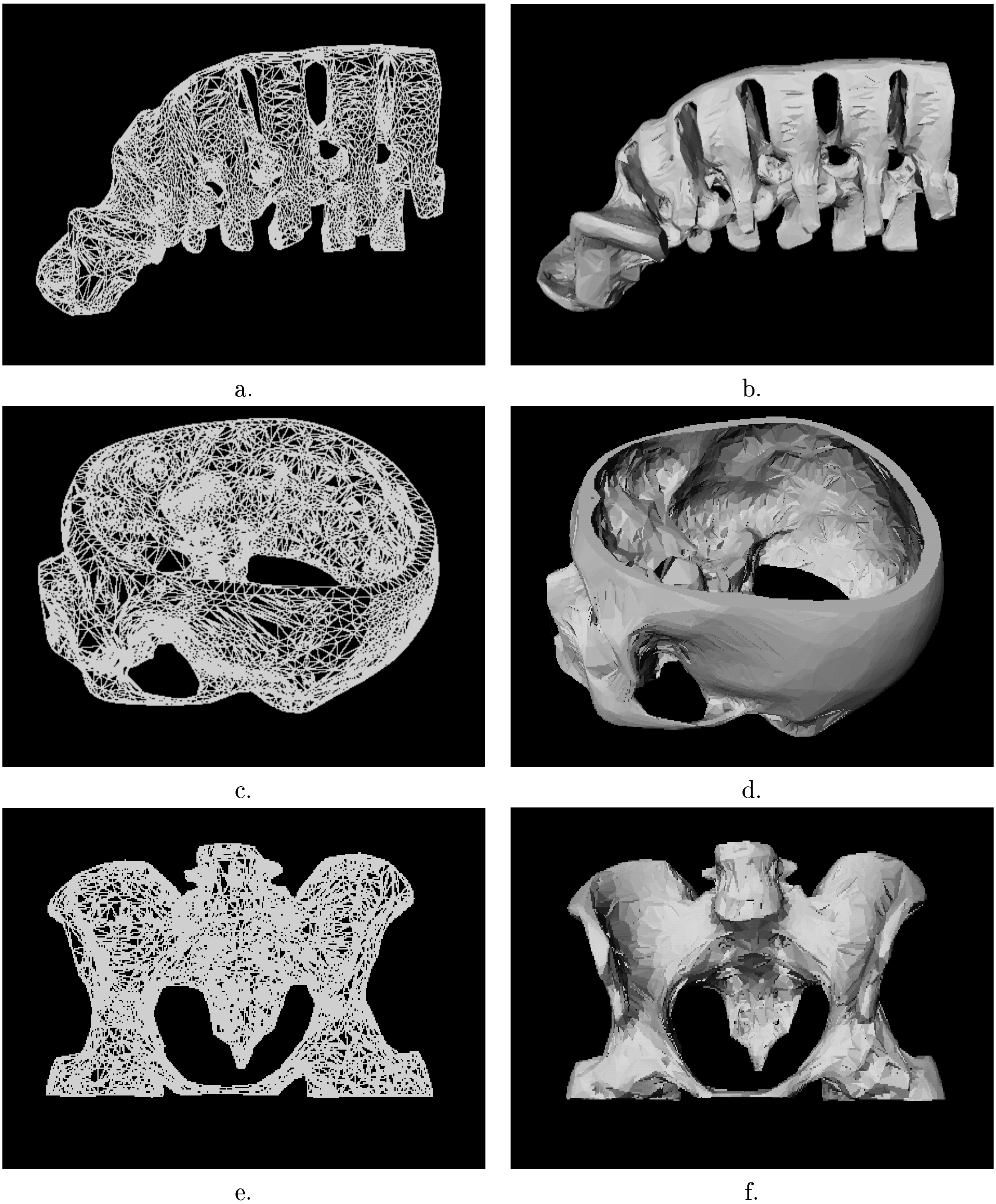

Figure 7.8: The 3D reconstruction algorithm was applied also to build 3D models of bones from CT images for use in Computer Assisted Surgery. The bone contours have been segmented in CT images. Using these contours, surface models have been obtained using our algorithms. This figure depicts some samples of objects rendered with our method. No tumor was presented on the original images. The CT images are acquired at Insel Spital Bern, Switzerland. Courtesy of Muller Institute, University of Bern.

Table 7.1: Experimental results

	Ratio points used	**Nr. tetrahedra generated**	**Ratio tetrahedra sculpted**	**Exec. time**
Skull 55 slices 74144 points	15.35%	71940	26.94%	0.33 min.
	22.72%	104900	22.64%	0.71 min.
	28.17%	127616	21.98%	1.38 min.
	32.58%	147674	21.49%	1.40 min.
	60.87%	283634	19.62%	10.88 min.
Spine 256 slices 147286 points	13.49%	131782	69.20%	0.46 min
	17.63%	171477	66.88%	0.80% min
	20.95%	204205	67.57%	1.11 min
	32.58%	315209	64.40%	2.55 min
Pelvis 119 slices 124357 points	18.51%	151563	22.88%	0.80 min
	21.83%	176867	22.64%	0.95 min
	35.46%	285096	20.61%	3.16 min
	67.22%	552366	18.41%	14.41 min
Knee 256 slices 85354 points	12.18%	66760	76.22%	0.20 min
	32.37%	174934	68.35%	1.31 min
	63.97%	348706	66.37%	6.28 min
Ribs 33 slices 24393 points	10.72%	16272	40.35%	0.033 min
	14.70%	22914	40.21%	0.066 min
	25.74%	40323	33.86%	0.11 min
	32.23%	51704	33.37%	0.21 min
	61.28%	109814	29.96%	1.05 min

Chapter 8

Conclusions

A system for interpretation of the thorax CT images was presented. Most important features include the use of a top-down approach and knowledge-based image processing philosophy. Our goal is to perform $3D$ analysis of CT scans in the same way the radiologist does it.

Therefore, the system contains three important components:

1. *Anatomical Structures Map* - with the aim of representing the anatomical knowledge used by radiologist while interpreting the CT images;

2. *Plan solver* - which contains the procedural knowledge, which specifies how to identify particular anatomical structures one-by-one;

3. *Top-down knowledge base architecture* - which links all the modules of the system (structural and procedural knowledge with the actual image processing algorithms). It makes it possible to cope with inter-patient variation.

Two kinds of problems related to radiation therapy planning have been solved using our knowledge base approach: segmentation of organ at risk (including the spinal cord) and detection of **Gross Tumor Volume** (lung tumors). Some sub-problems are also solved: the identification of spinal canal, lamina, lungs, ribs and thorax contour. The method for spinal cord segmentation was tested on image data from 23 patients and its accuracy is higher than 90%. The procedure for lung tumors detection has been tested on image data from 20 patients, with an accuracy higher than 90%. The analysis is fast (less than a second per slice on a normal workstation).

Also, a method for $3D$ reconstruction of organs from a stack of CT slices is presented in this thesis. The segmentation data is combined with a computational geometric algorithm, in form of Delaunay 3D triangulation. Thus, both surface and volume models of organs are obtained. The volumes are defined by tetrahedrical meshes, meanwhile the surface is given by triangles. The possibilities further are in interaction with these models (e.g. cuts using virtual tools).

8.1 Limitations and issues for further research

Meanwhile, several limitations have been identified and some questions remain unresolved. The solutions to these limitations and how these drawbacks might be improved in future work are discussed below.

1. *Some types of lung tumors cannot be detected. There are types of tumors which are located in the middle of the thorax, near or connected to the normal tissue (e.g. aorta).*

   These types of tumors are not easy to delimit in CT images, even for the radiologists. The question which arises is whether the CT images are to detect these tumors, or another imaging modality should be used (as PET). Still, a solution would be to administer a contrast agent to the tumoral images, which can highlight the tumors tissue.

2. *The contour quality of the detected tumors may and should be further improved.*

   The precision of the tumor contours can be improved. This problem can be solved, by adding more points (using geometrical relationships lung - ribs), and modifying them using a snakes-based algorithm. Special attention should be given to the number of points which will be added, and of course to the snakes parameters.

3. *The algorithms for spinal cord identification, have not been tested on patient images in which the spinal cord is affected by a tumor.*

   The availability of the image dataset poses currently a problem for validation of the different medical image processing algorithms. Even if database with reference images are created (or about to be created), there are not always sufficient image material available to the whole research community. This would be a good point for testing different rare case like a tumor, which affects the spinal cord.

4. *The smallest nodule detected has 7 mm diameter. The question is how could the method be improved so that nodules of 3-4 mm could be detected as well.*

   Information about the nodule texture would be a way to classify them with a higher accuracy. But, as stated previously, a lung nodules image database is required, so important statistical information about texture could be extracted. The current trend in image analysis is to go even further and analyze the healthy tissues and to predict possible apparitions of cancers.

5. *For some organs (e.g. liver) the segmentation strategy should be more complex.*

   For some organs like the liver, a simple technique like thresholding or region growing will fail. Still, our general approach could serve as a framework encompassing novel low level routines. Different reference objects might be found, which would guide a more complex algorithm like 3D active shape models, which are very sensitive to initial parameter settings.

6. *The algorithms have been tested on images acquired with a CT Picker scanner; is the system scanner dependent?*

   The *DICOM* standard (used by our system), and the use of *HU* normally will enable the use of these techniques in every hospital. Another scanner than Picker, might have another distribution of noise, which of course will affect the quality of segmentation algorithms. A possible new parameter calibration is required for each scanner.

7. *The uncertaincy is a parameter which is not yet taken into account when the top-down plan is generated.*

   A statistical model (e.g. a probabilistic network) could be introduced in future work, which for each submodule involved in image analysis, will give a success rate, based on previous applications of the algorithms (i.e. learning facility). In case the plan solver would have multiple choices for solving a task, this would be a good criterion to adopt the best decision.

8. *There is no capability of learning, in this stage of the system.*

   The learning component of the system might be essential for clinical use of this kind of system. A *Learning from failure* component may be necessary. This point is very related to the previous one.

9. *The extension of the knowledge based (adding new anatomical structures) could not be performed without a good knowledge of computer engineering.*

   Formalization of anatomical and procedural knowledge requires time and computer engineering knowledge. This problem is well-known from the research in expert systems and has been called the *knowledge elicitation bottleneck.* Although the *Anatomical Structures Map* may be partly reused, e.g., for automatic interpretation of MR images of the thorax, reverse engineering would be required to tailor the plan solver. A different image modality will, in general, require different low-level operators to find the same anatomic structures. Furthermore, the rather confined macro-anatomy of the human thorax makes it well-suited for representation in a frame-like hierarchical representation scheme such as the *Anatomical Structures Map.* This inconvenient could be overtaken either by adding a friendly interface, easy to use by non-computer specialists which will allow intuitive interactions with ASM, either by using high-level scripts or macros.

10. *There is no clear delimitation between the image datasets used for training and for testing.*

    The parameters for ASM have been tuned from a subset of images which have been used for testing the algorithms. A more clear delimitation between the training and test dataset should be marked. As improvement, a new dataset for testing the algorithms performance should be used.

11. *The prototype as it is now, could not be used in a daily clinical work.*

    At this stage the techniques and algorithms developed result in a prototype which work on a standard workstation. The system could not be used *as it is* in the daily clinical work of hospitals. From a computer engineering point of view, more steps should be performed to this aim:

- test the algorithms on images acquired with a different CT scanner;
- solve the copyright problems for a few modules which have developed in other university (modules which deal with input/output routines for CT images);
- write the software in order to meet normative IEC 601-1-4 (Europe) and FDA (USA) general requirements regarding safety for medical equipment;
- perform validation tests.

Some of these steps are part of the *Development Life Cycle* of any software based product. An important aspect is how this system could be used in a hospital. While a fully automatic system for medical image analysis would require an extensive validation by the medical community, its practical use would only be as a tool for *Computer Aided Diagnosis*. The system itself can be used as a tool which will propose a solution for contours obtained to the oncologists. They will assess the correctness of the algorithms. Hopefully, it can increase the medical doctors performance.

Even if the enumerated limitations exist, the methodology presented in this thesis has shown to be straight in solving contouring problems related to radiotherapy planning. Some of the proposed improvements (2,3,6,9,10) could be realized in a relative short term. It is possible to solve the problems related to the points 4,7,8 using the current state of the art techniques in statistics. Still the results will depend to the availability of the medical images database.

However, a very important but complex problem is related to the detection of the tumors. The artificial intelligence techniques used in this thesis have opened a way of detecting them. Still, a lot of work remains to be done, even in the particular case of lung tumors. The image processing techniques should follow the evolution of the screening modalities. It is very likely that the detection of the pathologies will be performed in the future using multiple sources of information, from different imaging modalities. This kind of information should be incorporated as well in an anatomical knowledge-based, as modality oriented properties of each structure. So, tumors less visible on CT images will be easier to detect using for the same patient a PET scan. For different tumors of different organs, algorithms for normal structures segmentation are needed first in our philosophy. E.g. detecting the liver tumors is easier to perform when the liver is identified first. More complex segmentation schemes are necessary for segmentation of other structures (see point 5).

The next important point is how the medical community will accept these techniques in a daily basis clinic operation. In the very near future, more and more tools for *Computer Aided Diagnostic* will penetrate in the hospitals. However, a huge amount of research has to be performed before the techniques for automatically image interpretation can be validated, accepted and used in the clinics.

In the ideal case, if technology is evolved enough, every person in our society will spend a couple of minutes per year in a scanning modality [65]. The acquired data will be analyzed automatically by a computer system. Potential hazards to the patient's health will be reported to medical experts, who will be able to detect and cure most diseases in time. The work presented here, even at the prototype level, is a further step in this direction.

Bibliography

[1] *Visualization toolkit*, www.kitware.com.

[2] *Prescribing, recording and reporting photon beam therapy*, International Commission on Radiation Units and Measurements, 7910 Woodmont Avenue Bethesda, Maryland 20814, USA, 1993.

[3] A. Aamodt and E. Plaza, *Case-based reasoning: foundational issues methodological variations, and system approaches*, AI Communications **7** (1994), no. 1, 39–59.

[4] R. Adams and L. Bischof, *Seeded region growing*, IEEE Transactions on Pattern Analysis and Machine Intelligence **16** (1994), no. 6, 641–647.

[5] U. Ahlrichs, J. Fischer, J. Denzler, C. Drexler, H. Niemann, E. Noth, and D. Paulus, *Knowledge based image and speech analysis for service robots*, Proceedings Integration of Speech and Image Understanding, 1999.

[6] W. E. Alexander, D. Reeves, and C. Gloster, *Parallel image processing with the block data parallel architecture*, IBM J. Res. Develop. **44** (2000), 681–701.

[7] O. Anders and H. Torp, *Encoding of a priori information in active contour models*, IEEE Transactions on Pattern Analysis and Machine Intelligence **18** (1996), no. 9.

[8] S. Ando, *Consistent gradient operators*, IEEE Transactions on Pattern Analysis and Machine Intelligence **22** (2000), no. 3.

[9] N. Archip, *3d visualization of anatomical structures*, Intern raport, 2001.

[10] N. Archip and P.-J. Erard, *Anatomical structures map - a way of encoding medical knowledge in a task oriented computed tomography image analysis*, Proceedings of The 2000 International Conference on Mathematics and Engineering Techniques in Medicine and Biological Sciences (Las Vegas, Nevada, USA), June 2000, pp. 377–383.

[11] N. Archip, P. J. Erard, J.-M. Haefliger, and J. Germond, *Lung metastaces detection and visualization on ct images – a knowledge-based method*, Jurnal of Visualization and Computer Animation **accepted for publication** (2002).

[12] Samuel G. Armato, Maryellen L. Giger, and Heber MacMahon, *Automated detection of lung nodules in ct scans: Preliminary results*, Medical Physics **28** (2001), no. 8, 1552–1561.

[13] H.K. Awwad, *Radiobiological and psysiological perspectives - the boundary zone between clinical radiotherapy and fundamental radiobiology and physiology*, Kluwert Academic Publishers, 1990.

[14] R. Baechler, H. Bunke, and L.P. Nolte, *Restricted surface matching - numerical optimization and technical evaluation*, Computer Aided Surgery **6** (2001), 143–152.

[15] C. Bajaj, K. Lin, and E. Coyle, *Arbitrary topology shape reconstruction from planar cross sections.*, Graphical Models and Image Processing **58** (1996), 524–543.

[16] G. Barequet and M. Sharir, *Piecewise-linear interpolation between polygonal slices*, Computer Vision and Image Understanding **63** (1996), 251–272.

[17] J. Berger, *Roentgen: Radiation therapy and case-based reasoning*, Proceedings of the Conference on Artificial Intelligence Applications (1994), 171–177.

[18] J. R. Beveridge, J. Griffith, R.R. Kohler, A.R. Hanson, and E.M. Riseman, *Segmenting images using localized histograms and region merging*, International Journal of Computer Vision **2** (1989), no. 3, 311–347.

[19] J. Bijhold, K.G.A. Gilhuijs, M. vanHerk, and H. Meertens, *Radiation-field edge-detection in portal images*, Physics In Medicine And Biology **36** (1991), no. 12, 1705–1710.

[20] J.D. Boissonnat, *Shape reconstruction from planar cross-section*, Computer Vision, Graphics, and Image Processing **44** (1988), 1–29.

[21] P. Brigger, J. Hoeg, and M. Unser, *B-spline snakes: A flexible tool for parametric contour detection*, IEEE Transactions on Image Processing **9** (2000), 1484–1496.

[22] M.S. Brown and et al., *Knowledge-based segmentation of thoracic computed tomography images for assessment of split lung function*, Med. Phys. **27** (2000), no. 3, 592–598.

[23] J. Canny, *A computational approach to edge detection*, IEEE Trans. Pattern Analysis and Machine Intelligence **8** (1986), 679–698.

[24] H.N. Christiansen and T.W. Sederberg, *Conversion of complex contour line definitions into polygonal element mosaics*, Computer Graphics **12** (1978), 187–192.

[25] P. Croisille, M. Souto, M. Cova, S. Wood, Y. Afework, J. E. Kuhlman, and E. A. Zerhouni, *Pulmonary nodules: Improved detection with vascular segmentation and extraction with spiral ct*, Radiology **197** (1995), 397–401.

[26] D. Davis and C. Taylor, *A blackboard architecture for medical image interpretation*, SPIE Vol. 1445 Image Processing (1991).

[27] K. De Geus and A. Watt, *Three dimensional stylization of structures of interest from computed tomography images applied to radiotherapy planning*, Int. J. Radiation Oncology Biol. Phys. **35** (1996), 151–159.

[28] S. Dickson, *Investigation of the use of neural networks for computerized medical analysis*, Ph.D. thesis, University of Bristol, 1998.

[29] A. M. DiGioia, B. Jaramaz, and B. D. Colgan, *Computer assisted orthopaedic surgery. image guided and robotic assistive technologies*, Clinical Orthopaedics and Related Research **354** (1998), 8–16.

[30] M. Egmont-Petersen, *Mental models as cognitive entities*, Proceedings of the Scandinavian Conference on Artificial Intelligence (B. Mayoh (Ed.),IOS Press, Amsterdam), 1991, pp. 205–210.

[31] M. Egmont-Petersen, P.C.W. Hogendoorn, R. v. d. Geest, H. A. Vrooman, H. J. v. d. Woude, J. P. Janssen, J. L. Bloem, and J. H. C. Reiber, *Detection of areas with viable remnant tumor in postchemotherapy patients with ewing's sarcoma by dynamic contrast-enhanced mri using pharmacokinetic modeling*, Magnetic Resonance Imaging **15** (2000), no. 5, 525–535.

[32] A. Eisvruch, *Phase i/ii study of conformal and intensity modulated irradiation for oropharyngeal cancer*, Tech. report, RADIATION THERAPY ONCOLOGY GROUP, URL: http://www.rtog.org/members/protocols/h0022/, 2002.

[33] A.B. Ekoule, F.C. Peyrin, and C.L. Odet, *A triangulation algorithm from arbitrary shaped multiple planar contours*, ACM Trans. Graphics **10** (1991), 182–199.

[34] P.J. Elliott, J. Diedrichsen, K.J. Goodson, R. Riste-Smith, and G.J. Sivewright, *An object-oriented system for 3d medical image analysis*, IBM System Journal **35** (1996), no. 1.

[35] K. Englmeier and et al., *Model based image interpretation of spiral ct scans of the abdomen*, Artificial Intelligence in Medicine (1993), 44–51.

[36] C. Favardin, *Détermination automatique de structures géométriques destinées à la reconstruction de courbes et de surfaces à partir de données ponctuelles*, Ph.D. thesis, Université Paul Sabatier, Toulouse, 1993.

[37] A. Fenster and A. Zahalka, *Automated segmentation method for 3-dimensional ultrasound*, Phys. Med. Biol. **46** (2001), 1321–1342.

[38] W. Frei and C.C. Chen, *Fast boundary detection:a generalized and a new algorithm*, IEEE Trans. Computers **26** (1977), no. 10, 988–998.

[39] H. Fuchs, Z. Kedem, and S.P. Uselton, *Optimal surface reconstruction from planar contours*, Communications of the ACM **20** (1977), 693–702.

[40] S. Ganapathy and T.G. Dennehy, *A new general triangulation method for planar contours*, Computer Graphics **16** (1982), 69–75.

[41] E. Gautier, R. Baechler, P. Heini, and L.P. Nolte, *Accuracy of computer-guided screw fixation of the sacroiliac joint*, Clinical orthopaedics and related research **393** (2001), 310–317.

[42] B. Geiger, *Three-dimensional modeling of human organs and its applications to diagnosis and surgical planning*, Technical report, 2105, France (1993).

[43] K.G.A. Gilhuijs, P.J.H. vandeVen, and M. vanHerk, *Automatic three-dimensional inspection of patient setup in radiation therapy using portal images, simulator images, and computed tomography data*, Medical Physics **23** (1996), no. 3, 389–399.

[44] C. Gitlin, J. O'Rourke, and V. Subramanian, *On reconstructing polyhedra from parallel slices*, Intern. J. Comput. Geom. Appl. **6** (1996), 103–122.

[45] L. Gong and C.A. Kulikowski, *Composition of image analysis processes through object-centered hierarchical*, IEEE Transactions on Pattern Analysis and Machine Intelligence **17** (1995), no. 10.

[46] R. Gonzales and R. Woods, *Digital image processing*, Addison Wesley, 1992.

[47] M. Grimnes and A. Aamodt, *A two layer case-based reasoning architecture for medical image understanding*, Lecture Notes in Computer Science **1168** (1996), 164–178.

[48] M.J.F. Grimnes, *Imagecreek: A knowledge level approach to case-based image interpretation*, Ph.D. thesis, University of Trondheim, 1998.

[49] W. E. L. Grimson, *Image understanding, medical imaging, neurosurgery: Medical application of image understanding*, IEEE Expert (1995), 18–28.

[50] M. Haddad and et al., *Scina: A case-based reasoning system for the interpretation of myocardial perfusion scintigrams*, Proccedings of EWCBR, 1996.

[51] E.J. Hall, *Radiobiology for the radiologist*, Lippincott, Williams & Wilkins, 2000.

[52] M. Held, *Vroni: An engineering approach to the reliable and efficient computation of voronoi diagrams of points and line segments*, Computational Geometry **18** (2001), 95–123.

[53] M.A. Holmes and et. al., *The application of correlated sampling to the computation of electron beam dose distributions in heterogeneous phantoms using the monte carlo method*, Physics In Medicine and Biology **38** (1993), 675–6888.

[54] H. Hoppe, *Surface reconstruction from unorganized points*, Ph.D. thesis, University of Washington, 1994.

[55] L. Itti, C. Koch, and E. Niebur, *A model of saliency-based visual attention for rapid scene analysis*, IEEE Transactions on Pattern Analysis and Machine Intelligence **20** (1998), no. 11, 1254–1259.

[56] P. Jackson, *Introduction to expert systems*, Addison-Wesley, 1999.

[57] M. Jacob, T. Blu, and M. Unser, *A unifying approach and interface for spline-based snakes*, Proceedings of the SPIE International Symposium on Medical Imaging: Image Processing, San Diego CA, USA (2001), 340–347.

[58] L. Jennifer, T.E. Boes, C. Weymouth, and R. Meyer, *Multiple organ definition in ct using a bayesian approach for 3d model fitting*, Vision Geometry IV, Proc. SPIE 2573, 1995, pp. 244–251.

[59] T. Kapur and E. Grimson, *Segmentation of brain tissue from magnetic resonance images*, Medical Images Analysis **1** (1996), no. 2, 109–127.

[60] M. Kass, A. Witkin, and D. Terzopoulos, *Snakes: Active contour models*, International Journal of Computer Vision (1988), 321–331.

[61] E. Keppel, *Approximating complex surfaces by triangulation of contours lines*, IBM J. Research Development **19** (1975), 2–11.

[62] J. P. Ko and M. Betke, *Chest ct: Automated nodule detection and assessment of change over time-preliminary experience*, Radiology **218** (2001), 267–273.

[63] H. Koch, K. Pakzad, and R. Tnjes, *Knowledge based interpretation of aerial images and maps using a digital landscape model as partial interpretation*, Workshop on Semantic Modeling of Topographic Information from Images and Maps, 1997.

[64] D. Koelma and A. Smeulders, *A black board infrastructure for object based image interpretation and maps using a digital landscape model as partial interpretation*, Third International Conference on Visual Information Systems, 1999.

[65] A.H. Konig and E. Groller, *3d medical visualization: Breaking the limits of diagnostics and treatment*, ERCIM News **44** (2001).

[66] V.P. Kumar and U.B. Desai, *Image interpretation using bayesian networks*, IEEE Transactions on Pattern Analysis and Machine Intelligence **18** (1996), no. 1.

[67] F. Kummert and al., *Control and explanation in a signal understanding environment*, Signal Processing **32** (1993), 111–145.

[68] M. Kunt, G. Coray, G. Granlund, J.P. Haton, R. Ingold, and M. Kocher, *Reconnaisance des formes et analyse de scènes*, Presses Polytechniques et Universitaires Romandes, 2000.

[69] K.F. Lai and R.F. Chin, *Deformable contours: Modeling and extraction*, IEEE Trans. Pattern. Anal. Mach. Intell. **17** (1995), 1084–1090.

[70] D.T. Lee, *Medial axis transformation of a planar shape*, IEEE Transactions on Pattern Analysis and Machine Intelligence **4** (1982), no. 4.

[71] Y. Lee, T. Hara, H. Fujita, S. Itoh, and T. Ishigaki, *Nodule detection on chest helical ct scans by using a genetic algorithm*, 1997 IEEE IASTED International Conference on Intelligent Information Systems (1997), 67–70.

[72] Philips T.L. Leibel, S.A., *Textbook of radiation oncology*, W.B. Saunders Company, 1998.

[73] D.I. Lewin, *Totally rad: Planning radiation therapy in 3d*, Computing in science and engineering **1** (1999), 6–9.

[74] H. Li, R. Deklerck, B. De Cyper, A. Hermanus, E. Nyssen, and J. Cornelius, *Object recognition in brain ct-scans: Knowledge based fusion of data from multiple feature extractors*, IEEE Transactions on Medical Imaging **14** (1995), no. 2, 343–360.

[75] Y. Ligier, O. Ratib, M. Logean, and C. Girard, *Osiris : a medical image manipulation system*, M.D. Computing Journal **11** (1994), no. 4, 212–218.

[76] J. Liu and Y.Y. Tang, *Adaptive image segmentation with distributed behavior-based agents*, IEEE Transactions on Pattern Analysis and Machine Intelligence **10** (1999), no. 6.

[77] S.L. Lou, C.L. Chang, K.P. Lin, and T.S. Chen, *Object based deformation technique for 3-d ct lung nodule detection*, Proc SPIE **3661** (1999), 1544–1552.

[78] R. Macura and K. Macura, *Macrad: Radiology image resource with a case-based retrieval system*, Case-Based Reasoning Research and Development (Veloso M. and Aamodt A. (eds.)), 1995, pp. 43–54.

[79] D. Marr and E.C. Hildreth, *Theory of edge detection*, Proc. Royal Soc. London **207** (1980), 187–217.

[80] T. McInerney and D. Terzopoulos, *Topologically adaptable snakes*, Proc. of the Fifth Int. Conf. on Computer Vision (ICCV '95) (Cambridge, MA, USA), June 1995.

[81] ——, *Deformable models in medical image analysis: A survey*, Medical Image Analysis **1** (1996), no. 2.

[82] W.S. Meisel, *Computer-oriented approaches to pattern recognition*, Academic Press, 1972.

[83] W. Menhardt and et al., *Knowledge based interpretation of cranial mr images*, Tech. report, Philips GmbH, Forschungslaboratorium Hamburg, POBox 540840 D-2000 Hamburg 54, 1990.

[84] M.L. Merriam, *Experience with the cyberware 3d digitizer*, NCGA Proceedings (1992), 125–133.

[85] D. Meyers, S. Skinner, and K. Sloan, *Surfaces from contours: The correspondence and branching problems.*, Proc. Graphics Interface (1991), 246–254.

[86] Giger M.L., K.T. Bae, and H. MacMahon, *Computerized detection of pulmonary nodules in computed tomography images*, Invest. Radiol. **29** (1994), 459–465.

[87] A.N. Moga and M. Gabbouj, *Parallel image component labeling with watershed transformations*, IEEE Transactions on Pattern Analysis and Machine Intelligence **19** (1997), no. 5, 441–450.

[88] D. Moore and K. Warren, *Approximation of dense scattered data using algebraic surfaces*, Tech. report, Rice University, 1990.

[89] F.H. Netter, *Atlas of human anatomy*, 2nd ed., Novartis Medical Education;, 1997.

[90] P. P. Ohanian and R.C. Dubes, *Performance evaluation for four classes of textural features*, Pattern Recognition **25** (1992), no. 8, 819–833.

[91] T. Okumura and et al., *Image processing for computer-aided diagnosis of lung cancer screening system by ct(lsct)*, Proc SPIE **3338** (1998), 1314–1322.

[92] J. O'Rourke, *Computational geometry in c*, Cambridge University Press, 1994.

[93] J.R. Parker, *Algorithms for image processing and computer vision*, Wiley Computer Publishing, 1997.

[94] T. Pavlidis, *Structural pattern recognition*, Springer-Verlag, 1977.

[95] I. Pitas, *Digital image processing algorithms and applications*, John Wiley and Sons, Inc., 2000.

[96] N.J. Pizzi, R.A. Vivanco, and R.L. Somorjai, *Evidenttm: a functional magnetic resonance image analysis system*, Artificial Intelligence in Medicine **21** (2001), 263–269.

[97] D. Popovic and V. P. Bhatkar, *Methods and tools for applied artificial intelligence*, MARCEL DEKKER, Inc, 1994.

[98] J.A. Purdy and G. Starkschall, *A practical guide to 3d planning and conformal radiation therapy*, Ed. Advacnced Medical Publishing, Inc., 1999.

[99] T. Randen and J.H. Husy, *Filtering for texture classification: A comparative study*, IEEE Pattern Analysis and Machine Intelligence **21** (1999), no. 4.

[100] Joseph M. Reinhardt, Neil D. D'Souza, and Eric A. Hoffman, *Accurate measurement of intrathoracic airways*, IEEE Transactions on Medical Imaging **16** (1997), no. 6, 820–827.

[101] R.A. Robb, B.M. Cameron, and S. Aharon, *Totally rad: Planning radiation therapy in 3d*, **1** (1999), 6–9.

[102] J.B.T.M. Roerdink and A. Meijster, *The watershed transform: definitions, algorithms, and parallellization strategies*, Fundamenta Informaticae **41** (2000), 187–228.

[103] E. Rogers, *Via-rad: a blackboard-based system for diagnostic radiology*, Artificial Intelligence in Medicine **7** (1995), 343–360.

[104] T. Schiemann, M. Bomans, U. Tiede, and K. Heinz, *Interactive 3d-segmentation*, Visualization in Biomedical Computing II, Proc. SPIE 1808, Chapel Hill, 1992.

[105] J. Schnabel and S. Arridge, *Snake implementation in the uk iue project*, University College London, Tech. report (1998), URL: http://www.cs.ucl.ac.uk/research/mip/mipue.

[106] J. Serra, *Image analysis and mathematical morphology*, Academic Press, 1982.

[107] Y. Shinagawa and T.L. Kunii, *The homotopy model: a generalized model for smooth surface generation from cross sectional data*, The Visual Computer **7** (1991), 72–86.

[108] K.R. Sloan and J. Painter, *From contours to surfaces. testbed and initial results*, Proc. CHI+GI (1987), 115–120.

[109] I. Sobel, *Neighborhood coding of binary images for fast contour following and general binary array processing*, CVGIP **8** (1978), 127–135.

[110] M. Sonka, G. Sundaramoorthy, and E.A. Hoffman, *Knowledge-based segmentation of intrathoracic airways from multidimensional high resolution ct images*, Medical Imaging 1994: Physiology and Function from Multidimensional Images (1994), 73–85.

[111] P. Suetens, P. Fua, and A.J. Hanson, *Computational strategies for object recognition*, ACM Computing Surveys **24** (1992), no. 1.

[112] R. Szeliski and D. Tonnesen, *Surface modeling with oriented particle systems*, Computer Graphics (SIGGRAPH '92 Proceedings) **26** (1992), 185–194.

[113] G.M. te Brake and N. Karssemeijer, *Segmentation of suspicious densities in digital mammograms*, Medical Physics **28** (2001), no. 2, 259–266.

[114] A. Teller and M. Veloso, *Pado: A new learning architecture for object recognition*, Symbolic visual learning (1995).

[115] J.C. Tilton, *A recursive pvm implementation of an image segmentation algorithm with performance results comparing the hive and the cray t3e*, Proceedings of Frontiers '99: The 7th Symposium on the Frontiers of Massively Parallel Computation, February 1999, pp. 146–153.

[116] R. Tombropoulos and et al., *A decision aid for diagnosis of liver lesions on mri*, Tech. report, Section on Medical Informatics, Stanford University School of Medicine, 1994.

[117] G. Turk and M. Levoy, *Zippered polygon meshes from range images*, Computer Graphics (SIGGRAPH '94 Proceedings) (1994).

[118] B. van Ginneken and B.M. ter Haar Romeny, *Automatic segmentation of lung fields in chest radiographs*, Medical Physics **27** (2000), no. 10, 2445–2455.

[119] G.L. Vernazza and et al., *A knowledge-based system for biomedical image processing and recognition*, IEEE Trans. Circuits and Systems **34** (1987), no. 11.

[120] O. Wegener, *Whole body computed tomography*, 2nd ed., Blackwell scientific, 1992.

[121] Josie Wernecke, *The inventor mentor : Programming object-oriented 3d graphics with open inventor*, Addison-Wesley Publishing Company, 1994.

[122] D.J. Williams and M. Shah, *A fast algorithm for active contours and curvature estimation*, CVGIP: Image Understanding **55** (1992), no. 1, 14–26.

[123] M. Worring and A.W.M. Smeulders, *Digitized circular arcs: Characterization and parameter estimation*, IEEE Pattern Analysis and Machine Intelligence **17** (1995), no. 6.

[124] K. Yanai, *An image understanding system for various images based on multi-agent architecture*, Proceedings of the Third International Conference on Computational Intelligence and Multimedia Applications, 1999.

[125] A. Yezzi, S. Kichenassamy, A. Kumar, P.J. Olver, and A. Tannenbaum, *A geometric snake model for segmentation of medical imagery*, IEEE Trans. Medical Imaging (1997), no. 16, 199–209.

[126] A. Zahalka and A. Fenster, *An automated segmentation method for three-dimensional carotid ultrasound images*, Physics in Medicine and Biology **46** (2001), 1321–1342.

[127] S.C. Zhu and A. Yuille, *Region competition: Unifying snakes, region growing, and bayes/mdl for multiband image segmentation*, IEEE Transactions on Pattern Analysis and Machine Intelligence **18** (1996), no. 9.